DSL LINE TESTER USING WIDEBAND FREQUENCY DOMAIN REFLECTOMETRY

A Thesis Submitted to the College of

Graduate Studies and Research

in Partial Fulfillment of the Requirements

for the Degree of Master of Science

in the Department of Electrical Engineering

University of Saskatchewan

Saskatoon

By

Bernardo Celaya de la Torre

Saskatoon, Saskatchewan, Canada

Permission to use

In presenting this thesis in partial fulfillment of the requirements for a Postgraduate degree from the University of Saskatchewan, I agree that the Libraries of this university may make it freely available for inspection. I further agree that permission for copying of this thesis in any manner, in whole or in part, for scholarly purposes may be granted by the professor or professors who supervised my thesis work or, in their absence, by the Head of the Department or the Dean of the College in which my thesis work was done. It is understood that any copying or publication or use of this thesis or parts thereof for financial gain shall not be allowed without my written permission. It is also understood that due recognition shall be given to me and to the University of Saskatchewan in any scholarly use which may be made of any material in my thesis.

Requests for permission to copy or to make other use of material in this thesis in whole or part should be addressed to:

Head of the Department of Electrical Engineering
57 Campus Drive
University of Saskatchewan
Saskatoon, Saskatchewan, Canada
S7N5A9

Abstract

Digital subscriber line (DSL) technology is used to provide high speed Internet access and, more recently, video services over twisted pair lines. Telephone lines have impairments that hinder DSL transmission, and some examples are coils and bridge taps that were introduced to aid voice telephony. Other faults are caused by physical damage that results in open circuits, short circuits or water in the line. Telephone companies have to locate and repair these faults to enable high-speed data services. It is also useful to "qualify" lines for future DSL service so that a new customer can be promptly informed whether high-speed service can be supplied.

This thesis proposes a novel technique called Wideband frequency domain reflectometry (W-FDR) to accurately locate impairments in telephone lines and estimate the reflection magnitude caused by faults. The measurement produces a result similar to the well-known time domain reflectometer (TDR), however, digital signal processing techniques are now applied to provide enhanced resolution and range. In addition to magnitude, the new technique is able to measure reflection angle which can help to determine the nature of the fault (wire in the cable, broken wires, etc).

The measurement technique consists of energizing the line with a sinusoid that increases from 50 kHz to 1300 kHz in discrete frequency steps after coherent detection. The amplitude of the reflected signal is recorded as a function of frequency for 2500 equally spaced frequencies. The Fourier transform and some signal processing are then used to estimate the complex reflection coefficient location of the faults in the telephone line. Lines with up to 4 reflection points have been accurately analyzed.

Results show distance measurement accuracy better than 1% and phase measurement accuracy better than 10 degrees for line lengths up to 5 km. These measurements exceed the performance of currently available TDR instruments.

Acknowledgments

I would like to express my most special recognition to my supervisor Professor David E. Dodds, for his very wisdom guidance that made so successful this project, and for the financial support that he provided me, which made possible my research.

I want to gratefully acknowledge TRLabs for the financial support and the excellent facilities that provided for my research, as well for the support that Jack Hanson and Garth Wells gave me during the project. I want to thanks the Canadian government for give me the great opportunity to come here to do my masters degree and this research.

A very special thanks to my parents for giving me everything and to support me in all the ways to made possible that I came here to make this work.

Finally, thanks to all the people that have helped me in my way, and to all the professors that gave me the knowledge to be here.

Table of contents

List of figures

List of tables

Abbreviations

ADC	Analog to digital converter
ADSL	asymmetric digital subscriber line
AWG	American wire gauge
CDSL	Rockwell's consumer digital subscriber line
CO	Central office
DFT	discrete Fourier transform
DSL	digital subscriber line
DSP	digital signal processing
FFT	Fast Fourier transform
FMCWR	Frequency modulated continuous wave radar
HDSL	high bit-rate digital subscriber line
IDFT	inverse discrete Fourier transform
IDSL	integrated services digital network digital subscriber line
ISC	Internet Systems Consortium
JWI	Jumper wire interface
LPF	Low pass filter
MDSL	moderate bit-rate digital subscriber line
OC	open circuit
PIC	Plastic insulated cable
RADSL	rate-adaptive digital subscriber line
SDSL	single line digital subscriber line
SSC	Spread spectrum correlation
TDR	Time domain reflectometry
Telco	telephone company
VDSL	very high rate digital subscriber line
W-FDR	Wideband frequency domain reflectometry

1. Introduction

1.1 Digital subscriber line

Digital subscriber line (DSL) is a technology for carrying high speed data to homes and small businesses over ordinary copper telephone lines. This technology increases data transmission rates by a factor of twenty or more by sending signals in previously unused high frequencies. Also, DSL allows users to receive voice and data simultaneously so there is no need for a separate phone line. For these reasons this technology became very popular and has been used by telephone companies around the world to deliver high-speed internet services using the telephone wires.

Originally, telephone lines were designed just to transmit voice. Nevertheless, over time, several applications like fax machines, dial modems, etc; have appeared. But all these applications were limited to the 3.4 kHz bandwidth provided for voice transmission. Therefore, this has limited data rate.

The introduction of xDSL (all the different DSL technologies) has increased the transmission bandwidth beyond 3.4 kHz. This allows higher data rate transmission in both, downstream (from network to customer) and upstream (customer to network) directions.

DSL techniques can be divided in 3 main categories. These categories are high bit-rate DSL (HDSL), asymmetric DSL (ADSL) and very high-bit-rate DSL (VDSL). These families are also divided in different technologies. Some of these technologies have been standardized, and some are variations on the standards, as depicted in Table 1.1 [1]. Next we explain these families.

High bit-rate DSL (HDSL) was introduced in 1992 for 1.5 Mb/s (using two pairs of wire) and 2 Mb/s (using two or three pairs of wire) symmetric transmissions on local lines. HDSL is used for private line services, and links to remote network nodes such as digital loop carriers remote terminals and wireless cell cites. In 2000,

HDSL2 was introduced to accomplish the same bit-rate and line reach as HDSL but using one pair of wires instead of the two pairs required for HDSL.

Asymmetric DSL (ADSL) service was introduced in 1995, and is used for applications benefiting from the bit-rate asymmetry, such as, high-speed Internet access and workstation access for small business offices and home work offices. ADSL supports downstream bit-rates up to 8 Mb/s and upstream bit-rates up to 900 kb/s on short lines (less than 1.8 km) with moderate line noise. However, ADSL is most often provided at bit-rates of 2 Mb/s and 128 kb/s upstream. ADSL signals are combined with 3.4 kHz analog voice signals with the ADSL signals in a higher frequency band. Fig. 1.1 shows the typical spectrum in a twisted pair that uses ADSL technology.

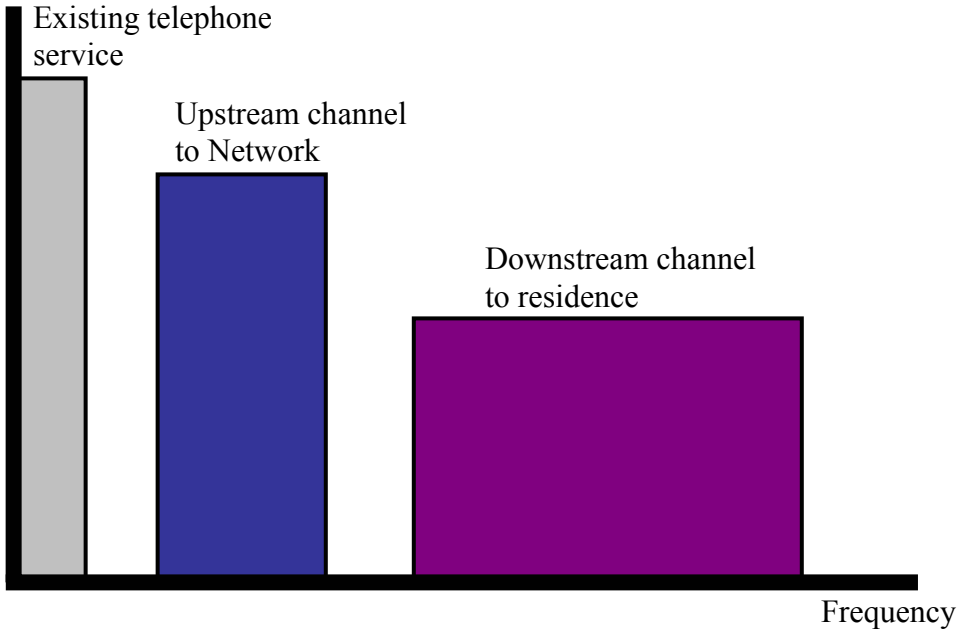

Fig. 1.1 ADSL spectral content on twisted pair

Very high-bit-rate DSL (VDSL) systems were used in fields trials in 2000. VSDL supports asymmetric bit-rates as high as 52 Mb/s downstream or symmetric bit-rates as high as 26 Mb/s. The key distinction of VDSL is its limitation to very short lines, as short as 1000 feet for the highest bit rate or up to about 4000 feet for the moderate data rates. VSDL provides simultaneous transmission of data and analog voice signal.

HDSL Family		**ADSL Family**		**VDSL Family**
Standards	**Variations**	**Standards**	**Variations**	
HDSL	MVL	ADSL	1-Meg Modem	
HDSL2	SDSL	RADSL	CDSL	
	MDSL	G.lite	EZ-DSL	
	IDSL			

Table 1.1 xDSL family (taken from [1])

If a twisted pair line is capable of supporting transmission using a standard DSL method, it is said that it “qualifies” for this service.

1.1.1 Internet and DSL Growth

The Internet has been growing nothing short of exponential in the last few years. For this reason telephone companies use DSL to offer high speed data transfer on their twisted pair lines, which runs to every residential home and small business.

To get an idea of the growth of the Internet, Fig 1.2 shows a statistic obtained from the Internet Systems Consortium, Inc. (ISC) [3], which shows the number of IP addresses or hosts on internet over the last years.

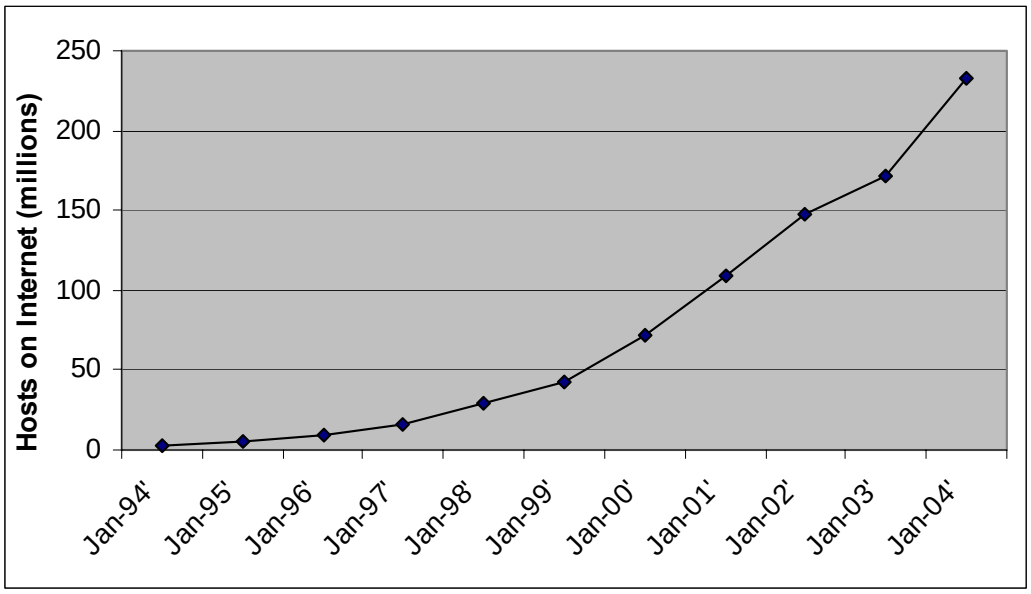

Fig 1.2 Growth of hosts on internet (data obtained from [3])

Along with the growth of Internet, digital subscriber lines or DSL has also been experiencing an explosive growth around the world. Just in the last year 2003, almost 28 million homes and business subscribed to a high-speed connection over the telephone line.

In the beginning of 2004, according to the analyst firm Point Topic [3], the number of DSL subscribers reached 63.84 million around the world. It is expected that, the number of DSL subscribers will reach 200 million by the end of 2005.

In the beginning of 2004, the number of DSL subscribers in North America, was 11 million, from which 9.1 million were in the United States and 2.1 million were in Canada. In the last year 2003, the number of DSL subscribers in North America increased by 3 million, from which 2.66 million were in the United States and 440 000 were in Canada. In this way, Canada had the eleventh largest growth of DSL subscribers in the world during 2003. Fig. 1.3 illustrates the growth of DSL

subscribers in North America from the beginning of 2000 to the beginning of the 2004, so we can appreciate the tremendous growth that DSL had in this region.

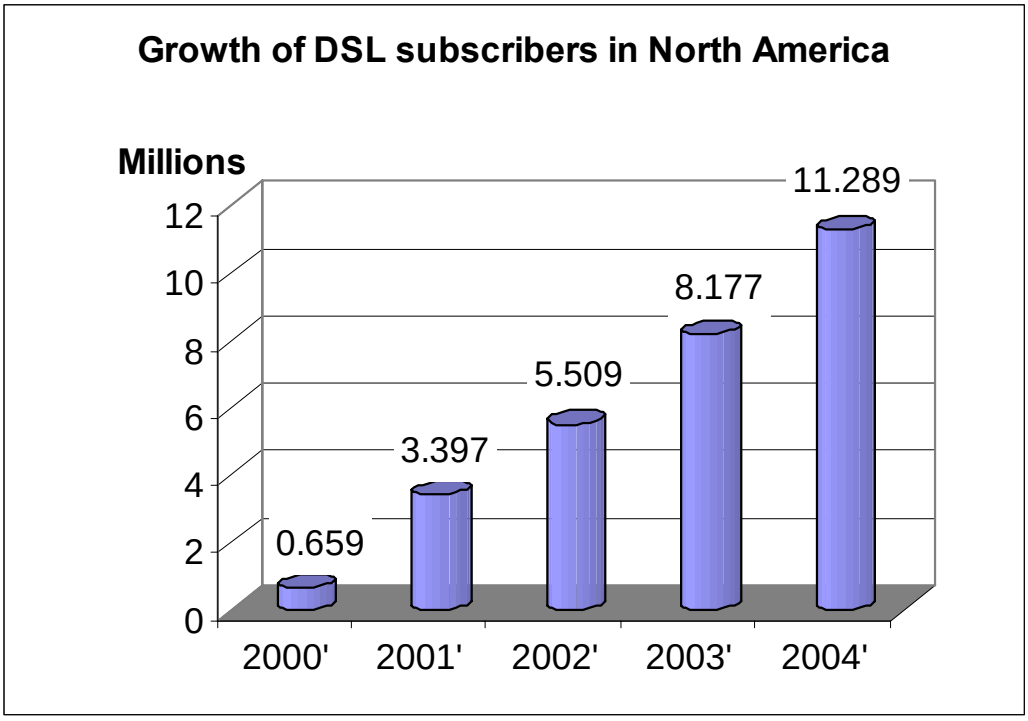

Fig. 1.3 Growth of DSL subscribers in North America
(data obtained form DSL forum [2])

Statistics collected by DSL Forum [2] show that at the beginning of the 2004, Canada occupied 9th place in the number of DSL subscribers compared with other counties, and 4th place in the number of DSL per capita. China has the largest DSL population in the world with 10.95 million (excluding Hong Kong). Table 1.2 shows the 10 countries with the most DSL subscribers in the world.

Global Ranking	Country	DSL subscribers (Beginning 2004)	DSL subscribers per 1000 people
1	China	10,950,000	8.5
2	Japan	10,272,052	80.9
3	USA	9,119,000	31.4
4	South Korea	6,435,955	133.3
5	Germany	4,500,000	54.6
6	France	3,262,700	54.2
7	Taiwan	2,800,000	123.8
8	Italy	2,280,000	39.3
9	Canada	2,170,243	67.4
10	UK	1,820,230	30.3

Table 1.2 Country ranking of DSL subscribers (data obtained from [2])

North America constitutes 17.7% of the global market of DSL subscribers, while the biggest market in the Asia-Pacific region with 32.1% of the global market. Fig. 1.4, shows the DSL subscriber market in 2004, distributed by regions.

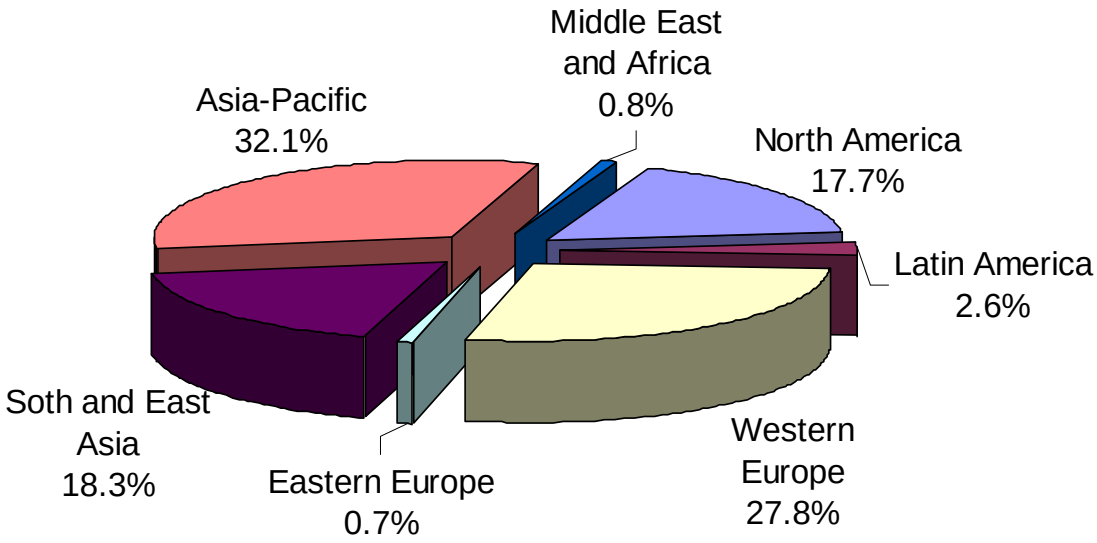

Fig. 1.4 Global DSL market by regions (data obtained from [2])

Globally, DSL has been experiencing an exponential growth in the last years, which indicates that DSL will continue to extend its lead as the world's best broadband technology in 2004. As an even wider variety of DSL services become available, it is expected that DSL services will become essential for consumers and businesses in the next years.

1.1.2 xDSL service qualification

As it was mentioned, DSL has been experiencing a large growth, and projections indicate that by 2005 the number of DSL subscribers will reach 200 million. This implies a great business for telephone companies, but at the same time it implies a great challenge to deploy their DSL services fast enough to satisfy the increasing demand. Telephone companies (Telco's) will only be able to capitalize

on this increasing demand for DSL services if they can overcome some obstacles to deployment.

There are several problems involved in the deployment of DSL services, and principally these problems are caused by impairments in the twisted pair line that cause attenuation and reflections at high frequencies. Therefore, telephone companies must remove these impairments to qualify the line for DSL.

Some of these impairments have been introduced by the telephone companies themselves to improve voice services. For example, loading coils were used on twisted pair lines to extend the range for voice signals; however, these coils or inductors have the effect of severely attenuating the high frequencies used for high speed data signals. Another example is increased wire size used at the end of long lines to reduce voice attenuation. But this change in the wire size also implies a change in the impedance of the line and this causes reflection of the high speed data signals. A third problem is bridge taps that have been added to twisted pair line to make it easier to add and delete costumers but they also introduce an impedance discontinuity at the junction and cause signal reflections that interfere with high speed data transmission [4].

In addition to these problems, there can be other faults, for example, water that gets into the cable casings, animals that chew the telephone wires, accidents that damage the line, etc. All these problems have to be located and fixed in order to provide high speed data services.

Telephone companies need a reliable technology to help them to determine if a telephone line has any impairment like coils, bridge taps, etc; that interfere with high speed data. In this way, telephone companies can test a line to qualify it for high speed data transmission, and if the line has any impairment, they can locate it and remove it to allow the line to provide DSL services such as high-speed Internet. This will enable telephone companies to capitalize the increasing demand for high speed Internet service and deploy xDSL service fast enough to satisfy the exponential demand.

1.2 Thesis proposal

The research presented in [1], is extended in this thesis to develop a technique called wideband frequency domain reflectometry (W-FDR), to locate impairments in telephone lines. This technique can locate multiple impairments in a telephone line, such as open circuits, short circuits, bridge taps, coils, etc. In this way, telephone companies can test telephone lines to qualify them for xDSL services, and in case of impairments on the line, they can accurately locate them and remove them permit high speed data services.

One goal of this thesis was to improve this technology, to increase the potential of the technique, so besides determining the location of the fault, this technique could also estimate the reflection angle of the fault, which is used to determine the nature of the fault (open circuits, water, bridge taps, etc). Other goals of the thesis were to improve the measurement range of the technique and the quality of the measurements, which means measurements with better resolution and with much more accuracy.

This new measurement technique consists of energizing the line with a sinusoid that increases in discrete frequency steps. The amplitude of the reflected signal is recorded as a function of frequency to form a trace, which is later processed using signal processing methods to estimate the location and reflection angle of the faults.

1.3 Thesis organization

This thesis is organized in 7 chapters.

Chapter 1 presents the motivation and the reasons for this thesis research, as well as the research goals.

Chapter 2 describes the different techniques that can be used to locate faults in telephone lines. These techniques include time domain reflectometry (TDR) and frequency modulated continuous wave radar (FMCW radar).

Chapter 3 provides information about transmission lines. There is a discussion about transmission line theory, parameters and constants of transmission lines, and the reflection coefficient. The chapter also describes twisted pair cable, and some common causes of impairments.

Chapter 4 describes the prototype system implemented in this project and shows how to test the telephone lines using frequency domain reflectometry.

Chapter 5 explains the steps used to process the data (trace), obtained with the W-FDR measurement system. There is an explanation of the digital signal processing used to estimate the location and reflection angle for the different faults.

Chapter 6 presents the results, obtained in the laboratory for several different line configurations and faults. These results were obtained using the W-FDR prototype system.

Chapter 7 presents the conclusions of this project based on the results obtained in the laboratory. It also presents ideas for improving the measurements.

2. Telephone line measurement techniques

In this chapter we are going to talk about different techniques that can be used to locate faults in telephone lines. There are four techniques that can be used for this purpose and these are: time domain Reflectometry (TDR) which is the most popular fault location technique in telephone lines, frequency modulated continuous wave radar (FMCW radar), spread spectrum correlation and wideband frequency domain reflectometry (W-FDR). This thesis focuses on the W-FDR technique. In this chapter we compare the advantages and disadvantages of the four methods.

2.1 Time Domain Reflectometry (TDR)

Time Domain Reflectometry is the most popular technique to locate faults in communication lines. This technique is used in all telephone line test equipments currently available on the market.

The TDR method works by sending an electric pulse through the line. This pulse can be changed in width and amplitude depending of how far we plan to measure. As farther is the measurement, it is necessary to increase the amplitude and width of the pulse in order to transmit more energy and be able to measure farther.

The transmitted pulse will travel through the line and if it encounters a discontinuity, a portion will be reflected back to the transmitter instead of reaching the terminating load at the end of the line, where it would normally be absorbed. This reflected pulse is described by the multiplication of the original pulse with the reflection coefficient of the discontinuity. The reflection coefficient can be calculated as follows:

$$\rho = \frac{Zr - Zo}{Zr + Zo} \tag{2.1}$$

Where Zr is the impedance at the discontinuity as "seen" by the traveling pulse and Zo is the characteristic impedance of the transmission line.

Using the reflected pulse from the discontinuity, it is possible to estimate the distance to the fault knowing the round trip delay of the pulse and using the next equation,

$$x = \frac{vt}{2} \tag{2.2}$$

where "*x*" is the distance from the test equipment to the fault, "*v*" is the velocity of propagation of the pulse in the line, and "*t*" is the time delay of the round trip of the pulse.

The type of fault can be estimated from the amplitude of the reflected pulse. For example, if the line has a short circuit then the reflection coefficient is -1. Therefore if we send a pulse, when this reaches the discontinuity it will be reflected with coefficient -1 and then it will have negative amplitude when it arrives back. We can determine from a negative amplitude in the reflected pulse that the fault on the line is ether a short circuit or a fault with Zr < Zo.

Fig. 2.1, shows an example of how a pulse propagates in a terminated line that has a bridge tap with an open circuit at the end of the lateral branch. The bridge tap has a reflection coefficient of -1/3, and the open circuit has a reflection coefficient of +1. Let's assume that the time that takes to the pulse to make a round trip to the bridge tap is 400 ns, and round trip from the bridge tap to the open circuit takes another 100 ns. In this way, we can see that at 400 ns we get the first reflection

coming from the bridge tap. This reflection has an amplitude of -1/3 the amplitude of the original pulse, because the original pulse was reflected back multiplied by the reflection coefficient of the bridge tap. After 1/3 of the signal was reflected back at the bridge tap, the remaining 2/3 continues traveling in the two lines. Then, the 2/3 of the signal reaches the open circuit at the end of the lateral branch, and is reflected back to the bridge tap multiplied by +1 (the reflection coefficient of the open circuit). Once the 2/3 of signal reaches for second time the bridge tap, the signal is multiplied again by -1/3 (the reflection coefficient of the bridge tap), and reflected back to the open circuit with an amplitude equal to (2/3)(-1/3) that is -2/9. The part of the signal that was not reflected back to the open circuit, this is 2/3 of the 2/3 of original signal continues traveling in the line and arrives back to the transmitter just 100 ns after the first reflection. The amplitude of this second reflection is equal to (2/3)(2/3) that is 4/9. The -2/9 of the signal that were reflected again to the open circuit, will keep bouncing between the bridge tap and the open circuit causing new reflections at the transmitter point every 100 ns. These reflections will have every time an amplitude equal to 1/3 of the amplitude of the reflection before. Therefore, we will receive a third reflection at 600 ns with amplitude equal to (4/9)(-1/3) that is -4/27, and a forth reflection at 700 ns with amplitude (4/9)(-1/3)(-1/3) that is 4/81, and so on.

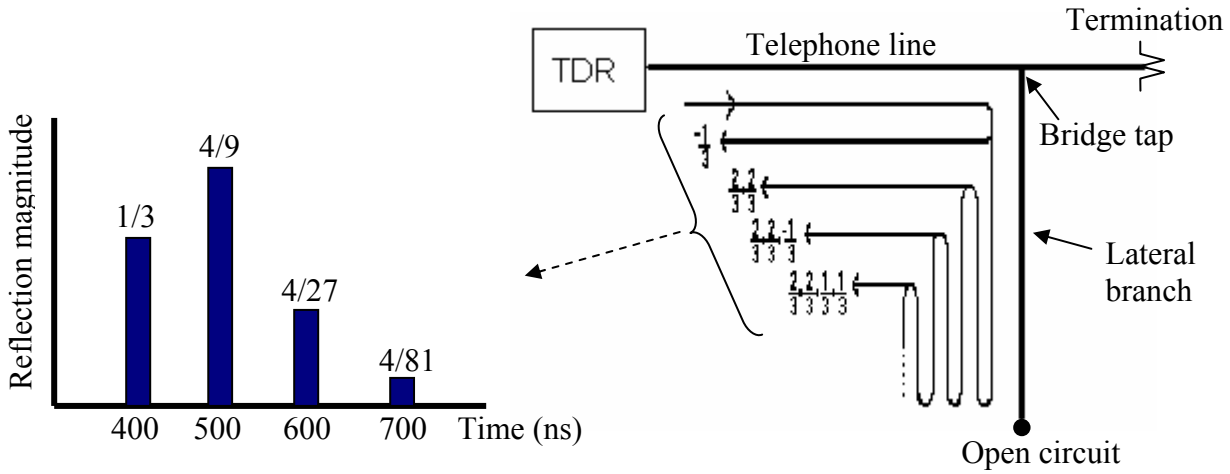

Fig. 2.1 Pulse reflection using TDR (adapted from presentation by Dodds)

Time domain reflectometry has several advantages compared with other techniques. It requires a very simple equipment to measure the lines, because with this technique there is no need of an oscillator to sweep the line or a hybrid coupler like the technique explained in section 2.4 (W-FDR); all it is needed is a pulse source and an oscilloscope to make basic measurements using this technique. Also this technique has the advantage that just by looking at the polarity of the reflected pulse, is possible to determine the kind of fault that is on the line.

This technique also has some disadvantages. The main one is that when the pulse propagates through the line it suffers from dispersion, as is shown in Fig. 2.2. This effect is caused by the differing velocity of propagation with frequency and is very difficult to compensate for when you use TDR. This effect of dispersion also forces the use of broader pulses, which reduces the measurement resolution. Another disadvantage of TDR is that using this technique is difficult to see several discontinuities on the same line, because each time the measuring pulse passes through one discontinuity it loses power and it becomes more difficult to see the next discontinuity.

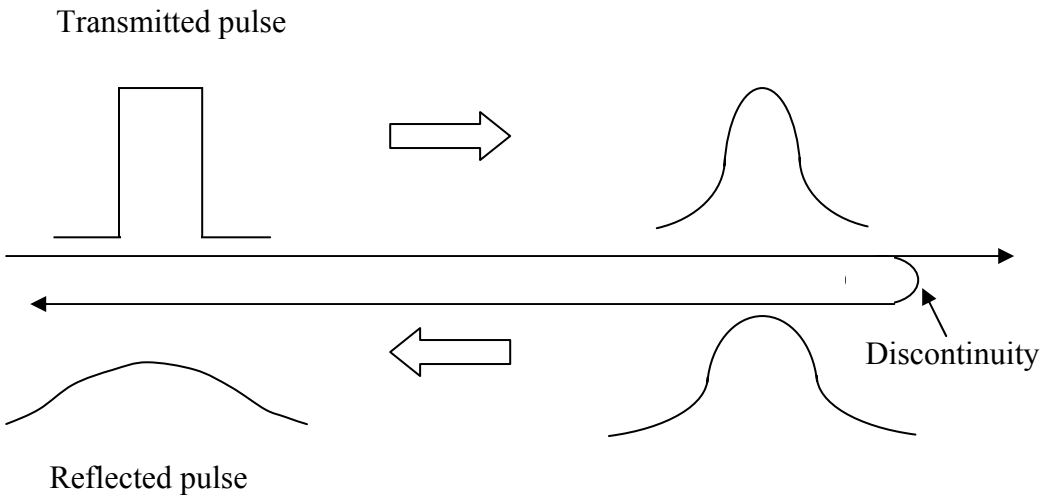

Fig. 2.2 Pulse dispersion in a transmission line

2.1.1 Two examples of commercial equipment

The CableShark test equipment from Consultronics [5] is the best instrument in the market to qualify lines for xDSL using TDR. Fig. 2.3 shows a measurement of an open circuit obtained with this test equipment and in Appendix B we can see some more measurements of this device.

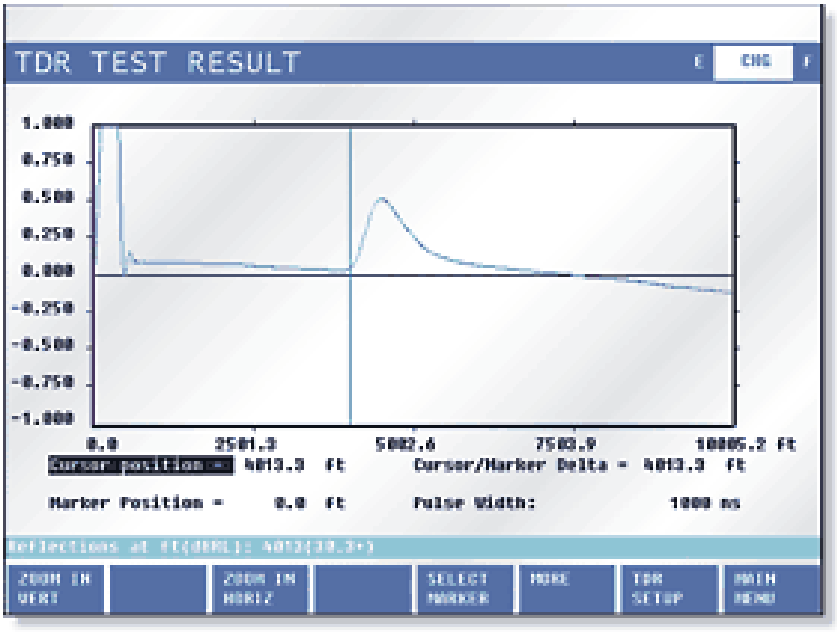

Fig. 2.3 CableShark measurement from an open circuit
(picture taken from Consultronics web page [5])

The 990DSL Copperpro is another DSL test equipment manufactured by FLUKE [6] that locates faults in telephone lines using time domain reflectometry (TDR). Fig. 2.4 taken from [6] shows a measurement of an open circuit at 2893 m (6078 ft) obtained with 990DSL Copper-pro. Some more measurements of this equipment are shown also in Appendix B.

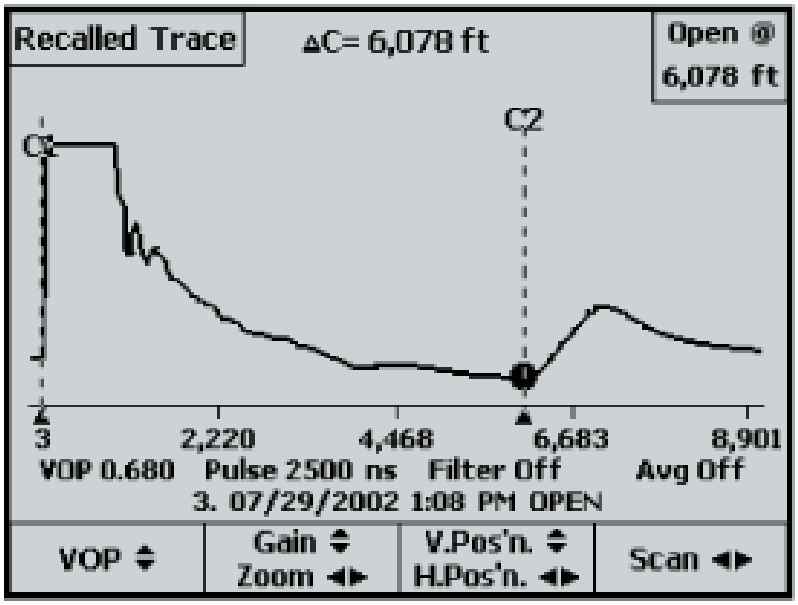

Fig. 2.4 990DSL Copperpro measurement from an open circuit (picture taken from Fluke web page [6])

In chapter 6 we show some measurements obtained with wideband frequency domain reflectometry, so we can compare the results of these TDR instruments with the ones obtained with W-FDR to see the improvement.

2.2 Chirp radar

Chirp radar, also known as frequency modulated continuous wave radar (FMCW radar), is a popular technique for distance measurements and it is used for sonar and radar. It is also possible to use it to test telephone lines to locate impairments.

When applied to transmission lines, the technique works as follows. A sinusoid signal is transmitted through the line, and its frequency is linearly increased to perform a linear frequency sweep to the line. The signal generated in the frequency sweep travels through the line and when it reaches an impairment, this signal is

reflected back. But the signal takes some time to do the round trip and by the time it arrives back to the transmitter, the transmitter will be already sending a signal with a higher frequency, since it is doing a linear swept frequency. So we can measure the difference in frequency between these two signals, which is called the beat frequency. This beat frequency is directly proportional to the delay of the reflected signal, and we can calculate this delay knowing 2 parameters, the time that takes the swept generator to do the whole sweep and the proportion of this that represents the beat frequency. Once we have calculated the delay of the signal in its round trip to the fault, we can estimate the distance, since we know already the propagation velocity of the line.

With this technique, it is also possible to locate several faults on the same line. When we have more than one fault on the line, we will receive a reflected signal of certain frequency from each discontinuity and all of them will be mixed in one signal. Therefore we can estimate the location of each discontinuity if we separate each reflected signal using a Fourier transform, since each one of them will have a different frequency. Then we just have to analyze separately each reflection in the same way we do when there is only one discontinuity. For example, Fig. 2.5 shows a measurement that contains 3 sinusoidal signals mixed together, that would correspond to the measurement of a line that has 3 discontinuities. Each beat frequency can be estimated using a Fourier transform. In this way, the location of each discontinuity can be estimated.

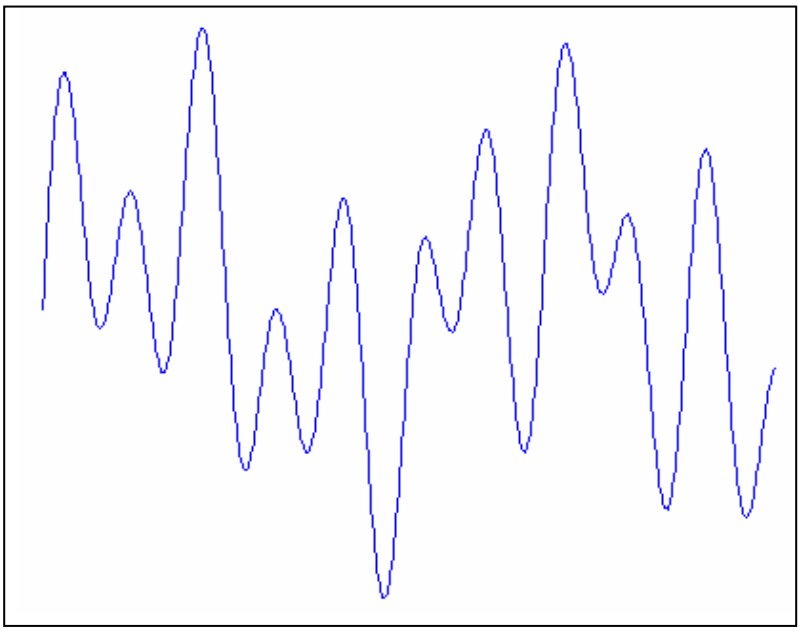

Fig. 2.5 Measurement of a line with 3 faults

A simple block diagram of a FMCW radar taken from [7] is illustrated in Fig. 2.6. The first block is the linear sweep waveform generator which performs a continuous linear frequency sweep to the line. Then the signal is separated in two ways, one goes to the line under test and the other to the mixer. The third block is the hybrid coupler, which separates the transmitted signal from the received signal, nevertheless, this separation is not essential. The fourth block is a band pass filter used to remove noise from the received signal, and also it can be used to compensate the received signal from the high frequency loss caused by the line. After the filter, the reflected signal goes to the mixer, where it is multiplied by the transmit signal to obtain the beat frequency. Then the signal passes through a filter to eliminate the double frequency component generated with the mixer and prevent aliasing at the ADC. Then the signal is digitized, and it goes to the DSP block. In this block a Fourier transform is applied to the received signal to obtain the beat frequency from each discontinuity and with these, estimate the location of each discontinuity on the line.

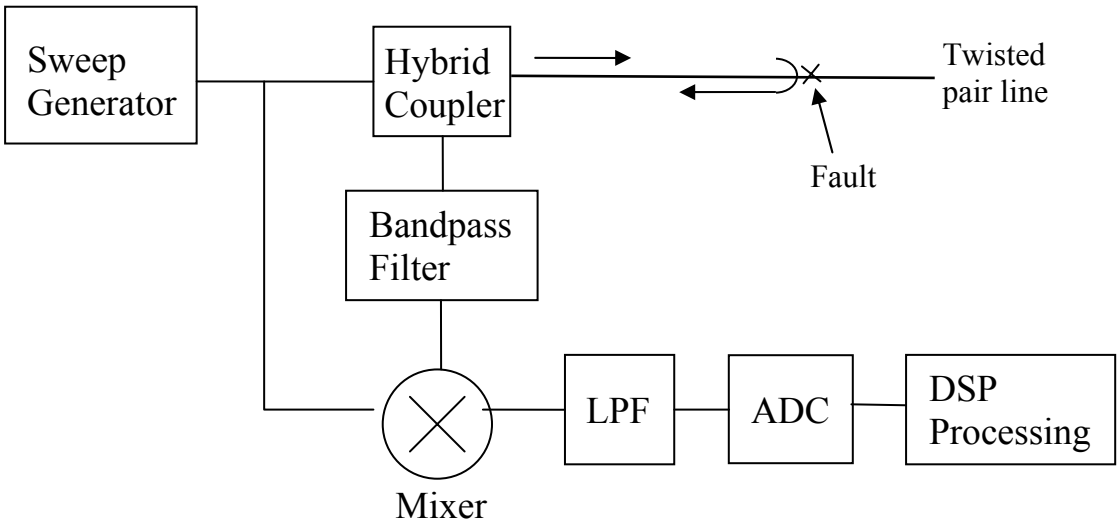

Fig. 2.6 FMCW radar Block Diagram

This technique to locate faults has some advantages. First, using this technique it is possible to use digital signal processing techniques to process the measurements. Another advantage of this technique is that it allows measuring several faults on the same telephone line using FFT to estimate each beat frequency in the received signal, and hence estimate the location of each fault. A disadvantage is that here there is no way to compensate for propagation velocity variation with transmitted frequency.

2.3 Spread spectrum radar

Spread spectrum radar is another technique that can be used to locate faults in telephone lines. This technique consists of sending a spread spectrum signal through the line that is reflected back at the discontinuity. This reflected signal is correlated with the transmitted signal as a function of delay. So, when the transmitted signal has completed its round trip to the discontinuity, the correlation between the reflected signal and the original transmitted signal will have its maximum value. In

this way, finding the maximum value of correlation we can estimate the delay of the round trip of the signal. Once this delay is known, it is easy to estimate the distance to the fault since the propagation velocity of the line is known. Fig. 2.7 shows a block diagram of spread spectrum correlation.

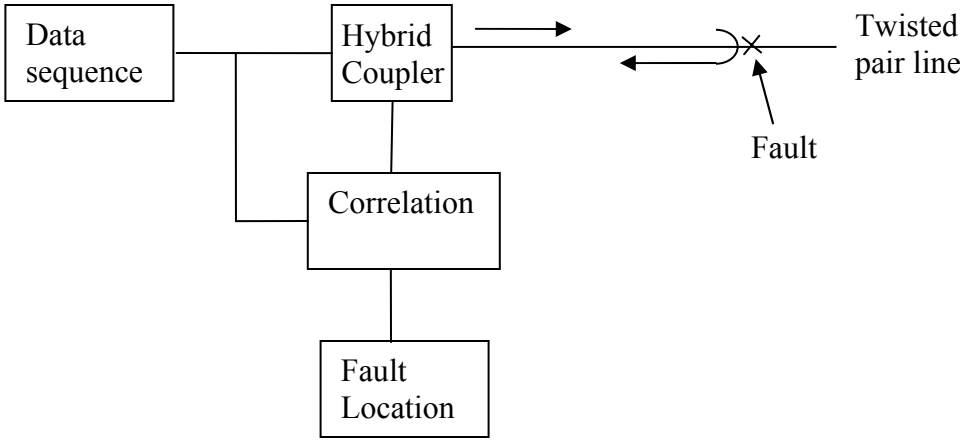

Fig. 2.7 Block diagram of spread spectrum radar

The correlation of the received signal with transmitted signal can be calculated using Equation 2.3, where x and y are the signals to be correlated and Tp is the period of the data sequence.

$$C(\tau) = \int_0^{Tp} x(t)y(t-\tau)dt \tag{2.3}$$

With this equation, the correlation C can be calculated as a function of the delay to locate the maximum value of the correlation and hence the delay to the fault.

If the line has more than one impairment, then the function of correlation vs. delay will have more than one peak, as shown in Fig. 2.8. Therefore, taking the delay of each correlation peak, we can estimate the location of multiple faults.

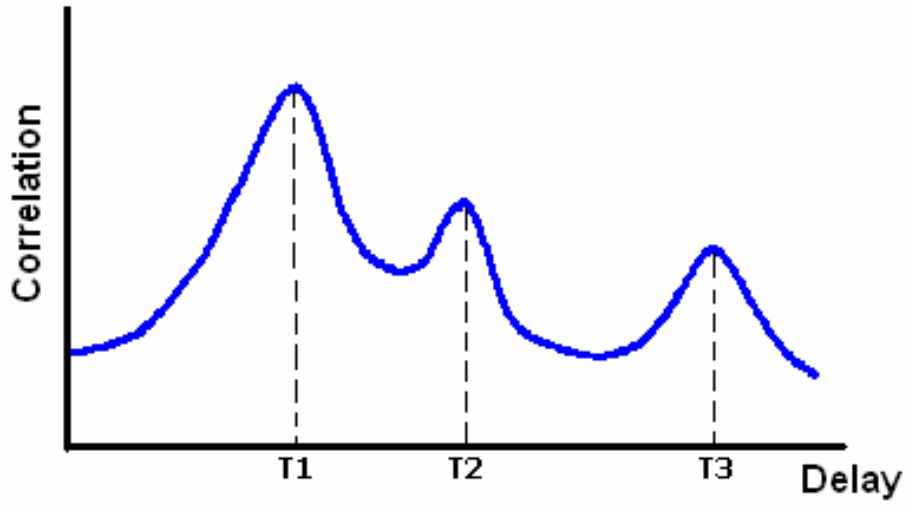

Fig. 2.8 Illustration of correlation vs. delay from line with 3 impairments

The disadvantage of using this technique is that it requires complex system since it needs to generate a spread spectrum signal and also requires hybrid coupler.

2.4 Wideband frequency domain reflectometry

Wideband frequency domain reflectometry is the technique proposed in this thesis for fault location. Next is a description of the advantages and disadvantages of this technique, and further chapters will explain the way this technique works.

This technique has several advantages that make this technique very attractive. Using this technique, one can compensate for the line characteristics like variable propagation velocity and variable attenuation with frequency. This allows measurements with much more resolution and accuracy than other techniques (such as the popular TDR). 2) This technique has the advantage that it has a measurement range over 5 km, which is better than other techniques. 3) It can calculate the reflection coefficient angle, to determine the kind of fault that it is measuring (open

circuit, loading coils, water, etc). 4) It can locate multiple faults on the same line, and it can tell the nature of each fault. 5) This technique could test a line while operating with voice telephony due to the high frequencies that it uses to test the line.

The disadvantage of W-FDR are that this technique requires some hardware for its implementation like a swept frequency generator and a hybrid coupler that is not needed in other techniques like TDR. This could increase the price of the portable instrument and perhaps make it a little bigger in size.

2.5 Summary of TDR, FMCWR, SSR and W-FDR

These four techniques for fault location in telephone lines present different advantages and disadvantages. From a study of each technique, we conclude that TDR is the simplest of the four techniques and therefore it has a low cost of implementation. This is the reason why this technique is the one currently used in the equipments of the market. Nevertheless, W-FDR and FMCW have the advantage over TDR that with these techniques it is easier to apply different DSP techniques to improve the quality and resolution of the measurements. Another good point for these techniques is that their cost of implementation has been going down since the price of the DSP chips also has been going down. This makes now these techniques much more attractive to be commercially implemented. And W-FDR has also the advantage over FMCW radar that now it can also detect the kind of discontinuity on the line, which FMCW radar can not do.

3. Transmission line theory

A transmission line is defined as a medium used to transmit energy between two distant points; consequently the twisted pair cable used in telephony is

considered a transmission line. When the length of a transmission line is longer than 1/10 of the wavelength, the transmission of the signal should be analyzed using transmission line theory [8]. Telephone lines have a length shorter than 5 km from the central office to the home. Therefore; for frequencies about 1 kHz, where the propagation velocity is 100000 km/s and the wavelength is 30 km, it is required to apply transmission line theory in the analysis of these lines.

3.1 Primary Constants

Like all transmission lines, a twisted pair wire can be described by its fundamental electrical characteristics, or primary constants. The primary constants are inductance l, shunt capacitance c, shunt conductance g, and resistance r. These are described in customary electric units per unit length. Fig. 3.1 shows a T-equivalent circuit commonly used to represent telecommunication transmission lines.

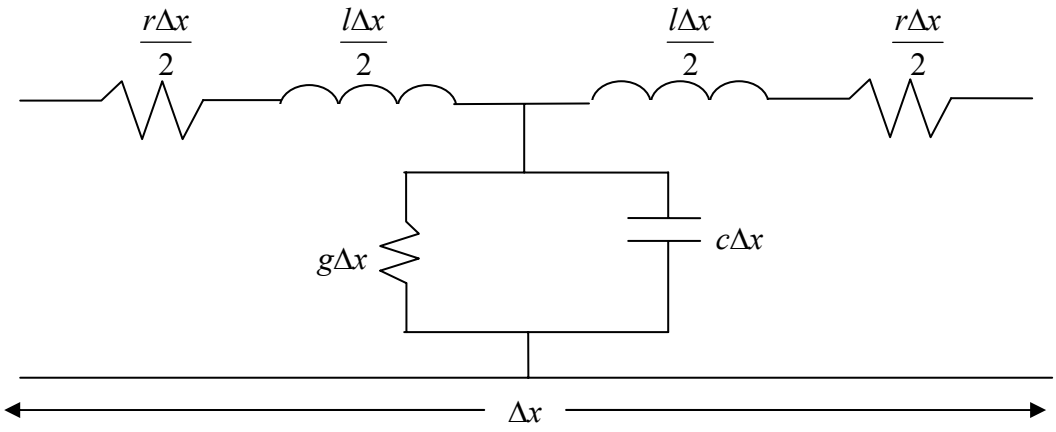

Fig. 3.1 Transmission line T-equivalent circuit in terms of primary constants

The inductance per unit length, l, of a typical cable depends on the geometry of the conductors and it is affected by the magnetic flux distribution within and around the conductors. Due to skin effect, inductance starts to decrease at about 20 kHz and continues to decrease to at least 5 MHz. Inductance has a small variation with

temperature. It can change 1.8% from -18° to +49°C. Fig. 3.2, shows the variation of the inductance with frequency.

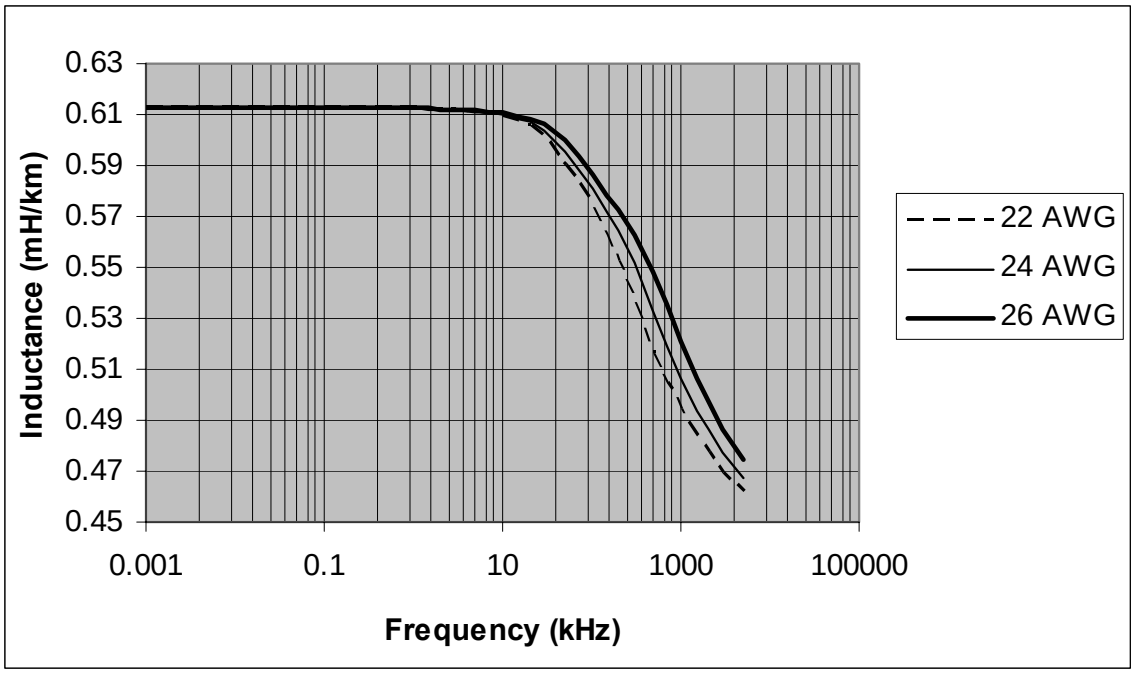

Fig. 3.2 Twisted pair inductance vs. frequency for PIC at 20° C

The capacitance per unit length, *c*, depends of the geometry of the twisted pair and its dielectric. Typically the capacitance of a twisted pair cable is 52 nF/km. The capacitance of the conductor can change with temperature due to a decrease in the insulation density, cable expansion, and a decrease in the dielectric constant with temperature increase. In filled cables, it can decrease linearly at a rate of 0.016% per °C over the frequency range of 1 kHz to 3 MHz.

The resistance per unit length *r* depends on the resistivity of the conductor and the current distribution within itself. It is constant at lower frequencies but is approximately proportional to the square root of frequency at higher frequencies. Fig. 3.3 shows the variation of the resistance with frequency. Also the resistance is

highly dependant on the temperature. It increases about 4% for each 10 °C at voice frequencies and 2 to 3% at frequencies higher than 10 kHz.

The conductance per unit length *g* depends on the dielectric medium between the conductors. It increases by a factor of 10 for each decade in frequency. Its value can vary considerably with different insulations and core filling compound, however it varies negligibly with temperature. Fig. 3.4 shows the variation of the conductance with frequency.

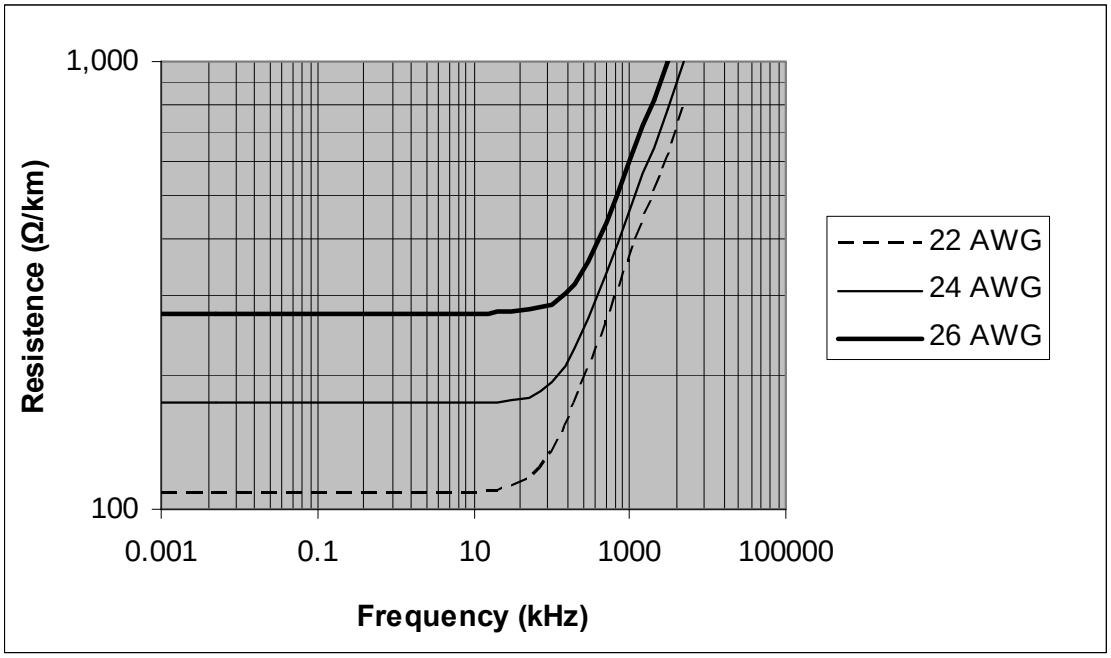

Fig. 3.3 Twisted pair resistance vs. frequency for PIC at 20° C

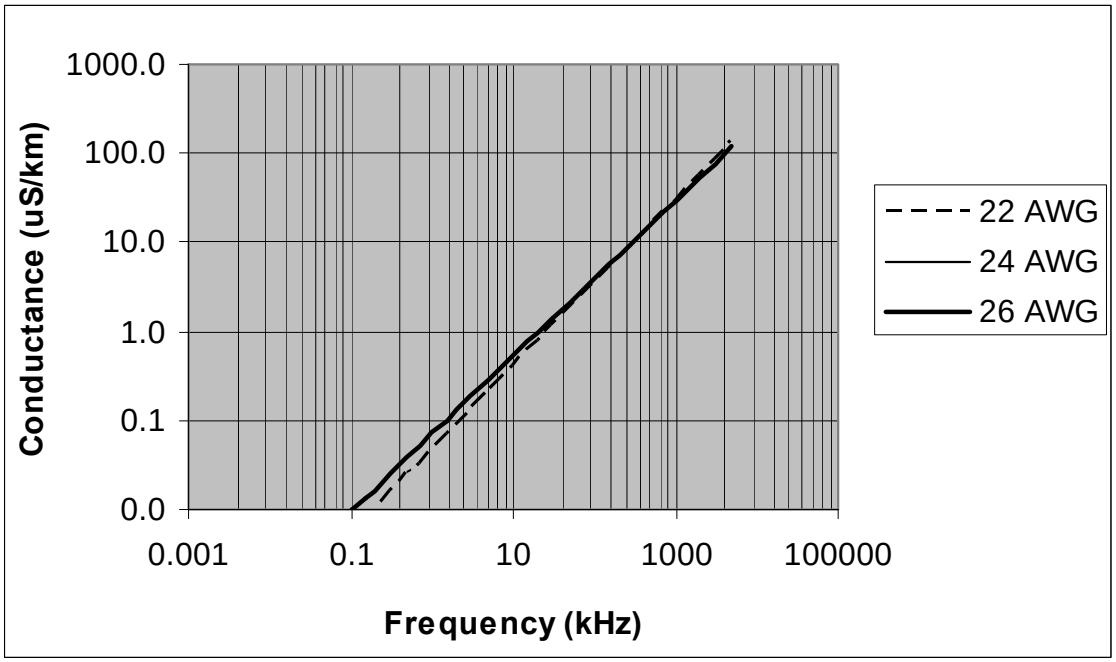

Fig. 3.4 Twisted pair conductance vs. frequency for PIC at 20° C

Table 3.1 shows sample values of the primary constants for different gauges of cable at different frequencies. In Appendix A, more complete tables with these values are given, and some polynomial functions that describe the behavior of the primary constants with frequency.

FREQ (kHz)	*r* (Ω/km)	*l* (mH/km)	*c* (nF/km)	*g* (us/km)
19 AWG				
1	52.82	0.60	51.51	0.13
40	61.35	0.57	51.51	5.18
192	115.82	0.51	51.51	24.87
772	230.33	0.47	51.51	99.74
1,576	324.49	0.46	51.51	203.42
22 AWG				
1	106.30	0.60	51.51	0.13
40	112.21	0.58	51.51	5.18
192	165.36	0.55	51.51	24.87
772	330.72	0.50	51.51	100.07
1,576	463.28	0.48	51.18	203.42
24AWG				
1	168.32	0.59	51.51	0.13
40	173.89	0.57	51.51	5.18
192	219.83	0.55	51.51	24.87
772	418.98	0.50	51.51	100.07
1,576	597.47	0.48	51.18	203.42
26 AWG				
1	269.04	0.60	51.51	0.13
40	274.29	0.58	51.51	5.18
192	309.73	0.56	51.51	24.90
772	524.30	0.52	51.51	100.07
1,576	755.61	0.50	51.51	203.42

Table 3.1 Air core PIC, cable pair primary constants, 20 °C, taken from [9]

3.2 Secondary Parameters

The propagation constant and the characteristic impedance are known as the secondary parameters and are described in equations 3.1 and 3.2. These secondary parameters are used to describe the characteristics of a transmission line, and can be found from primary constants, where *r* is the resistance, *l* the inductance, *g* the conductance and *c* the capacitance.

$$\rho = \alpha + j\beta = \sqrt{(r + j\omega l)(g + j\omega c)} \tag{3.1}$$

$$Zo = \sqrt{\frac{r + j\omega l}{g + j\omega c}} \tag{3.2}$$

The characteristic impedance is independent of the length of the transmission line and it is measured in ohms per unit length. The propagation constant is a complex number that describes the attenuation and phase shift per unit length of the line. The real portion of this constant is called the attenuation constant α and it can be obtained from the primary constants as is shown on equation 3.3 [10]. This equation gives the attenuation in Nepers per unit length but can be converted to dB per unit length by multiplying the result by 8.686. The imaginary portion of the propagation constant is called the phase constant β and it can be also obtained from the primary constants as is shown on equation 3.4. This equation provides the phase shift of the signal on the line and it is measured in radians per unit length. The delay of the signal at any certain frequency can be calculated by dividing the phase shift, which is in radians per unit length by the frequency ω, which is in radians; and the result is given in seconds.

$$\alpha = \sqrt{\frac{1}{2}(\sqrt{(r^2 + \omega^2 l^2)(g^2 + \omega^2 c^2)} + rg - \omega^2 l c)} \tag{3.3}$$

$$\beta = \sqrt{\frac{1}{2}(\sqrt{(r^2 + \omega^2 l^2)(g^2 + \omega^2 c^2)} - rg + \omega^2 l c)} \tag{3.4}$$

3.3 Reflection Coefficient

Next is showing the process to obtain the equation to calculate the reflection coefficient. First, let us consider that the voltage at any point of a line with a discontinuity is the sum of the incident voltage V_1 and reflected voltage V_2:

$$V_r = V_1 + V_2 \tag{3.5}$$

In the same way, the current at any point of a line with a discontinuity will be the sum of the incident current I_1 and the reflected current I_2:

$$I_r = I_1 + I_2 \tag{3.6}$$

Where I_1 and I_2 (which goes in opposite direction than I_1) can be found dividing the incident voltage V_1 and reflected voltage V_2 by the line impedance Z_0:

$$I_1 = \frac{V_1}{Z_0} \tag{3.7}$$

$$I_2 = -\frac{V_2}{Z_0} \tag{3.8}$$

The impedance of the discontinuity can be calculated as:

$$Z_r = \frac{V_r}{I_r} \tag{3.9}$$

Combining equation 3.5 and 3.6 it results:

$$Z_r = \frac{V_1 + V_2}{I_1 + I_2} \tag{3.10}$$

Substituting 3.7 and 3.8 in 3.10 and reworking the equation, results:

$$Z_r = Z_0 \frac{V_1 + V_2}{V_1 - V_2} \tag{3.11}$$

Solving this for V_2 gives:

$$V_2 = V_1 \frac{Z_r - Z_0}{Z_r + Z_0} \tag{3.12}$$

The last step to obtain the reflection coefficient is to take the ratio of reflected voltage to incident voltages, and this result as follows:

$$\rho = \frac{V_2}{V_1} = \frac{Z_r - Z_0}{Z_r + Z_0} \tag{3.13}$$

3.4 Twisted paired wire properties

Twisted pair cables are used to connect telephone subscriber sets to the central office (CO). These connections are done using several cables in series. Feeder cables connect the central office to main junction points. Then, distribution cables are used from these main junction points to distribution terminals such as pedestals. Finally, service wires connect the distribution terminal and the customer device, which can be at an office or a residential establishment.

The size of the conductor in a paired cable is standardized for Canada and USA as American Wire Gauge (AWG). The most common sizes are 22, 24 and 26 AWG. In the telephone network, AWG 26 PIC (polyethylene insulated cable) is the most common for voice transmission. AWG 24 and AWG 22 cables are used in 1.544 Mbits/s T1 trunks or other types of toll trunks [8]. Next is an analysis of the behavior of the propagation constants for the most common AWG gauges of cable.

The twisting of the wire pair is to provide equal interface exposure to each wire in the pair. When the wire pair is operated in differential mode, this minimizes the

electromagnetic interference from neighbor pairs, power lines, etc. One common way to drive the line in differential mode is using a transformer called balun (balanced-to-unbalanced), to transform the signal from single-end mode to differential mode. See Fig. 3.5

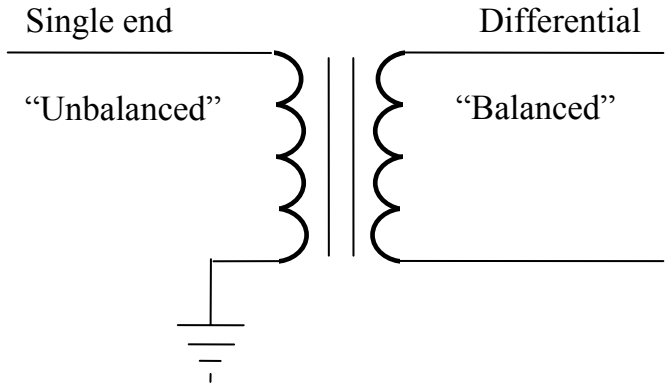

Fig. 3.5 Conversion from single-end mode to differential

Twisted pair lines have a propagation delay (inverse of propagation velocity) that decreases at higher frequencies. The delay parameter doesn't change much with the different gauges of cable. This can be seen in Fig. 3.6**,** where the delay curves of the most common AWG sizes show to have almost the same behavior**.** Nevertheless, larger sizes of cables have a smaller delay at lower frequencies and at higher frequencies the delays are almost the same for all cables. It mainly depends on the dielectric constant of the plastic insulation. The variable delay at different frequencies (especially at low frequencies) is called delay distortion. In this project a compensation for the delay distortion is applied. The delay can be calculated from the primary constants dividing the phase constant β/ω, where β is determined from equation 3.4.

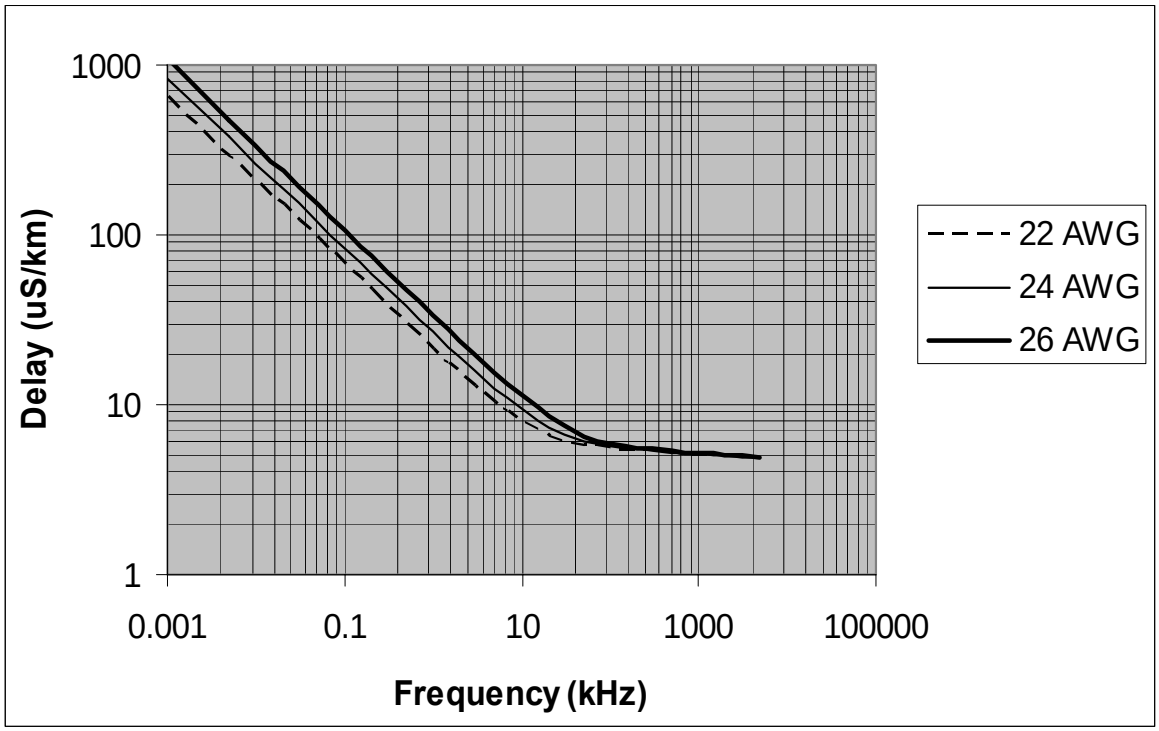

Fig. 3.6 Twisted pair delay vs. frequency

The attenuation constant, at certain frequencies, can have a wide variation among the different gauges of cable. In Fig. 3.7 we can see the attenuation behavior for the different gauges of cable. The attenuation for these cables is similar at low frequencies, but at high frequencies there are significant differences. The attenuation of large wire cables grows more slowly at high frequencies than in cables of smaller wire sizes. Therefore, larger sizes of cable have a wider bandwidth and are better for high speed data transmissions. This variable attenuation at different frequencies is called attenuation distortion. In this project a compensation for the attenuation distortion is applied.

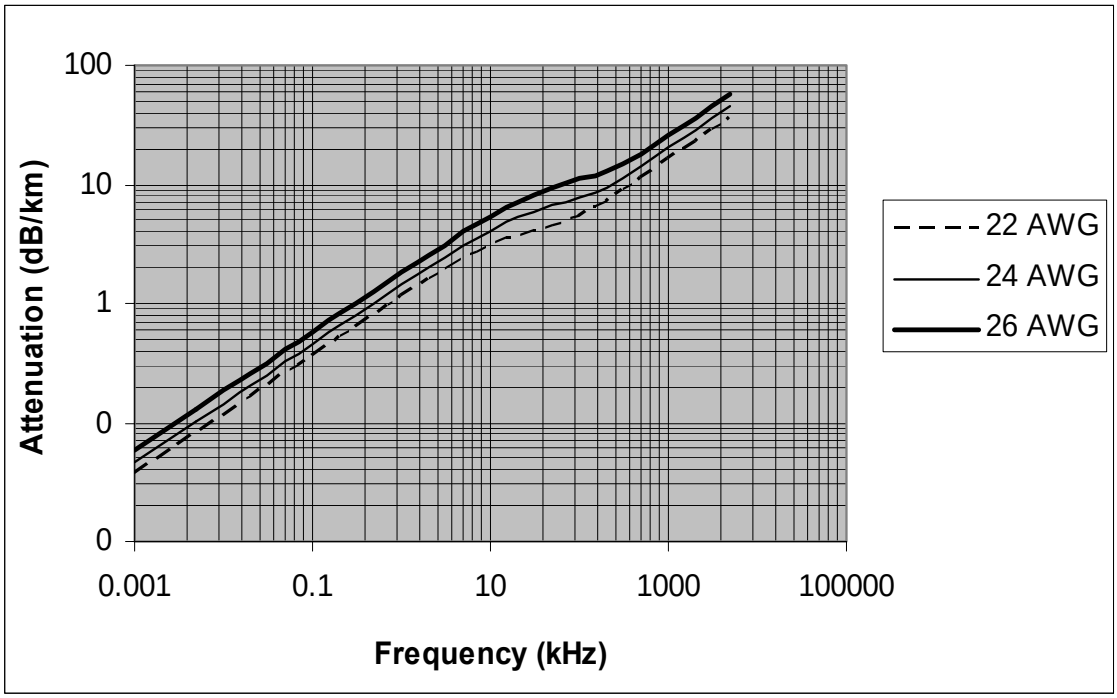

Fig. 3.7 Twisted pair Attenuation vs. frequency

The characteristic impedance is another secondary parameter that has a wide change with frequency. Fig. 3.8 and Fig. 3.9 show the curves of magnitude and angle for the characteristic impedance in different gauge cables. As we can see in these figures, the impedance of the line is high at lower frequencies, but as the frequency increases the impedance of the line decreases to about 100 Ω. Also, the angle of the impedance has a drastic change as the frequency increases from 10 kHz to 1 MHz. Therefore, when a hybrid coupler is used on the line, it is very complicated to find a balance impedance to match the line impedance over a wide frequency range. Hence the hybrid couplers always have some leakage signal caused by the impedance difference between the line and the balance impedance.

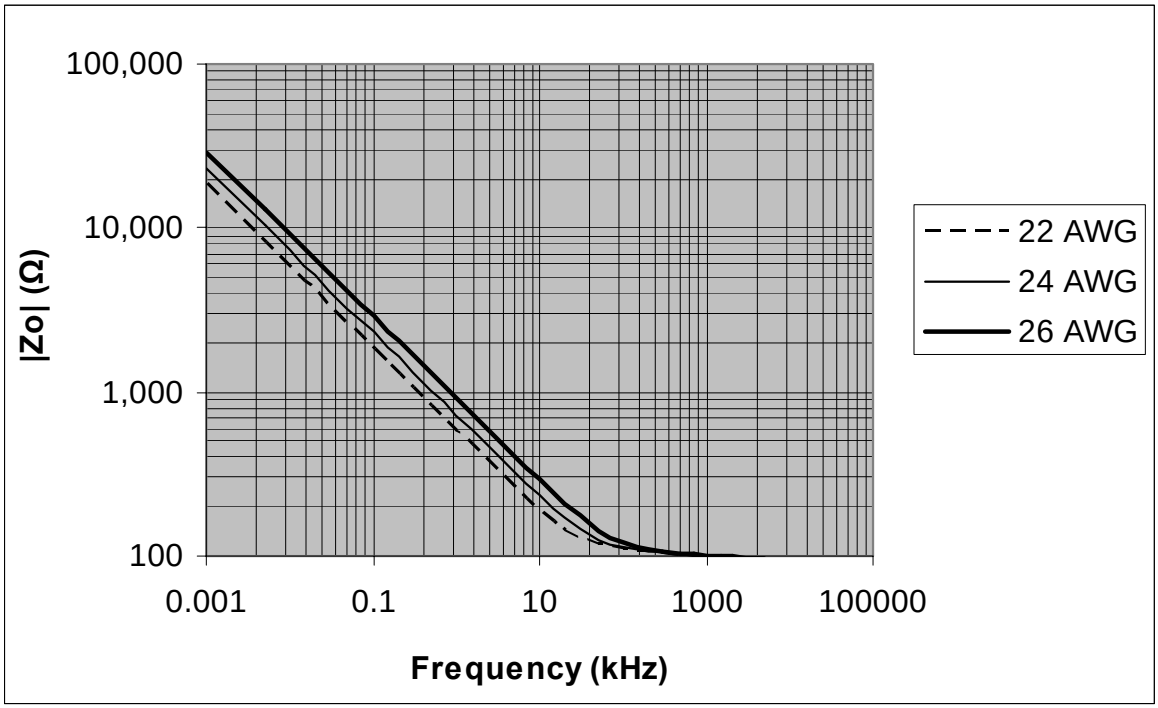

Fig. 3.8 Twisted pair Characteristic impedance vs. frequency

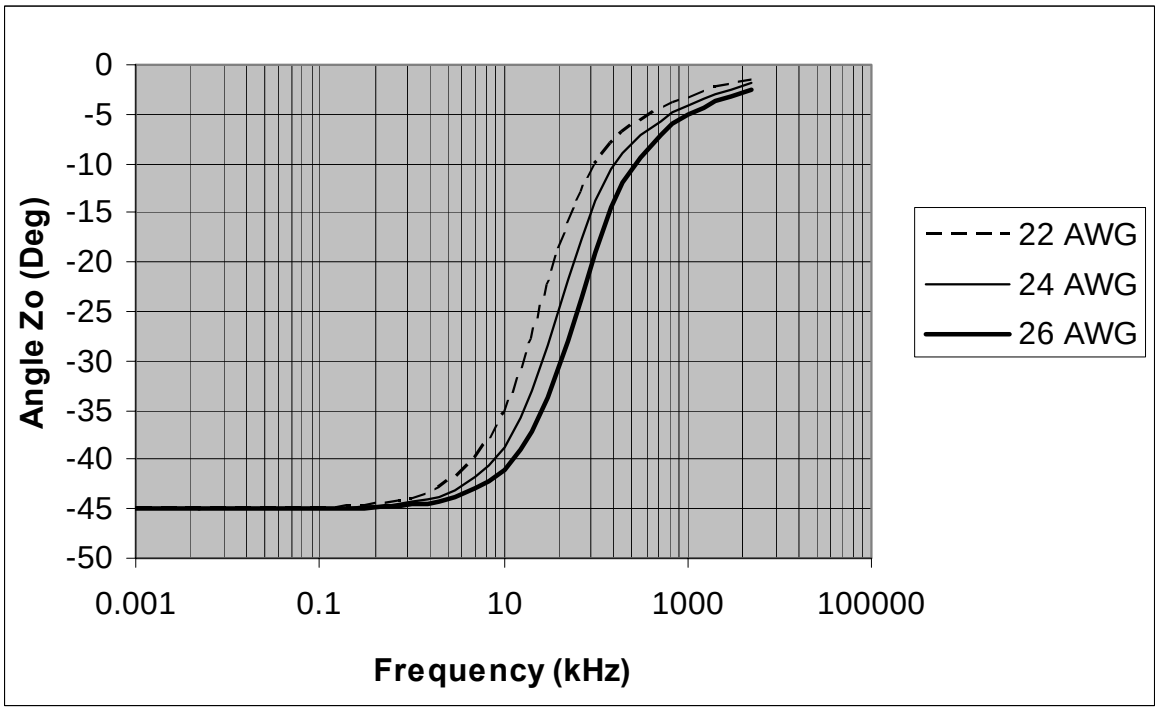

Fig. 3.9 Characteristic impedance angle vs. frequency

3.5 Transmission line impairments

There are several kinds of impairments on twisted pair lines. The most common impairments are open circuits, and bridge taps.

A *bridge tap* is a piece of open circuit transmission line connected in parallel somewhere between the ends of an operating telephone pair. These bridge taps are used by telephone companies to have more flexibility to meet the variable demand of service. A bridge tap is formed when a new service is connected part away along an existing wire pair. Fig. 3.10 illustrates a bridge tap.

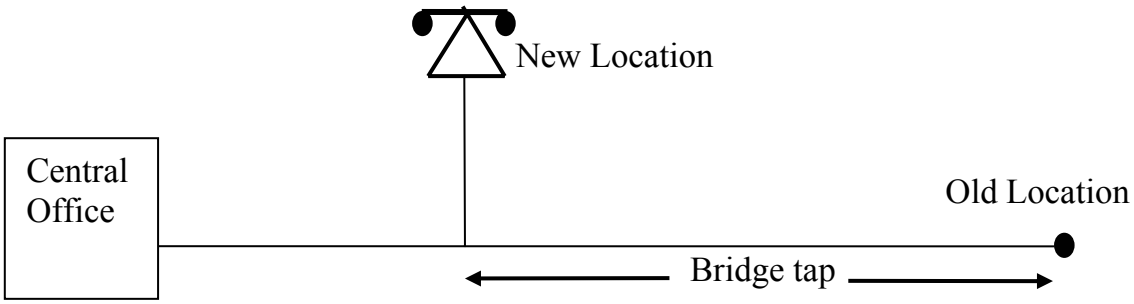

Fig. 3.10 Bridge tap illustration

A bridge tap reflects a portion of the signals back towards the service. A bridge tap has a reflection coefficient of -1/3 or $1/3 \angle 180°$. This reflection coefficient can be calculated using equation 3.13**,** where Z_r is obtained as the parallel of the line impedance (Z_o) with the impedance of the cable branch, which is also Z_o . Therefore Z_r is equal to $\frac{Z_o}{2}$.

Bridge taps don't have much effect on transmitted voice signals; nevertheless bridge taps constitute a big problem for high frequency signals that are required for high-speed Internet service. This is because the signal travels down the line and, at the bridge tap, a portion travels down the lateral branch and is reflected back. If the length of the tap is small compared to the signal wavelength, (like is the case in voice band due that it uses relatively low frequencies) the reflected signal rejoins the original signal after a minimal phase shift and there is a little attenuation of the original signal. However, when the bridge tap length approaches one forth of the signal wavelength, the reflected signal rejoins with a phase difference nearing 180 degrees and causes significant attenuation.

To understand this better, let's select a frequency signal that has a wavelength of 800 m. If the line has a 200 m bridge tap (1/4 of the wavelength) means that the portion of the signal that goes through the bridge tap and is reflected back to the line at the end of the bridge tap, will have travel 400 m in the bridge tap before rejoining the line. Therefore, once this signal rejoins the line, it would have already traveled 400 m (half wavelength) more than the signal that is arriving at the same junction point directly from the transmitter. So, considering that the wavelength of the signal is 800 m, then, these two signals will have a phase difference of half wavelength or 180 degrees at the junction point, which will cause the attenuation of the transmitted signal. For this reason, bridge taps must be removed in order to have a high speed transmission.

An *open circuit* consists of a broken wire (either one wire or both) that causes that the signals traveling down the line be reflected back, without any change in its phase. This is caused because the reflection coefficient for an open circuit is equal to 1 or $1\angle 0°$. This can be obtained using the reflection coefficient equation and considering the impedance of the discontinuity (Zr) equal to infinite.

A *short circuit* also causes the reflection of the signals like an open circuit, but this one also introduces a phase shift of 180° to the reflected signal. This is caused because its reflection coefficient is equal to -1 or $1\angle 180°$. This can be obtained

considering in the reflection coefficient equation, the impedance of the discontinuity (Zr) equal to 0.

From the analysis of these discontinuities, it is clear that the phase shift of the reflected signal is caused by the reflection coefficient angle, and this angle has a specific value for each kind of discontinuity. Therefore, measuring the phase of the reflected signal coming from a discontinuity, it is possible to estimate the kind of discontinuity that caused the reflection (open circuits, bridge taps, loading coils, water, etc).

4. W-FDR Test System

This chapter describes the implementation of a frequency domain reflectometer to test telephone lines. The system performs a stepped frequency sweep on the line, to measure return signal vs. frequency. A plot of this measurement will be called a "trace". This trace contains the information required to estimate the location and nature of the fault. The processing of this trace to locate the fault and the reflection coefficient angle will be described in the next chapter.

To have an overview of the system, Fig. 4.1 shows a block diagram of the W-FDR system. As we can see in this diagram, the blocks that constitute the system are the waveform generator, the amplifier, hybrid coupler, high pass filter for the high frequency loss compensation, coherent detector and the signal processor. In Appendix D, we show the schematic diagrams of the circuits used to implement this system.

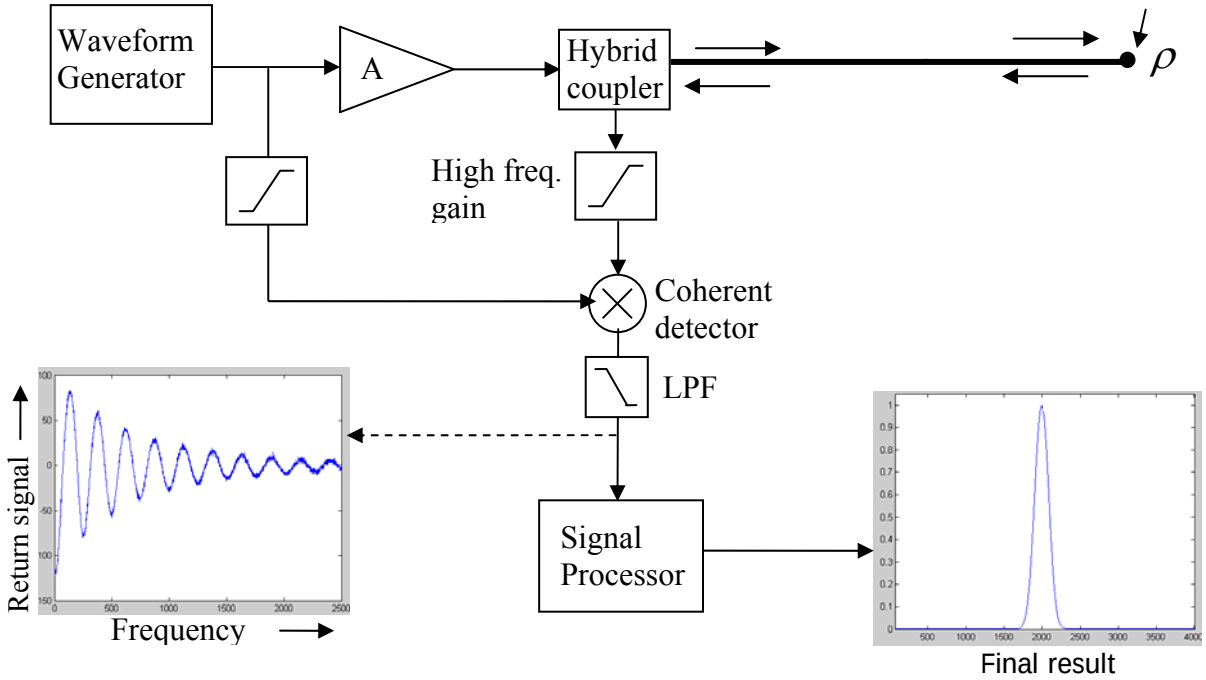

Fig. 4.1 Hardware block diagram of W-FDR system

4.1 Principle of operation

In order to understand the effect of the stepped frequency sweep, first let's consider a line that has just one fault. If this line is energized with a single sinusoid, this will travel through the line until it reaches the fault. Equation 4.1 describes the sinusoid voltage at any point *x* along the transmission line.

$$V(t,x) = A\sin(\omega t - \beta x) \tag{4.1}$$

Once the sinusoid signal reaches the fault, a portion of the energy is reflected back to the transmitter. This portion that is reflected back (the reflected signal), will have a phase difference with respect to the transmitted signal. This is caused by the delay of the round trip and also by the angle of the reflection coefficient. This phenomenon is illustrated in Fig. 4.2, where the transmitted signal travels through the line and when it reaches the open circuit, it is reflected back and

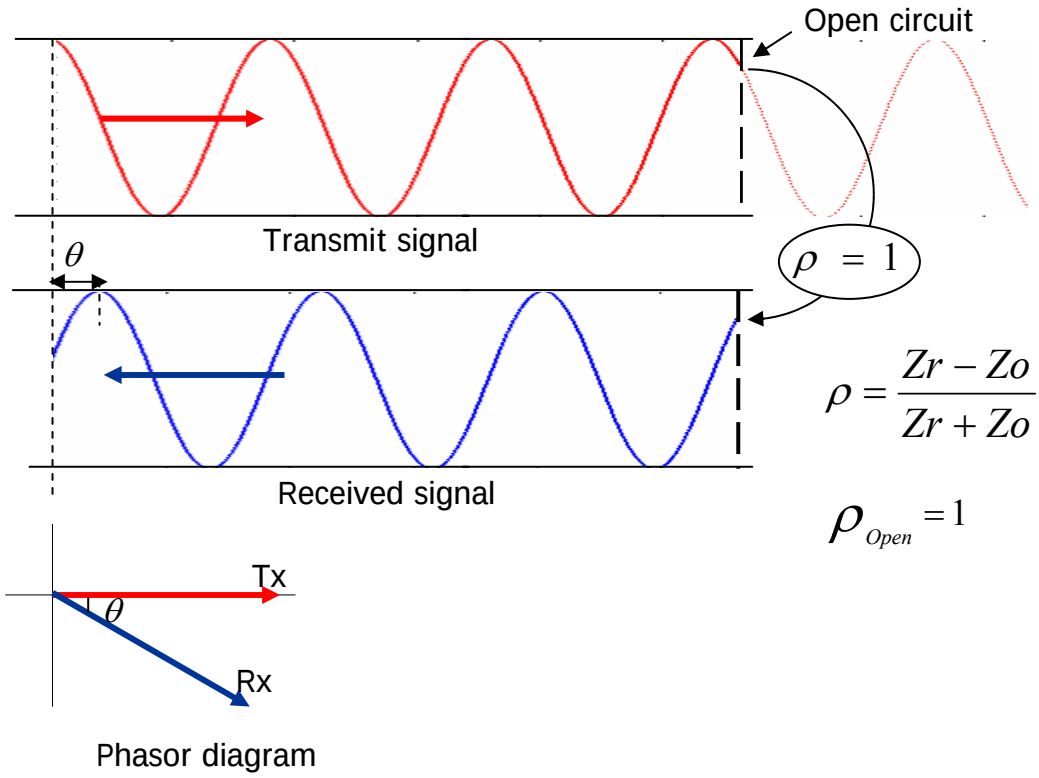

Fig. 4.2 Signal reflection

multiplied by the reflection coefficient. In this case the reflection coefficient is equal to +1, therefore it doesn't change the phase or magnitude of the signal when it is reflected. When the reflected signal arrives back to the transmitter, it has a phase difference with respect to the transmitted signal due to the propagation time of the round trip. This phase difference between the two signals can be represented by a phasor diagram as it is shown in Fig. 4.2.

So, the delay of the reflected signal during the round trip causes a phase difference between the transmitted and received signals at the receiver point. With fixed delay, this difference of phase between these two signals will increase as the frequency of the sinusoid increases. This is illustrated in Fig. 4.3. In this figure we show two cases where the transmitted and received signals have the same time delay between each other at the receiver. The phase difference in degrees between these

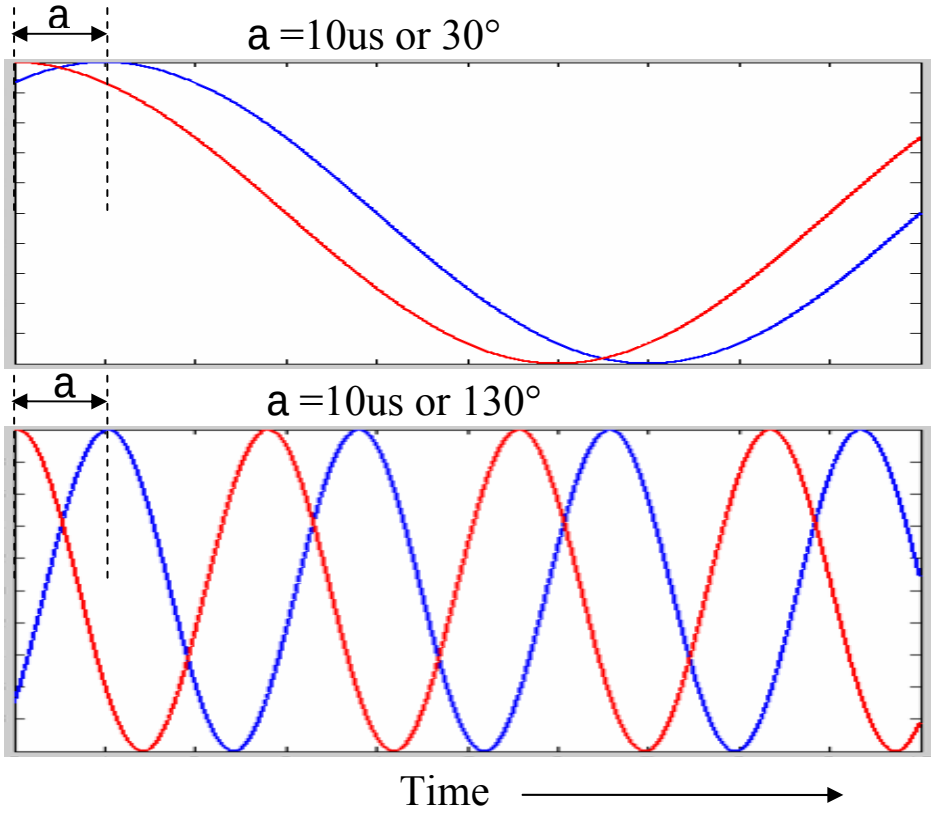

Fig. 4.3 Change of phase with frequency

two signals is different for each case, because the frequency of the signals is also different for each case. In the first case, where the frequency is low, the delay between the two signals represents a phase difference of 30°, while in the second case where the frequency is much higher, the same delay represents 130°.

Therefore, as the frequency of the sweep increases, the phase between the transmitted and received signal increases too. So, if we represent the transmitted signal (Tx) and received signal (Rx) with a phasor diagram, we would see that the phasor representing the received signal will rotate with respect to the phasor of the transmitted signal as the frequency increases during the sweep. Also, as the phasor representing the received signal rotates, it would also become smaller because the attenuation of the wire increases at higher frequencies. Fig. 4.4 illustrates the rotation of the received signal phasor with respect to the transmitted signal phasor during the frequency sweep.

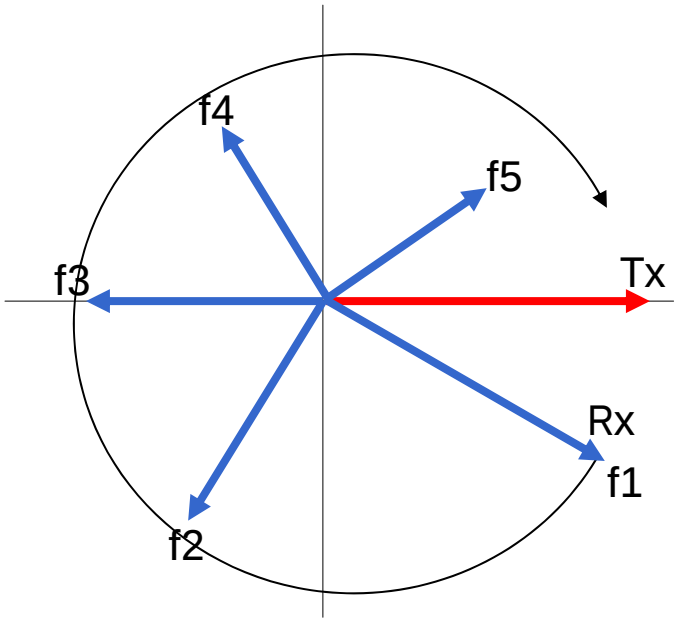

Fig. 4.4 Effect of frequency sweep

4.1.1 Coherent detector

Coherent detection is used in this project to obtain the component of the reflected signal that is in phase with the transmitted signal. In this way, after the frequency sweep (over the range 50 kHz – 1.3 MHz) we can obtain a trace of reflected signal vs. frequency, and this trace is used to estimate the location and nature of the fault. Fig. 4.5 show examples of the trace obtained after the coherent detection.

To have a better understanding of the output of the coherent detector, in the phasor diagrams of Fig. 4.5, we show some phasors representing the transmitted signal Tx, the received signal Rx and the portion of the received signal that is in phase with the transmitted signal. This in-phase phasor is the result of passing the received signal through a coherent detector. If we plot the magnitude of this phasor

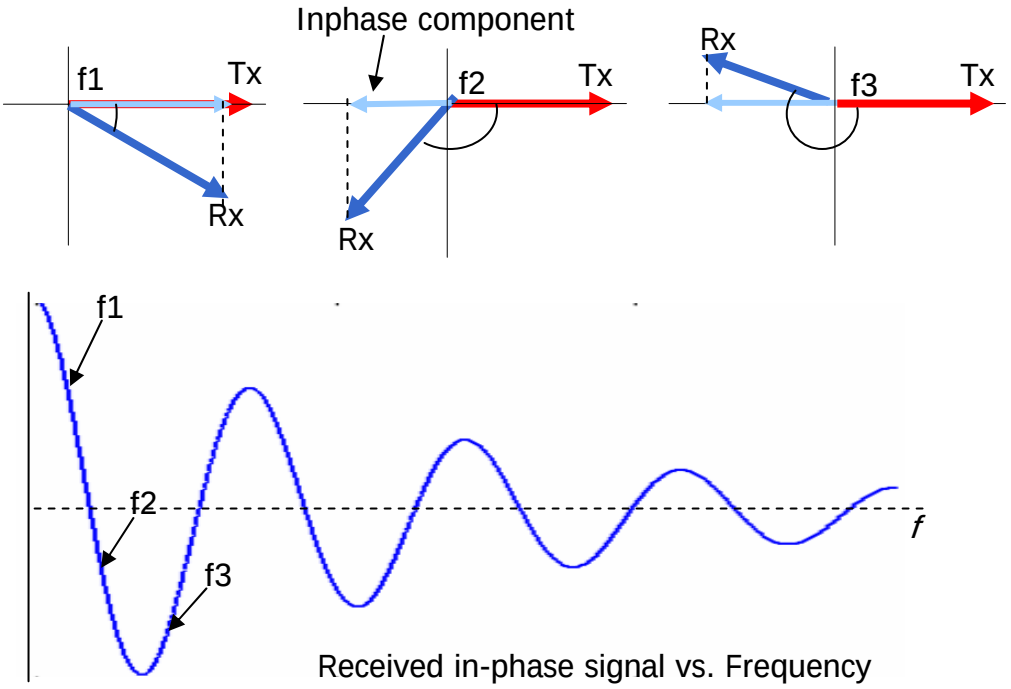

Fig. 4.5 Coherent detection of reflected signal

along the frequency axis, we obtain a decaying sinusoidal trace. As we saw in Fig. 4.4, as the frequency increases the phasor representing the received signal rotates with respect to the transmitted signal phasor. Therefore, as this phasor rotates, the magnitude of this phasor that is in phase with the transmit signal (which is the output of the coherent detector) will describe a sinusoid trace. The decaying of the trace is because, as the frequency increases, the magnitude of the received signal becomes smaller due to the attenuation properties of the line.

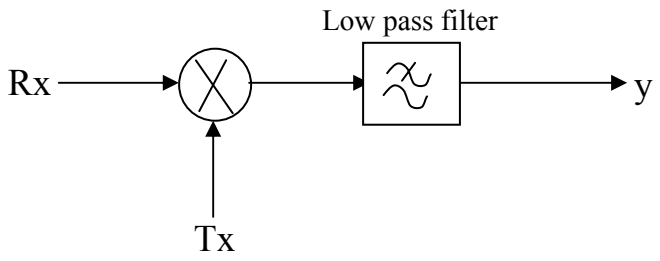

Fig. 4.6 Coherent demodulation process

The coherent demodulation is composed mixing and low pass filtering as is illustrated in Fig. 4.6. To understand the principle by which this works, let us assume that the transmitted signal has unity magnitude and zero phase.

$$V_t = \cos(\omega t) \tag{4.2}$$

Once the transmitted signal travels down the line and is reflected back, the signal will be received with a different amplitude and phase which are represented by A and Θ, but the frequency will remain the same. So, the received signal is represented by

$$V_r = \mathrm{A}\cos(\omega t + \Theta) \tag{4.3}$$

The first step for the coherent detection is to multiply the transmitted signal by the received signal. Using the trigonometric identity

$$\cos(\alpha)\cos(\beta) = \frac{\cos(\alpha+\beta)+\cos(\alpha-\beta)}{2} \tag{4.4}$$

the mixing of the two signals results in,

$$V_t \cdot V_r = \cos(\omega t)\, A\, \cos(\omega t + \Theta) = \frac{A[\cos(\omega t - \omega t + \theta) + \cos(\omega t + \omega t + \theta)]}{2}$$

$$= \frac{A}{2}\cos(\theta) + \frac{A}{2}\cos(2\omega t + \theta) \tag{4.5}$$

However, after the mixing of the signals comes the low pass filter that eliminate the upper frequency, and this just leaves

$$I_r = \frac{A}{2}\cos(\theta) \tag{4.6}$$

where I_r represents the component of the received signal that is in phase with the transmitted signal.

As it was shown in Fig. 4.4, the received signal rotates with respect to the transmitted signal during the frequency sweep. As a result, the phase angle Θ between the two signals will increase during this sweep. Therefore, if Θ is increasing, equation 4.6 would describe a sinusoidal trace.

The effect of the increasing attenuation of the line at higher frequencies can be represented multiplying equation 4.6 by an exponential that decays as a function of frequency, which leaves equation 4.6 as follows

$$I_r = \frac{A}{2}\cos(\theta)\cdot e^{-k(\omega)} \tag{4.7}$$

Therefore, as the frequency increases, equation 4.6 would describe the decaying sinusoidal trace that we see.

4.2 Waveform Generator and amplifier

We used the HP 33120A waveform generator to perform the stepped frequency sweep. This device was chosen because it can be controlled using a computer program like Labview. This allows sweeping the line using 2500 points or frequencies, to give a smooth shape to the trace.

The signal from the waveform generator doesn't have the power to test the line. Therefore, this signal has to pass through an amplifier to get enough power before it is sent to test the line.

The signal amplifier is an important part of the system because it increases the power of the signal from the waveform generator. In this way, the signal can have sufficient amplitude to be measured after the round trip despite of the attenuation caused by the line. Therefore, giving a good amplification to the transmitted signal helps to obtain long distance measurements.

To implement the signal amplifier in the W-FDR system we used a differential amplifier. This amplifier is connected to the hybrid coupler shown in Fig. 4.11, to drive the line in a differential mode. For this reason, the amplifier has a positive and a negative output as shown in Fig. 4.7. The schematic diagram of the circuit for this amplifier is shown in Appendix D.

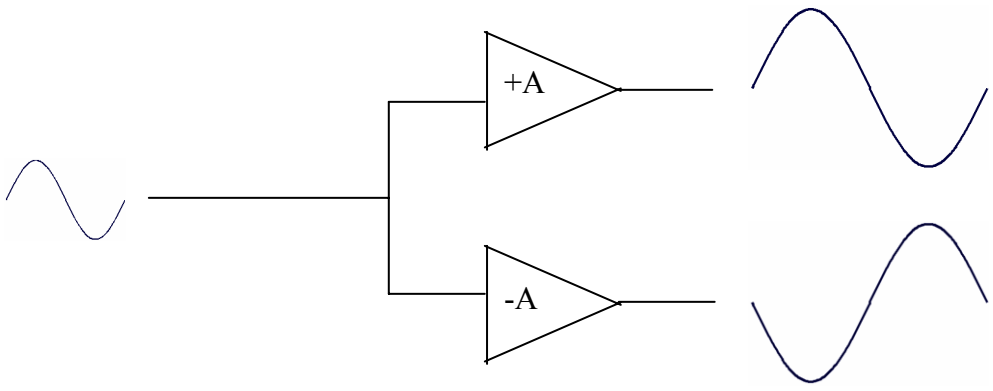

Fig. 4.7 Differential amplifier

4.3 Hybrid Coupler

The hybrid coupler is used to separate the received signal coming from the fault from the transmitted signal. In this way it is possible to compensate the received signal for the high frequency loss suffered during the round trip to the fault. Another advantage of separating these signals is that it makes easier to process the received signal once it has been separated from the transmitted signal.

The hybrid coupler is a circuit that has been in used for many years in telephone lines to separate two voice signals. Fig. 4.8 shows a diagram of a general hybrid coupler. Next is explained each part of the hybrid coupler and the way it functions.

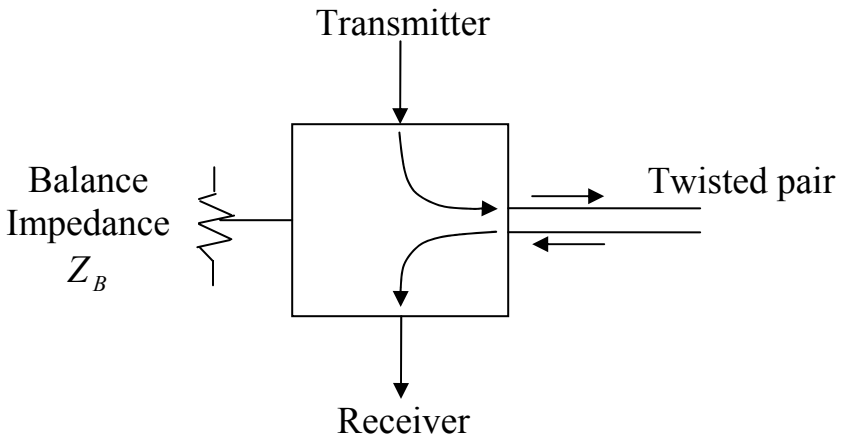

Fig. 4.8 General hybrid coupler

There are several configurations to implement a hybrid coupler. Fig. 4.9 shows a diagram of an electronic hybrid coupler [8]. An electronic hybrid coupler consists of a resistive bridge and an operational amplifier. The resistive bridge divides the transmitted voltage in two branches of the circuit - voltage dividers that are well balanced. One branch has $R_1 = R_2$, and the other has $Z_B = Z_L$. In this way, the transmitted voltage in each branch is divided in half. This forces each branch to

have exactly the same voltage regardless of the voltage that was transmitted. Therefore if we subtract the voltage in each branch using an operational amplifier, the resulting voltage will be zero regardless of the transmitted voltage. But if a signal comes back from the fault to the receiver of the hybrid coupler, this will increase the voltage in one of the branches of the circuit and the resulting voltage after the subtraction would be equal the voltage of the receiver signal. In this way the hybrid coupler separates the received signal from the transmitted signal.

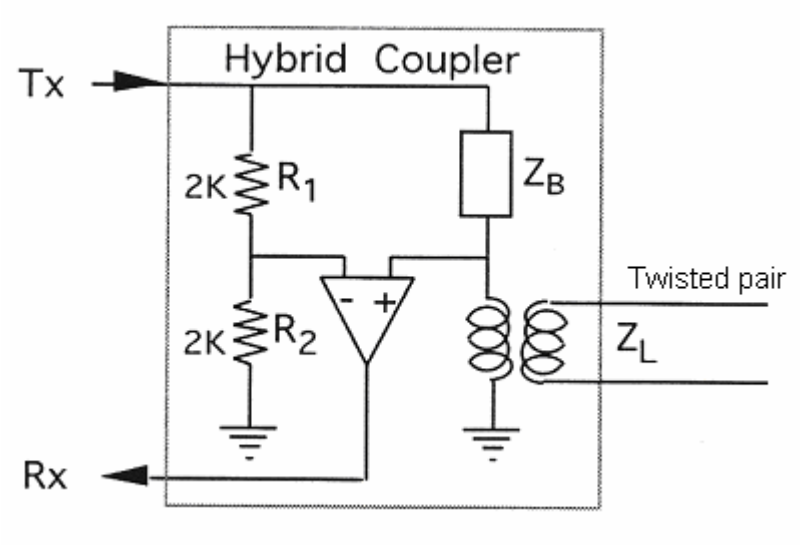

Fig. 4.9 Electronic hybrid coupler
(reproduced from EE816 notes with permission from D.E. Dodds [8])

Another example of hybrid coupler is the two transformers hybrid coupler, which provides electronic isolation and symmetry to the line. The transformer winding isolates electronic amplifiers from power feed and transient voltages found on transmission lines. This configuration is useful in long distance transmission circuits where signal reflections from hybrid couplers can cause serious echo and oscillation problems. Fig. 4.10 shows an example of the two transformer hybrid coupler [8].

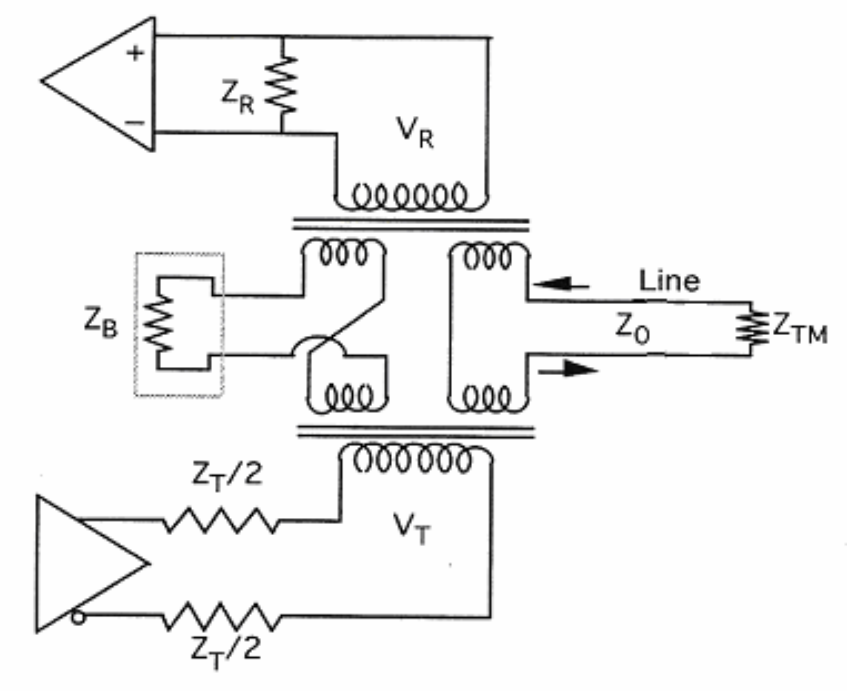

Fig. 4.10 Traditional hybrid coupler

(Reproduced from [8] with permission from D.E. Dodds)

4.3.1 Implemented hybrid coupler

For this project was required a hybrid coupler that could convert the transmitted signal from single-end mode to differential mode to drive the twisted pair line. Therefore we implemented the electronic hybrid coupler shown in Fig. 4.11.

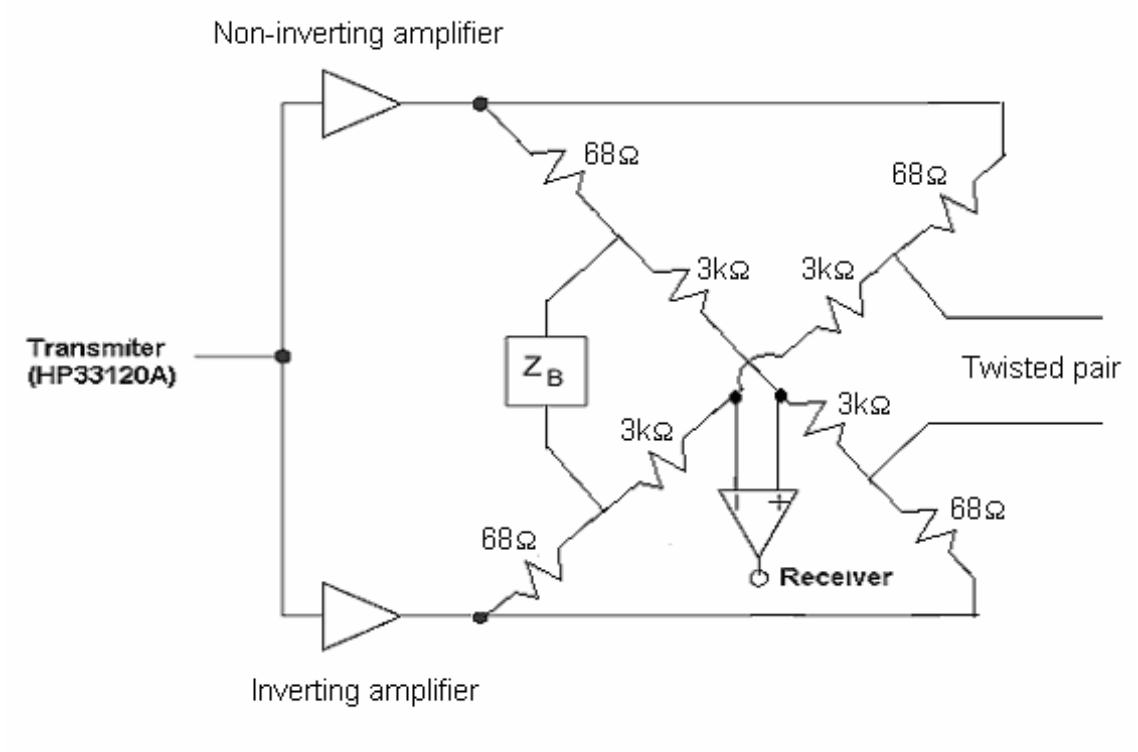

Fig. 4.11 Implemented hybrid coupler

This hybrid coupler provides balanced differential drive to the line and does not require a transformer; nevertheless, it requires an inverting and a non inverting amplifier to convert the single-end source to differential mode. These amplifiers need to be able to drive a twisted pair line at the frequencies required for the test.

This hybrid coupler is more complex than the electronic hybrid coupler shown in Fig. 4.9, but it uses the same principles. This hybrid coupler also has a resistive bridge that has two branches with the same impedance, to force the voltage in both branches to be equally distributed. This will cause the voltage at the receiver (difference of voltages between the two branches) to be zero regardless of the transmitted voltage (if there is no signal coming back to the hybrid coupler). In this way, any received signal coming from the twisted pair will unbalance the voltages between the two branches, and this will cause that the voltage at the receiver to be proportional to the voltage of the signal coming back from the fault. Hence, the

transmitted signal and the received signal will be separated. Once the received signal, which was reflected from the fault, is separated from the transmitted signal, it can be easily processed. The schematic diagram of the implement hybrid coupler is shown in Appendix D.

4.3.2 Balance impedance

The balance impedance is used in the hybrid coupler to match the impedance of the line. As it was explained in section 4.3.1, the principle of the hybrid coupler implemented in this project, is based in a resistive bridge that has two braches with the same relation of impedance, to force the voltages in both branches to be the same. Therefore, to have two branches with the same relation of impedance it is necessary to have a balance impedance in one branch to match the impedance of the line that is in the opposite branch. In this way both branches can have the same impedance and hence the transmitted voltage can be equally distributed in both branches.

The balance impedance consists of a network that matches the line impedance in magnitude and phase along the frequency range used for the frequency sweep. This balance network has branches of resistances and capacitors that are estimated based in the values of impedance that we want the network to have at certain frequencies. Therefore, the more branches the network has, the better the impedance of the network matches the line, because it is possible to impose more conditions for the value of its impedance along the frequency.

For the purpose of this project, we implemented a 3 branches balance network, as is shown in Fig. 4.12, to match the characteristic impedance of 26 and 24 AWG wire (which are used on typical urban telephone lines). It will always remain a small mismatch between the balance impedance and the line impedance at some frequencies, but this can be compensated as is explained in section 5.2.

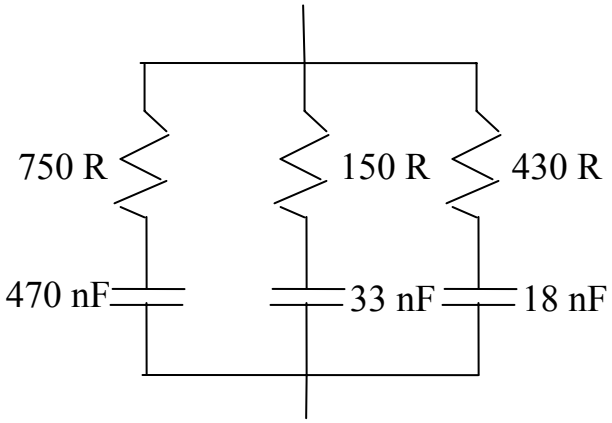

Fig. 4.12 Balance network

4.4 High frequency loss compensation

In Chapter 3 we showed that telephone lines have higher attenuation at higher frequencies. Therefore, when we sweep the line, the received signal coming from the fault gets more attenuated as the frequency is increased. This causes the loss of information at higher frequencies, and therefore, it also causes the loss of resolution in the measurements. For this reason, it is necessary to provide gain that increases with increasing frequency to compensate the received signal for the attenuation suffered during the round trip.

There can be several ways to compensate for the attenuation of the line. In this project it was decided to use an analog compensation, so as to maintain a larger signal input to the D/A converter. To do an analog compensation of only the received signal, it was necessary to use a hybrid coupler, as explained in section 4.3, to separate the received signal from the transmitted signal and then apply the compensation. In this way, once the signals were separated with the hybrid coupler, the received signal can be compensated for the high frequency loss using an active high pass filter. The frequency response of the filter attenuates at lower frequencies

and provides increasing gain as the frequency is increased to 1.3 MHz, and then provides a constant gain at higher frequencies.

The filter used for this compensation was an active first order high pass filter because the rate of gain of this filter is reasonably close to the attenuation rate of the wire. Therefore, using this filter with a gain of 12 dB it is possible to achieve a good compensation for the attenuation properties of the wire. Fig. 4.13 shows the frequency response of this filter.

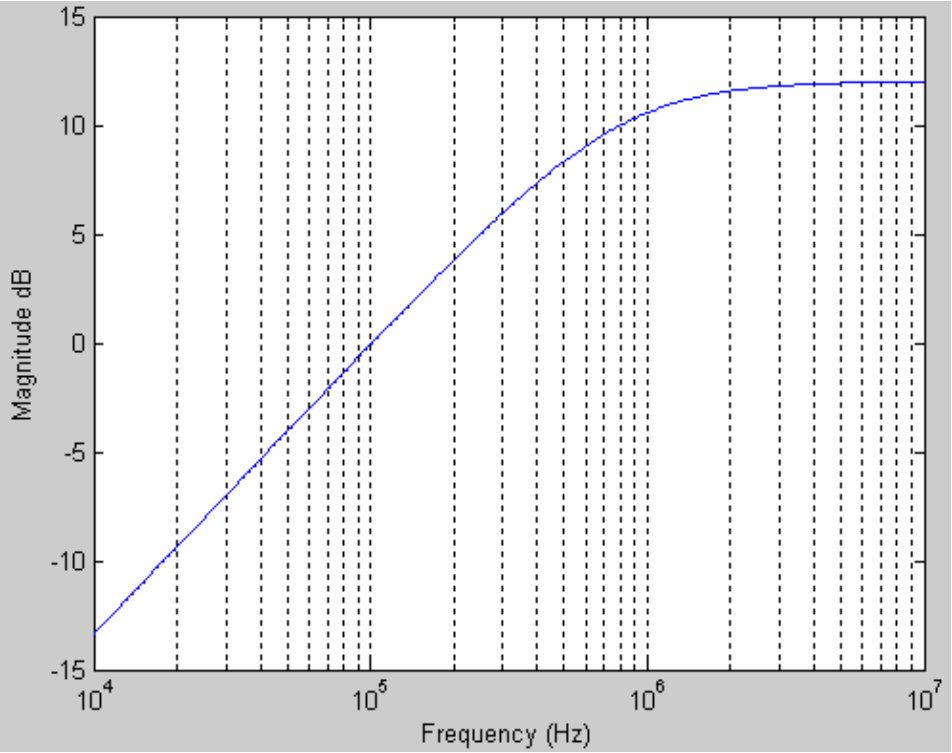

Fig. 4.13 Magnitude response for the first order high pass filter

To properly implement coherent detection, it is necessary to use two of these compensation filters. The reason for this is because if only one filter is applied to the received signal, at the output of the hybrid coupler, the phase of the signal will be altered by the filter and this will change the result after this signal is multiplied by

the transmit signal at the coherent detector. Therefore, to avoid this problem, another identical filter is placed before the multiplier of the coherent detector, to give to the signal coming from the transmitter the same phase shift that the received signal suffers with the compensation filter. By doing this, the phase of the signal that results from the multiplication between the received signal and the signal coming from the transmitter will not be altered since both signals get exactly the same phase shift. The use of the two filters, besides canceling the effect of the phase shift made by a single filter has another effect. There is a compounding of the high frequency gain compensation after both signals are multiplied.

Fig. 4.14 shows the phase response of the first order high pass filter. Here we can see that at low frequencies the filter alters the signal with almost 90°, although, the effect of this phase shift is cancelled when the second filter is placed as was described above.

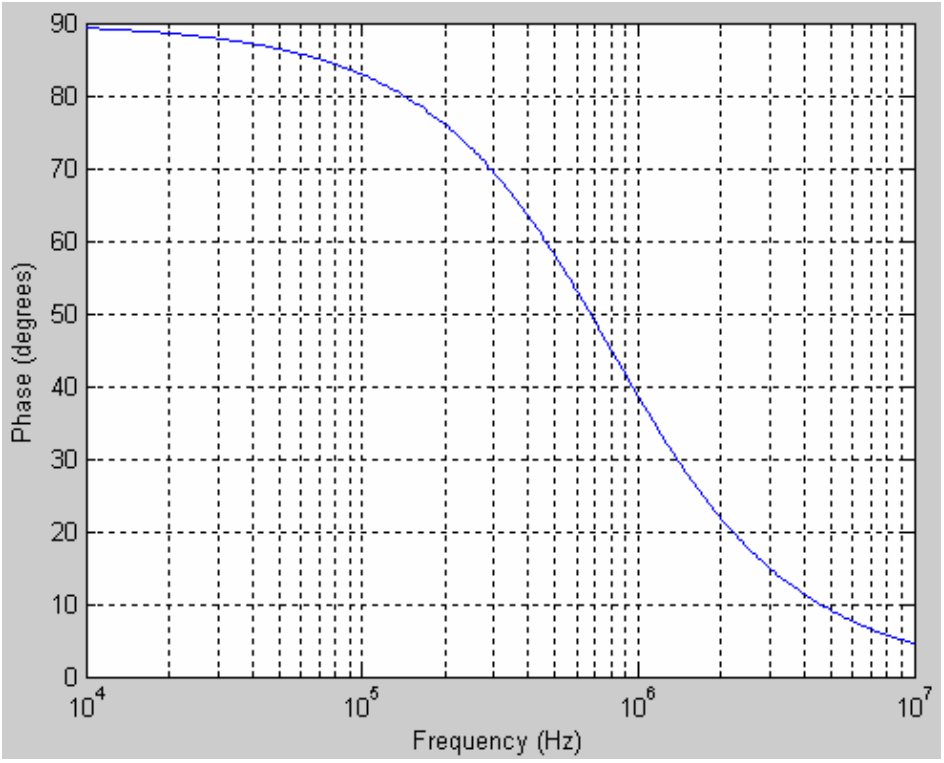

Fig. 4.14 Phase response for first order high pass filter

The figures below illustrate the effect of the compensation for the high frequency loss of a 1200 meter wire terminated in an open circuit. Fig. 4.15 illustrates the received signal without any compensation. Thus, in this figure we can clearly see the exponential decay of the trace caused by the attenuation properties of the line. On the other hand, Fig. 4.16 shows the received signal using the compensation filters for the high frequency loss. In this we can see how the filters have reshaped the trace giving it an attenuation of lower frequencies and an amplification of higher frequencies without altering the phase of the trace (otherwise the calculation for the reflection angle would be inaccurate). The overall effect is the taper of the signal at either end, which decreases the spectral leakage. Spectral leakage will be discussed in the windowing section of Chapter 5.

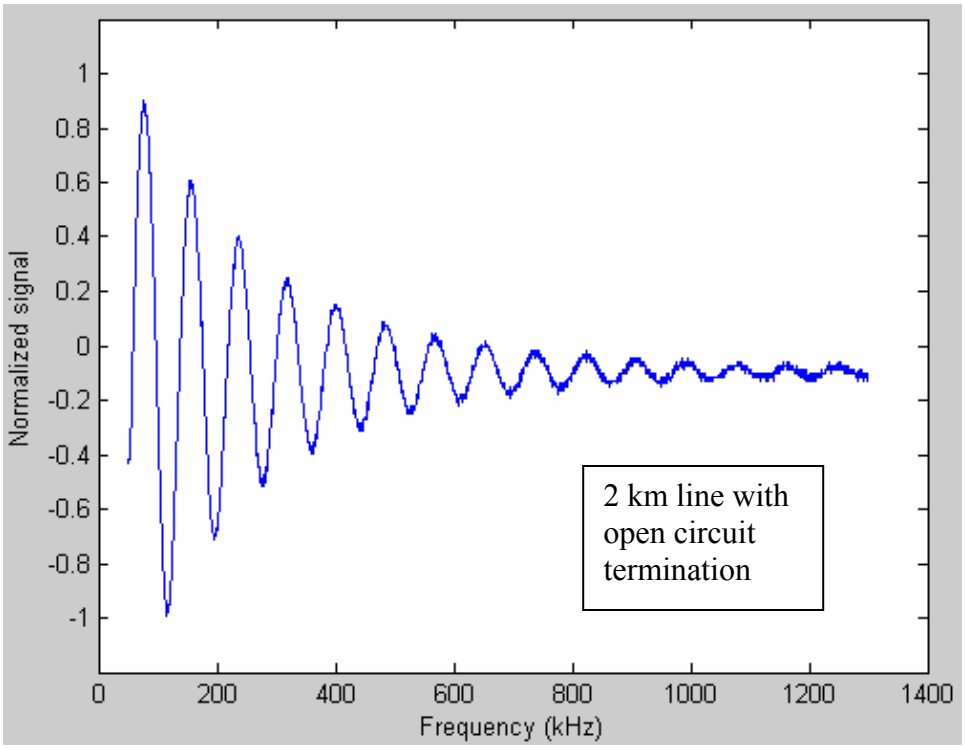

Fig. 4.15 Received in-phase signal without compensation

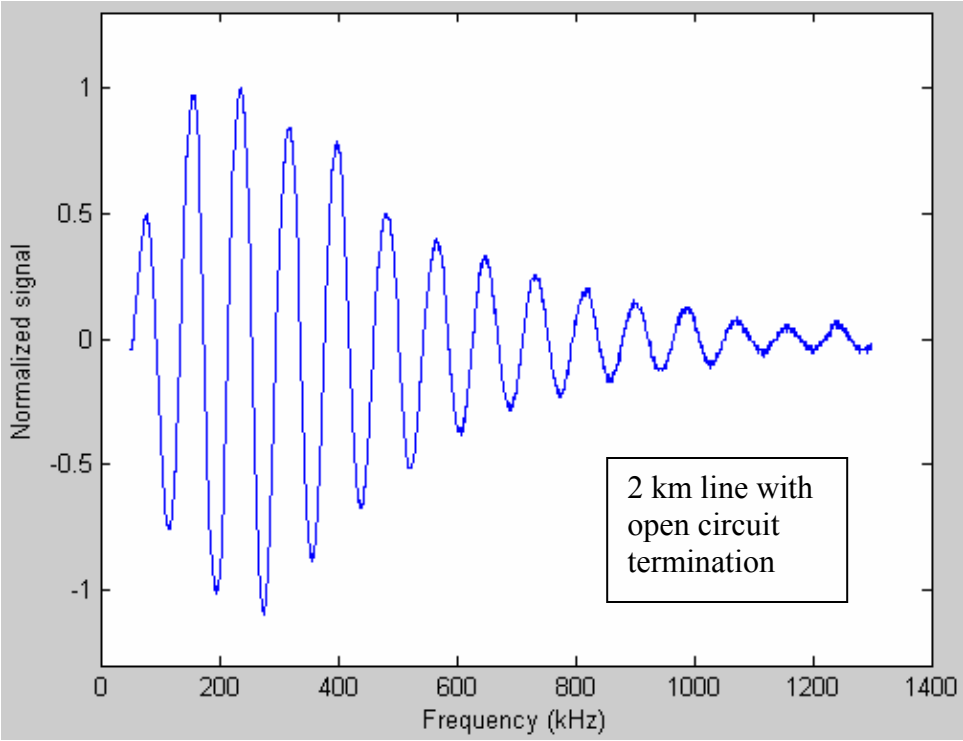

Fig. 4.16 Received in-phase signal with compensation

4.5 Data acquisition

To digitize the inphase reflected signal at the output of the coherent detector, we used the oscilloscope TDS220. This oscilloscope gives the opportunity to send the measured data to a computer file using its GPIB port. In this way the measurement can be processed using MATLAB.

This oscilloscope has 8 bits of resolution as all the oscilloscopes in the market. This resolution is good to digitize the trace at low frequencies, where the trace has good amplitude. Nevertheless, at high frequencies, where the amplitude of the trace is much smaller, this resolution might not be enough and can cause quantization noise. To solve this problem without increasing the resolution of the quantizer, the amplitude of the trace at higher frequencies is increased. This is done using the high frequency loss compensation described in section 4.4.

5. Signal processing

This chapter explains the different steps used to process the trace obtained with the W-FDR system.. These steps are a) warping of the frequency axis (to convert the frequency axis to inverse wave length), b) high frequency loss compensation, c) baseline compensation, d) windowing of the data, and e) Fourier transform to calculate the magnitude and phase of line fault reflections and the distances to the faults. Fig. 5.1 shows the block diagram of the signal processing used to locate the fault distance and estimate the reflection angle after the trace has been obtained from with the W-FDR system. The MATLAB code used for the signal processing is shown on Appendix C.

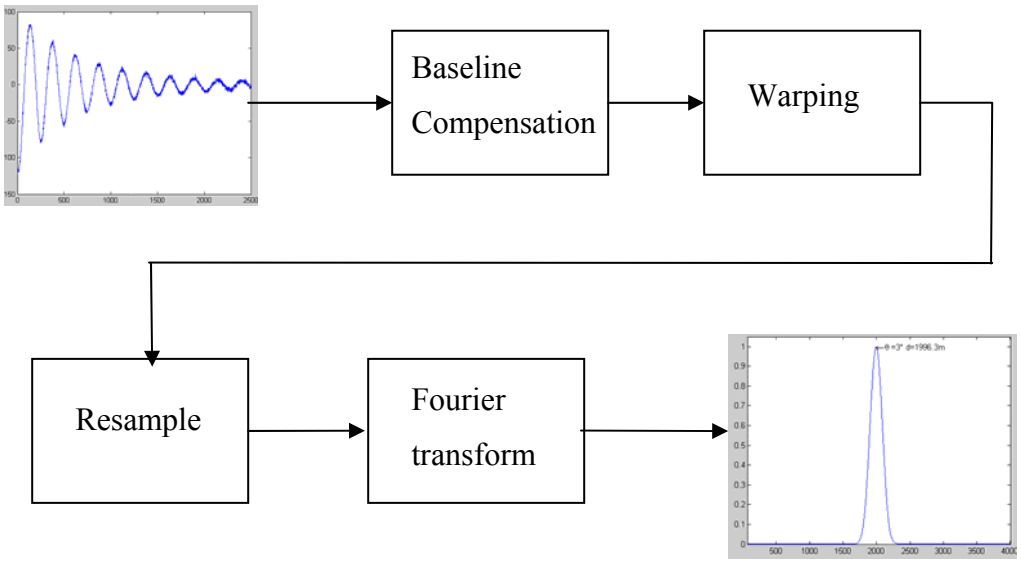

Fig. 5.1 Block diagram of the signal processing used by the W-FDR system

5.1 Sampling of the trace

The minimum number of samples required for the measurement of a trace will depend of the rate of variation (frequency) of the trace, or the number of cycles it has. This depends of the distance to the fault, as is explained in 5.5.1.

Digital subscriber lines have a maximum length of 5 km. Nevertheless, considering an extreme case of a measurement at 5.5 km, where the trace is measured in a frequency range from 50 kHz to 1.3 MHz. The number of cycles in this trace would be 68, because the rate of variation in a trace measured at this distance is 0.0544 cycles/kHz.

According to the Nyquist sampling theorem, a signal has to be sampled with a frequency at least two times the frequency of its highest frequency component. This means that we need to have at least 2 samples in each cycle of this component. However 4 samples per cycles is commonly used to better sample the signal. Given an extreme case of a trace that has 68 cycles (a measurement at 5.5 km), and that we want to have at least 4 samples per cycle, then we would need at least 272 samples is in the trace. Therefore, the minimum number of samples required for any trace is 272. In our measurements, we chose to use 2500 points because we wanted to have smooth shape of the trace and this number of points was the maximum we could get with the system.

5.2 Baseline compensation

The baseline is the trace obtained when measuring a telephone line that does not have any faults. This trace should be zero at all frequencies, but it is not because the hybrid coupler is not ideal. Compensation for this baseline is used to cancel its effect in the trace.

There are some factors that influence the baseline, for example, component variations. The principal reason is attributed to imprecise balance impedance match between the hybrid coupler and the test line. Recall from section 4.3.2, it is difficult to implement a balance impedance that will match the line for the entire range of frequencies used in the frequency sweep. Therefore, there is some mismatch between the balance impedance and the impedance of the line. This causes a small reflection of the transmited signal between the hybrid coupler and the line, and this signal goes right to the receiver. This slight leakage of signal to the receiver varies at different frequencies depending of the mismatch of the balance impedance. This results in the baseline that we obtain.

We measure the baseline trace by using a very long line (we used 6000 m during the experiments), and terminating the line with the same balance impedance as the hybrid coupler. Any small reflections from the termination are attenuated by the long line. In this way we guarantee that there will be almost no reflection coming from the line, and all we measure is the leakage signal of the hybrid coupler. This trace is called baseline of the hybrid coupler. This is a unique trace that depends on the component values for each hybrid coupler. To obtain the true measurement of the line under test, the baseline is subtracted from this trace. In this way we eliminate the baseline from the measurement. Fig. 5.2 shows the trace obtained from an open circuit at 1200 m before subtracting the baseline, Fig. 5.3 shows the baseline, and Fig. 5.4 shows the trace after subtracting the baseline. These figures were obtained without using the filters for high frequency loss, in order to illustrate the effect of the baseline itself.

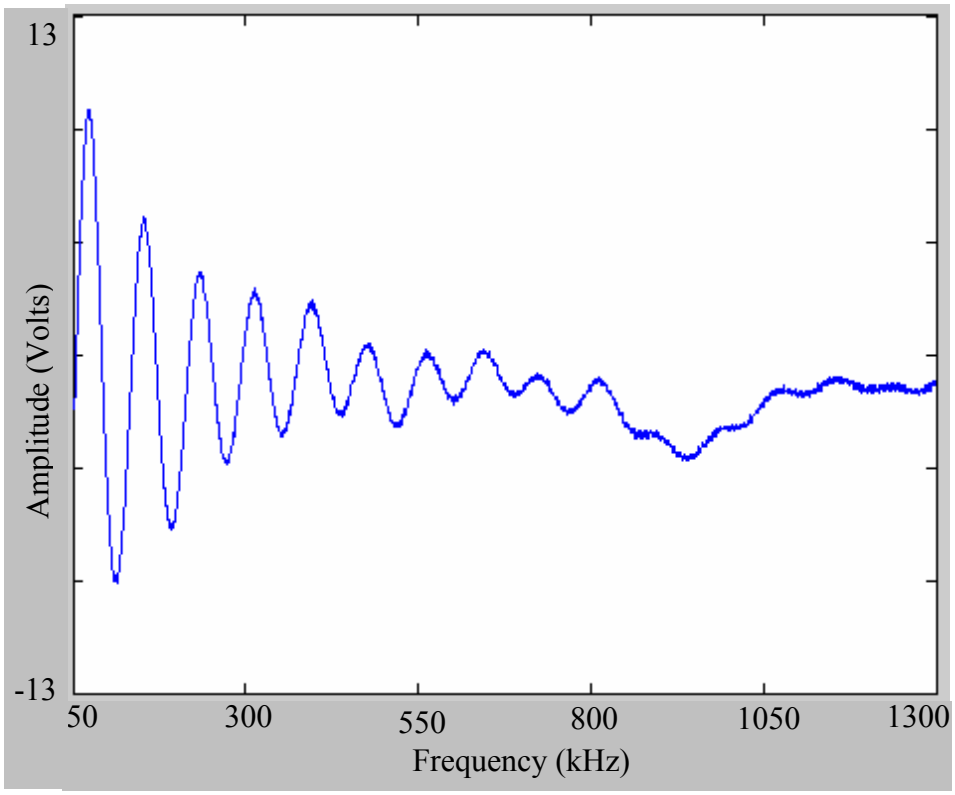

Fig. 5.2 Trace of an open circuit at 1200 m before subtracting baseline

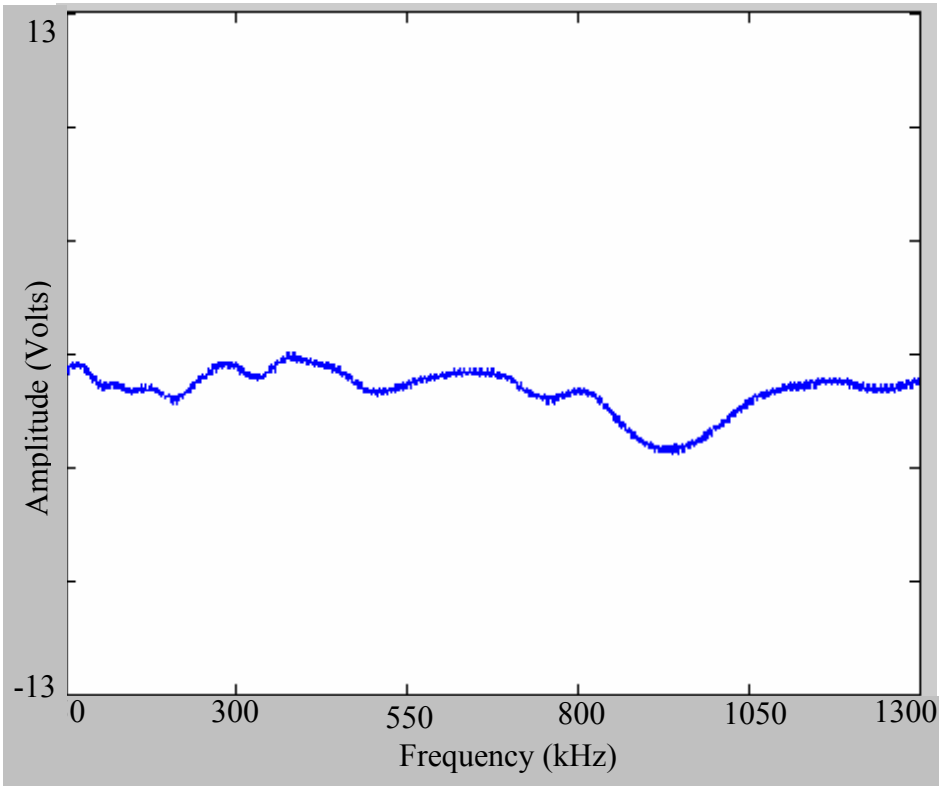

Fig. 5.3 Baseline of the implemented hybrid coupler

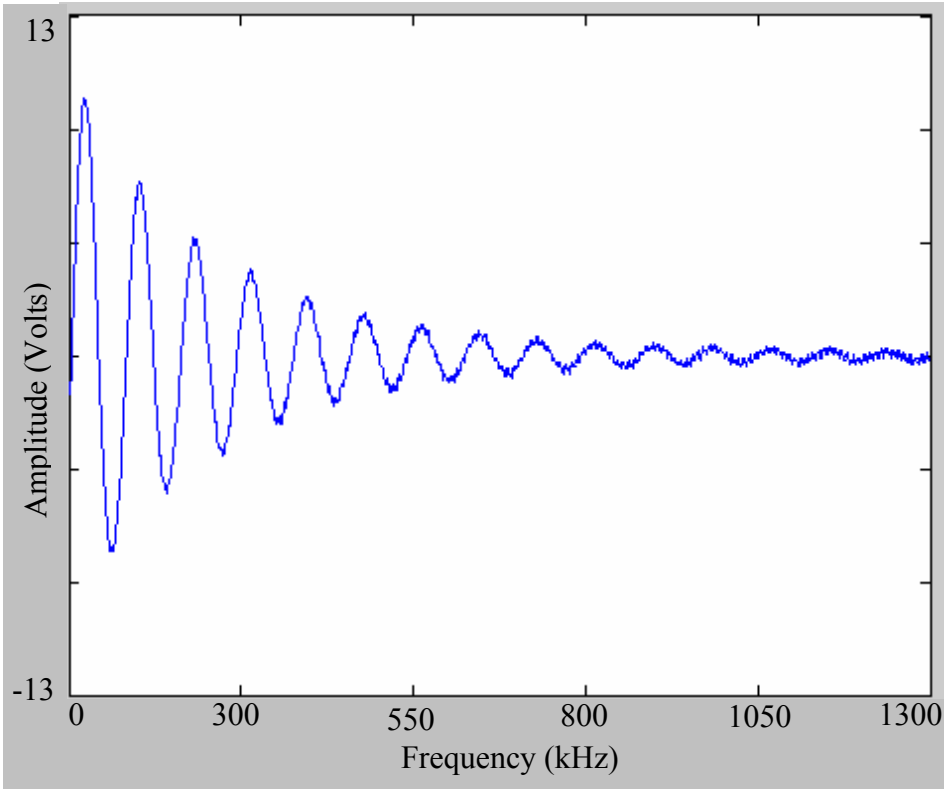

Fig. 5.4 Trace of an open circuit at 1200 m after subtracting the baseline

5.3 Warping of the frequency axis

Transmission lines have propagation velocity that changes as a function of frequency. This is described in equation 5.1, where β is the phase constant and f is the frequency. This causes telephone lines to have a reduced propagation velocity at low frequencies.

$$v = \frac{2\pi f}{\beta} \tag{5.1}$$

Therefore the trace from a single point of reflection will have a shorter period at lower frequencies, and this will affect the resolution when determining the distance to the fault. For this reason, it is necessary to compensate for the variable propagation velocity by warping the frequency axis of the trace. The MATLAB code of the warping functions is shown in Appendix C.

To warp the frequency axis, it is necessary to multiply each frequency of the axis, which is in Hz or *cycles/sec*, by the inverse propagation velocity or warping function as we call it. Inverse propagation velocity is measured in *sec/meter*, thus the result of this multiplication is in *cycles/meter* or inverse wave length (1/λ). In this way we convert the frequency axis to inverse wave length. When we apply the Fourier transform to the warped data, this will convert the axis which is in *cycles/meter* in to *meters*, (in the same way as the Fourier transform traditionally converts the frequency axis from *cycles/sec* to *seconds)*. Therefore, once the Fourier transform has converted the warped axis from *cycles/meter* to *meters*, it is possible to estimate the location of the fault.

To calculate the warping factor, we begin with the phase constant β (*rad/meter*) as given in [10].

$$\beta = \sqrt{\frac{1}{2}\left[\sqrt{(r^2+\omega^2 l^2)(g^2+\omega^2 c^2)} - rg + \omega^2 lc\right]} \tag{5.2}$$

Dividing β by ω, which is in *rad/sec*, yields the warping factor or inverse propagation velocity in units of *sec/meter*. A plot of the warping factor is shown in Fig. 5.5, and its warping function *X*, is described in the equation below.

$$X = \frac{\beta}{\omega} \tag{5.3}$$

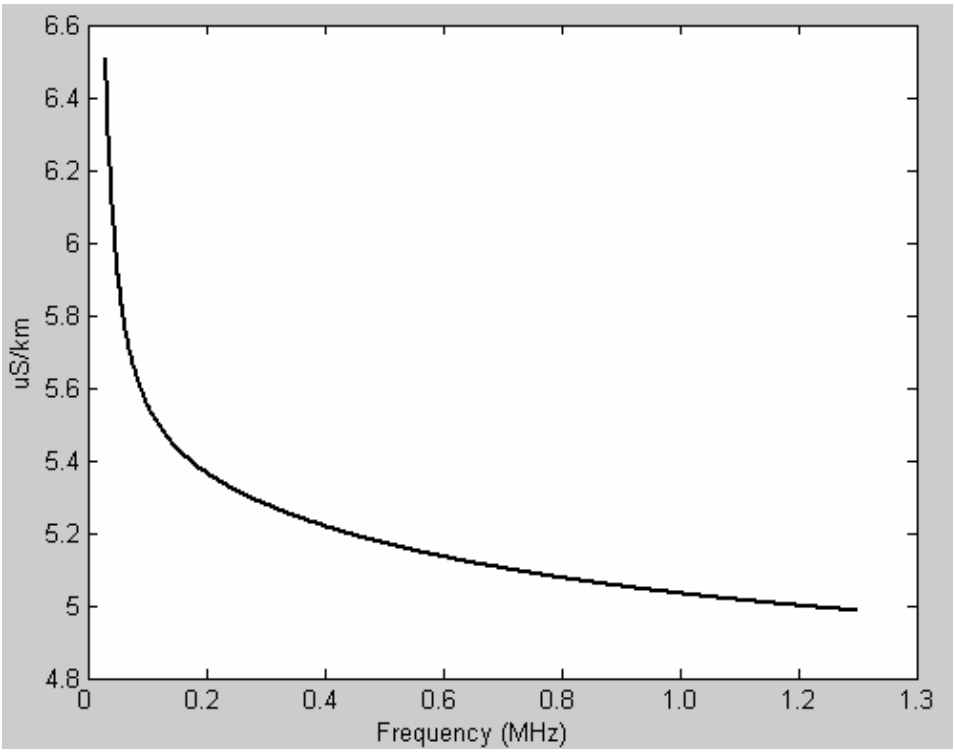

Fig. 5.5 Warping factor

To see the effect of the warping factor, Fig. 5.6 illustrates a trace affected by changes in the propagation velocity due to frequency. In this graph we can see that as frequency increases, the period of the trace at higher frequencies gets larger compared to the period at lower frequencies.

To compensate for this effect, we use the warping factor. Fig. 5.7 illustrates the trace shown in figure Fig. 5.6, after applying the warping function. In this trace we notice that the period of the trace is uniform and the frequency axis has changed to inverse wave length (*cycles/km*) after being multiplied by the warping factor.

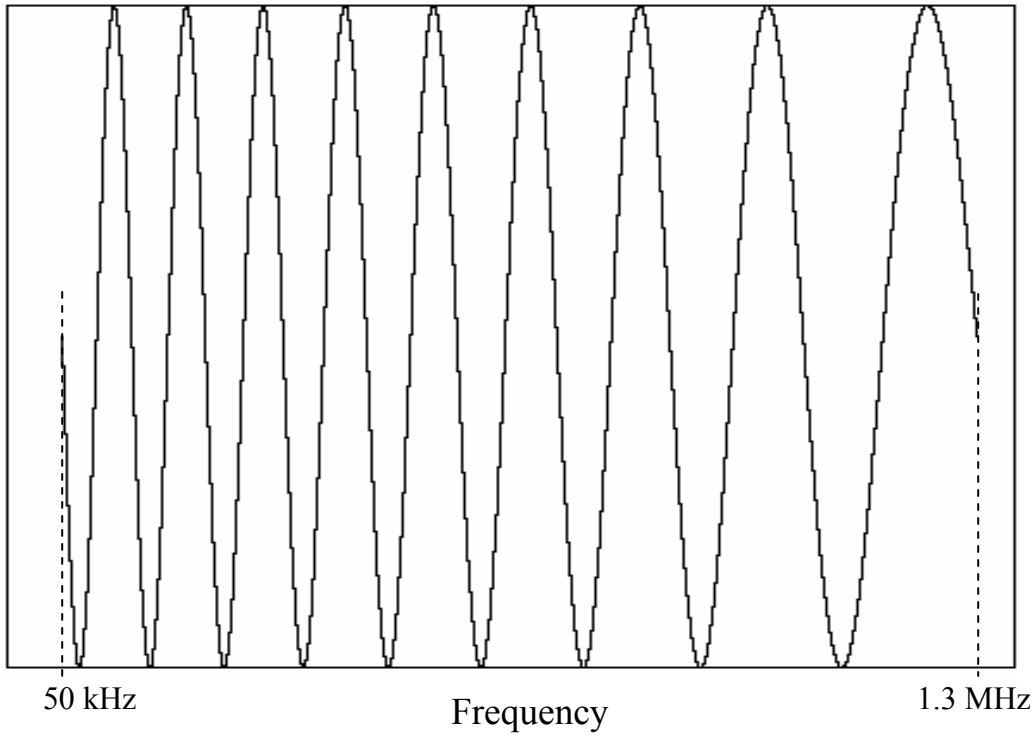

Fig. 5.6 Example of a trace prior to warping application

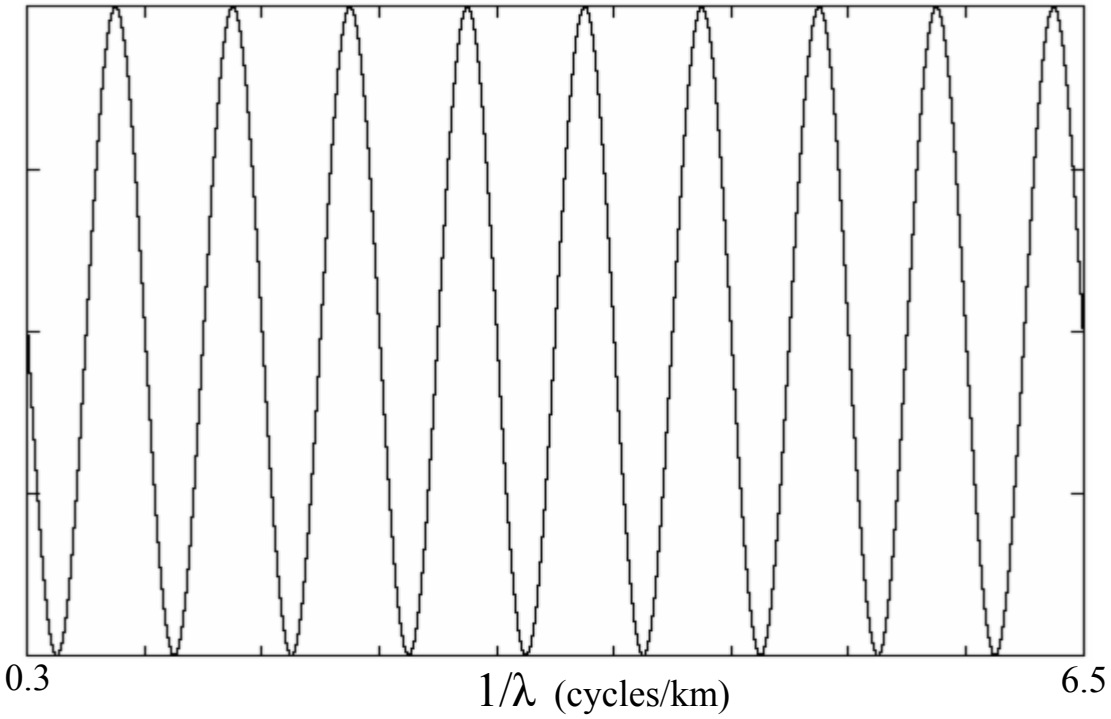

Fig. 5.7 Example of a trace after the warping application

5.4 Resampling

After warping, the sample points of the trace are no longer uniformly spaced because this last process, compress or expands the horizontal spacing between the points. These points must be equally spaced to be processed using the Fourier transform. For this reason, the resampling algorithm is used in order to make the points of the trace equally spaced. The MATLAB code of the resampling functions is shown in Appendix C.

Starting with this irregularly spaced set of data, we used a linear interpolation routine to make the set of data equally spaced. The algorithm consists of two primary steps. The first step is the recalculation of a new equally spaced sample points on the x-axis. The second consists in the recalculation of the y-axis values based on the new sample points on the x-axis. The old sample points on the x axis after the warping are designated $x_1, x_2 .... x_N$ and the new sample points after interpolation are designated $X_1, X_2 .... X_N$.

To determine the new x-axis spacing, a sample size needs to be selected. The distance between the two closest points on the existing x-axis was selected to be the new sampling space. After warping, the two closest points are the last two points of data that constitute the trace, which are selected to be the new sampling space.

The initial point for the new x-axis corresponds to the initial point of the existing x-axis ($X_1 = x_1$). Therefore, the new x-axis points are defined to be:

$$X_n = x_1 + (n-1)(x_N - x_{N-1}) \tag{5.4}$$

where *n* is the sample number in the new x-axis $2 \leq n \leq$ N, and N is the total number of data samples.

After calculating the new x-axis X_n, the next step is to calculate the corresponding new y-axis Y_n. To do this we use linear interpolation and the new y-axis values are found from:

$$Y_n = \left(\frac{y_n - y_{n-1}}{x_n - x_{n-1}}\right)(X_n - x_{n-1}) + y_{n-1} \tag{5.5}$$

Fig. 5.8 [1], shows a discrete sequence plot of a position of the original data sequence and its resampled version. The data was obtained from a 400 m open circuit line. The sample in the far left corresponds to the initial data point of both the original and resampled data sequence. By definition these two points are the same. Towards the right of the plot, the effects of the resampling process are more pronounced. Also in this figure, we show an example of how the newly resampled data was calculated. X_{14} lies between x_{14} and x_{13}, according to the value calculated from equation 5.4. The value for Y_{14} is found from equation 5.5.

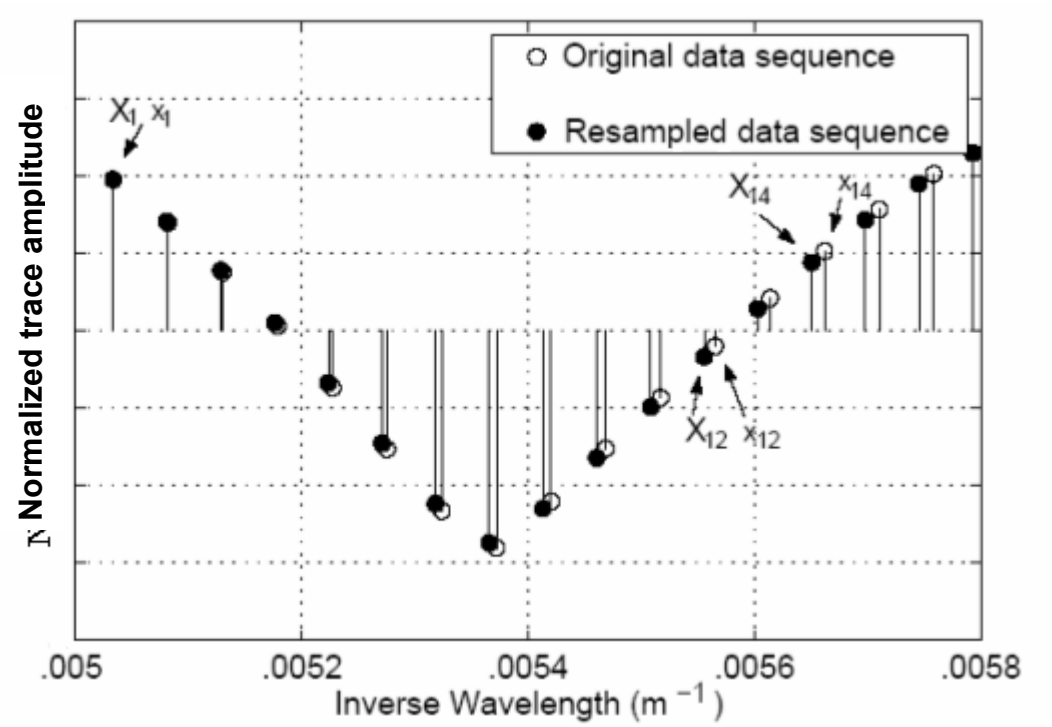

Fig. 5.8 Illustration of resampling (taken from [1])

5.5 Fourier transform

The Fourier transform is used to analyze the trace and estimate the location and nature of a fault. When we have just one single fault on the line, the obtained trace looks like a sinusoid with an exponential decay (caused by the increasing attenuation of the line at high frequency) as shown in Fig. 4.15. The rate of variation (or frequency) of this sinusoid trace is proportional to the distance to the fault, and its phase will depend of the nature of the fault. If we have more than one fault on the line, we will obtain a trace that is the mix of several sinusoids of different frequency and phase, each corresponding to a different fault. Using the Fourier transform we can analyze this trace and estimate the frequency and phase of each sinusoid. Hence, we can locate several faults in the same line and determine their nature. Fig. 5.9 shows an example of a trace that is the mix of two sinusoids. This trace was obtained from a measurement of a 200 m bridge tap at 800 m that ends in an open circuit. In the next chapter we show the results obtained after the analysis of this trace using the Fourier transform.

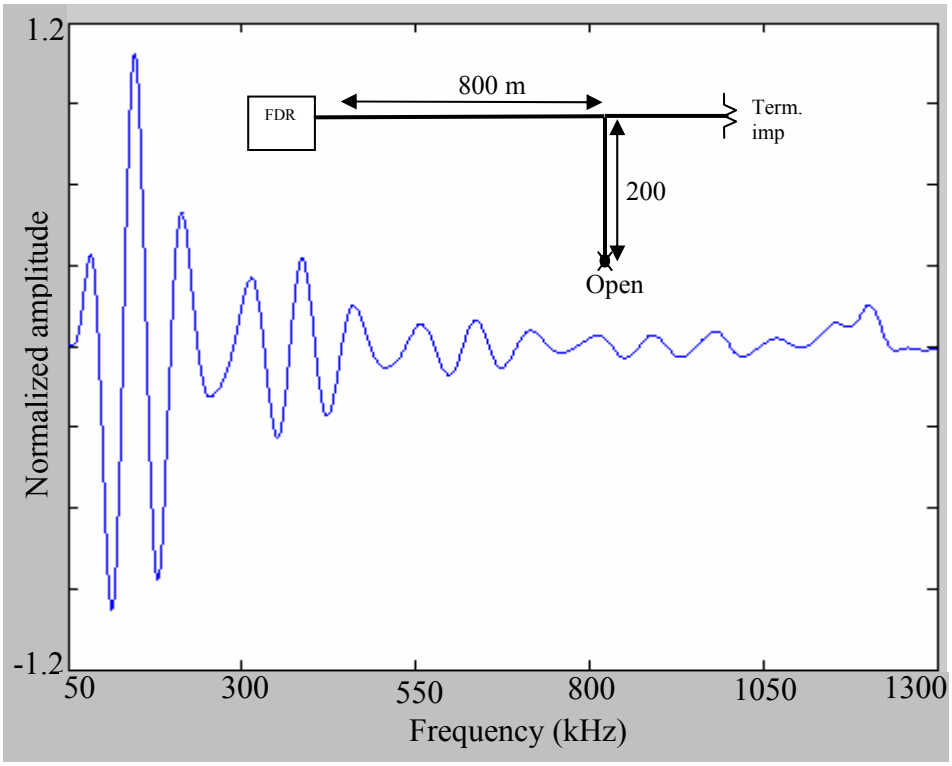

Fig. 5.9 Trace composed by two sinusoids

The Fourier transform obtains a frequency spectrum of the sinusoids that compose the trace. In this way it is possible to analyze each component separately.

In the case of analog continuous time signals, the Fourier transform can be determined using the following equation:

$$X(f) = \int_{-\infty}^{\infty} x(t) e^{-j2\pi ft} dt \tag{5.6}$$

where *X(f)* is the frequency spectrum of a time signal *x(t)*. The signal must have finite energy in order for its Fourier transform to exist [11]; the energy of the signal is calculated as

$$E = \int_{-\infty}^{\infty} | x(t) |^2 \ dt \tag{5.7}$$

Equation 5.6 transforms a time domain signal into its frequency domain components. The inverse transformation, to pass from frequency domain to time domain, is shown below.

$$x(t) = \int_{-\infty}^{\infty} X(f) e^{j2\pi ft} dt \tag{5.8}$$

To apply the Fourier transform to a discrete signal it is necessary to use the discrete Fourier transform or DFT. The DFT is used in the project to analyze the trace and estimate the location and nature of the faults. The DFT is calculated as

$$Z(k) = \sum_{n=0}^{N-1} x(n) e^{\frac{-j2\pi kn}{N}} \tag{5.9}$$

where *k* is the frequency index, *X(k)* is the discrete Fourier transform and *x(n)* is the discrete signal and *N* is the total number of data samples. To calculate the inverse discrete Fourier transform or IDFT, we use the following equation:

$$x(n) = \frac{1}{N}\sum_{n=0}^{N-1} X(k) e^{\frac{j2\pi kn}{N}} \tag{5.10}$$

5.5.1 Fault location

The rate of variation of the trace is proportional to the distance of the fault. An example of this is given in the next figures. Fig. 5.10 shows the trace obtained from an open circuit at 800 m, and Fig. 5.11 shows the trace obtained from an open circuit at 1600 m. The 1600 m trace shows a rate of variation that is twice the rate shown in the 800 m trace. Therefore, using the Fourier transform, as is explained next, we can estimate the rate of variation (frequency) of the trace, and hence we can estimate the distance to the fault since they are proportional.

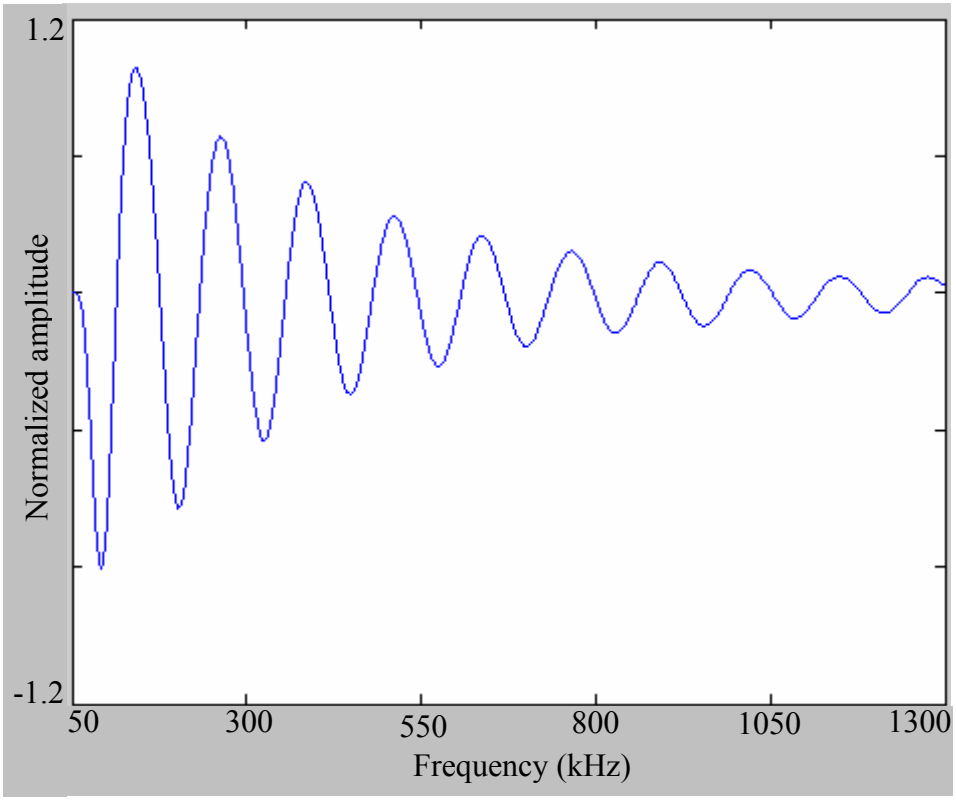

Fig. 5.10 Trace from an open circuit at 800 m

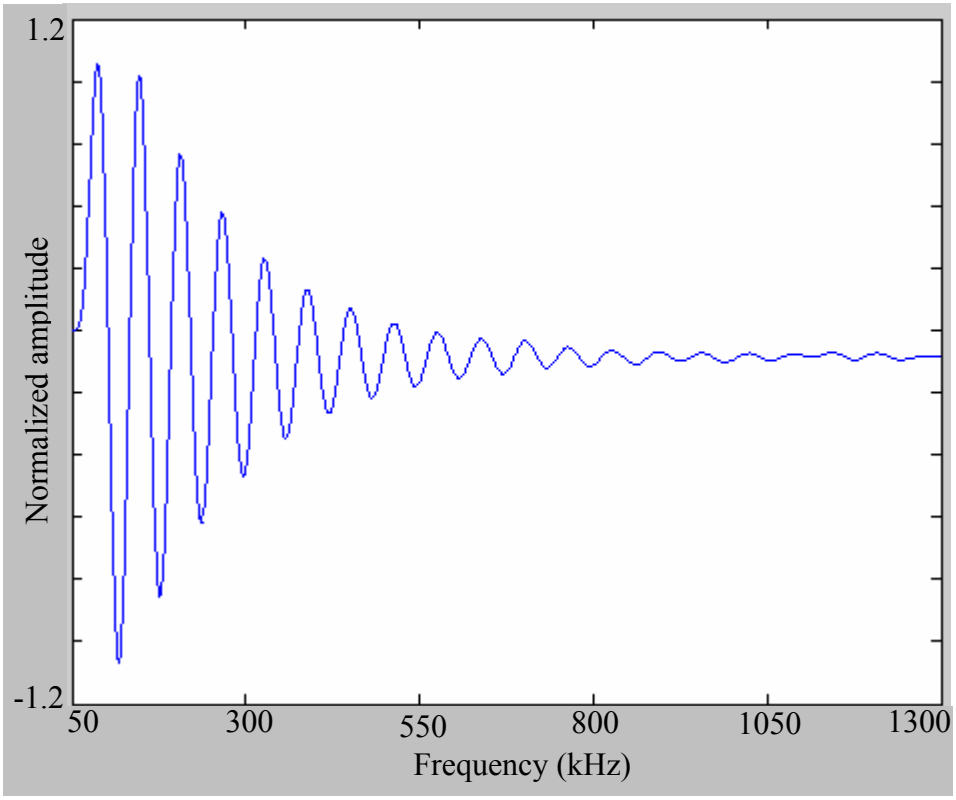

Fig. 5.11 Trace from an open circuit at 1600 m

In order to process the trace and estimate the distance to the fault, we can choose ether the Fourier transform or the inverse Fourier transform. The Fourier transform is applicable because the obtained trace is composed of sinusoids (one from each fault on the line). Therefore, the Fourier transform will give us the frequency spectrum of the trace. We can then analyze each component of the trace and estimate the rate of variation (frequency) of each component. This will give us the location of each fault.

The inverse Fourier transform can also be used because this function will convert the x-axis of the trace from *cycles/meter* (the warping function previously changed this axis from frequency to *cycles/meter*) to *meters*, in the same way as it usually converts the frequency axis from *cycles/second* to *seconds*. This conversion of the x-axis then indicates the location of the fault (which is in meters).

Since it is the same to use ether the Fourier transform or the inverse Fourier transform to process the trace and obtain the location of the faults, we will use the Fourier transform. This will make easier to understand the processing of the trace described in the next sections.

5.5.2 Measurement precision

To implement the Fourier transform and determine the location of the faults we used the DFT. This allows to obtain a final result (plot of normalized reflection amplitude vs. distance) with as many samples as we want regardless of the number of samples in the trace. In this way we can obtain high precision measurement and a smooth shape of the final result.

In this project, first we use the DFT to obtain a measurement of normalized reflection amplitude vs. distance with 4500 points. Therefore, the distance between samples, which is equal to the maximum distance in the measurement divided by the number of samples, is around 1 meter per sample. With this measurement we determine the location of the fault. Then, to get the measurement with high precision, we use again the DFT to calculate another 2500 points in the portion of the graph where the fault was located. This portion is equal to the distance between two samples, which is around 2 meters. Therefore, the precision of the measurement is around 0.8 mm.

5.5.3 Calculation of the Reflection Angle

In Chapter 3 we explained the equation used to calculate the reflection coefficient. For convenience, this reflection coefficient equation is again shown,

$$\rho = \frac{Z_r - Z_0}{Z_r + Z_0} \tag{5.11}$$

where *Zr* is the impedance of the discontinuity and *Zo* is the impedance of the line. This reflection coefficient can be represented as a complex number with magnitude "*r*" and phase angle Θ. This is,

$$\rho = re^{j\theta} = r\angle\theta \tag{5.12}$$

The phase angle Θ of the complex reflection coefficient will be different for different kinds of faults. Therefore, by determining the angle of the reflection coefficient we can determine the nature of the fault (short circuit, water, loading coils, bridge tap, etc).

Using the W-FDR technique, it is possible to measure this reflection coefficient angle to determine the nature of each fault on the line. It was illustrated in Fig. 4.4 that the received vector rotates as frequency increases and at 0 Hz, there is no rotation. Thus, at 0 Hz the received signal has a phase shift (relative to the transmitted one) that is equal to the angle of the reflection factor.

The first step in calculating this reflection angle is to extrapolate the trace from the start frequency down to 0 Hz. Once the trace is extrapolated we measure the phase of each frequency component on the trace (each variation frequency corresponds to one fault) to estimate the reflection coefficient angle for each fault on the line. To have a better understanding of this, we will analyze a case where there is only one fault on the line.

As explained, when we have one fault on the line, what we obtain from the W-FDR system is a decaying sinusoidal trace of in-phase reflected signal amplitude vs. frequency that ranges from the start frequency of the sweep to the last frequency. Fig. 5.12 represents the traces obtained from a frequency sweep that ranges from 50 kHz to 1.3 MHz for two different lines, one with an open circuit and the other with a short circuit.

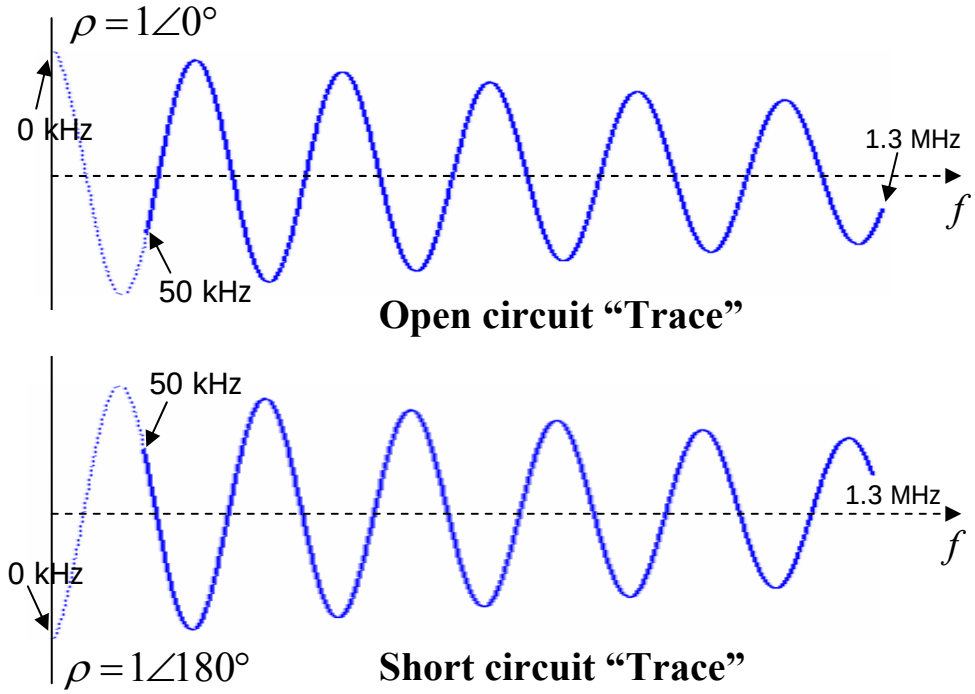

Fig. 5.12 Calculation of reflection angle

The first step to calculate the reflection angle was to extrapolate the trace from the start frequency down to 0 Hz. This extrapolation is represented in Fig. 5.12 by the dotted line that goes from 50 kHz down to 0 Hz. Once the traces are extrapolated down to 0 Hz, we notice that the trace corresponding to the open circuit has a phase angle of 0° (compared to a cosine function). This is the same angle that we would obtain if we calculate the complex reflection coefficient from an open circuit using equation 5.11 (where Zr is equal to ∞ in this case). Similarly, we can notice that the trace corresponding to the short circuit has a phase angle of 180° after extrapolation. This is the same angle that we would obtain if we calculate the complex reflection coefficient of a short circuit using equation 5.11 (where Zr is equal to 0 for this case). Therefore, measuring the phase of the extrapolated trace we can estimate the phase angle of the reflection coefficient and determine the nature of the fault.

In order to extrapolate the trace and measure the phase, we first zero pad the trace down to 0 Hz. Fig. 5.13 shows a sinusoid trace zero padded from 50 kHz down to 0 Hz. The dotted line in the beginning of the trace represents the part of the trace that is missing, since the sweep begins at 50 kHz.

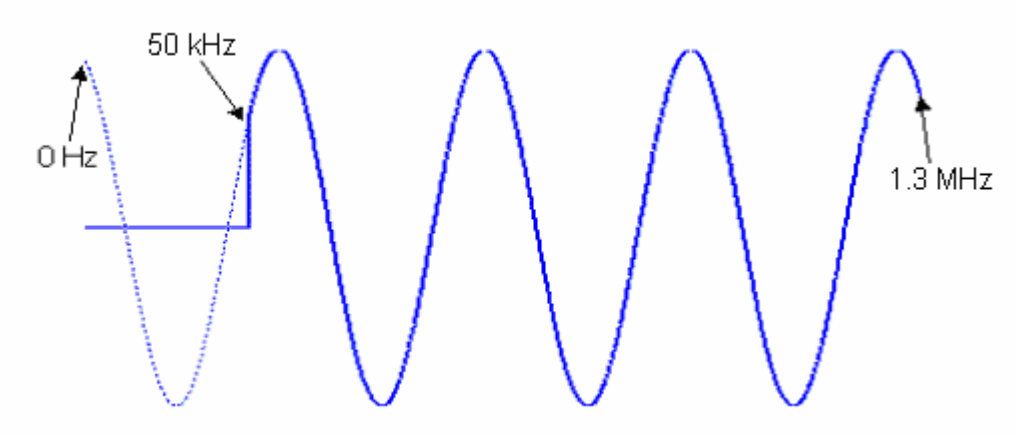

Fig. 5.13 Extrapolation zero padding the trace

Once the trace has been zero padded, its phase can be measured using the Fourier transform to estimate the angle of the reflection coefficient. To understand how the Fourier transform measures the phase of the trace, first we have to rewrite the equation of the discrete Fourier transform (5.9), substituting the exponential part using the following propriety,

$$e^{-j\phi} = \cos(\phi) - j\sin(\phi) \tag{5.13}$$

and the discrete Fourier transform results

$$Z(k) = \sum_{n=0}^{N-1} x(n)\cos(\frac{2\pi k}{N}n) - j\cdot\sum_{n=0}^{N-1} x(n)\sin(\frac{2\pi k}{N}n) \tag{5.14}$$

This shows that the real part of the Fourier transform correlates the trace (represented by *x(n)*) to a cosine of frequency $\frac{2\pi k}{N}$. The result of this is the component of the trace that is in-phase with the cosine. The imaginary part of the Fourier transform correlates the trace to a sine wave (of the same frequency), and the result of this is the component of the trace that is in-phase with the sine. The sine and the cosine are two orthogonal functions that form a two-dimensional basis function *x, y*. Therefore, when we apply the Fourier transform to a sinusoid trace, this one correlates the trace to a sine and a cosine to obtain the coordinates *x, y* that represent the trace in the base function formed by the sine and the cosine. Each value calculated by the Fourier transform is a complex number that represents a coordinate *x, y*. This is $Z(k) = X(k)+jY(k)$, where *k* determines the frequency, *X(k)* is the real part of the Fourier transform and *Y(k)* is the imaginary part. Fig. 5.14 is a graphical example of how the Fourier transform correlates the sinusoid trace to the basis functions formed by the sine and the cosine.

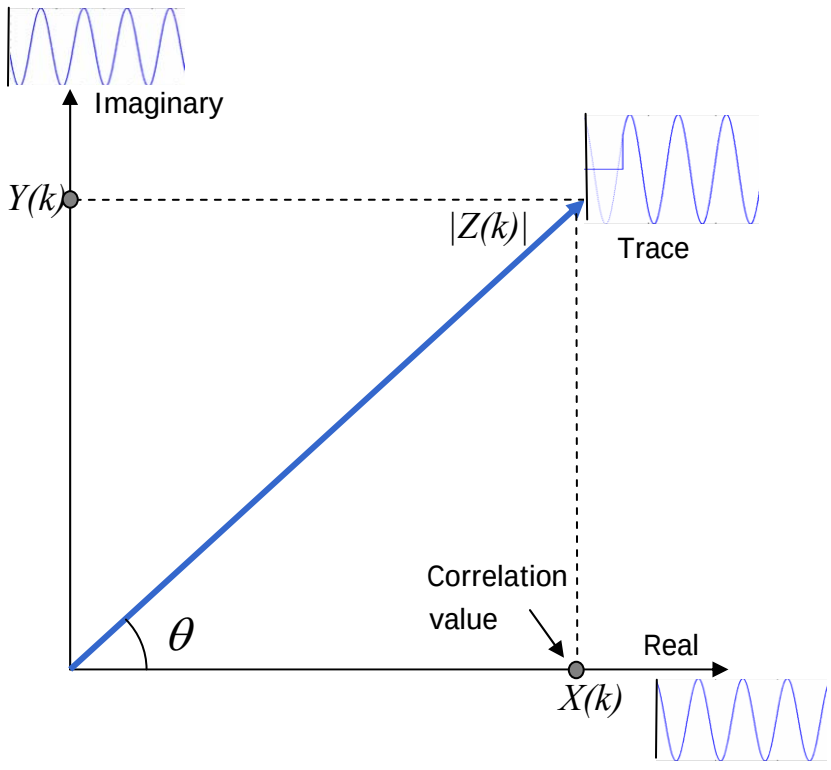

Fig. 5.14 Phase Θ of the reflection angle

Once the components *X(k)* and *Y(k)* are calculated with the Fourier transform, the phase angle Θ of the trace can be easy estimated as

$$\theta(k) = \tan^{-1}(\frac{Y(k)}{X(k)}) \tag{5.15}$$

where *k* represents the harmonic of which we are measuring the phase.

We have shown that the Fourier transform correlates the zero padded sinusoidal trace, with a two dimensional basis function formed by a sine and a cosine of the same frequency as each component of the trace. But a problem arises when we consider that the frequencies of the components of the trace are initially unknown. Nevertheless, this problem is solved because the Fourier transform repeats several times the process described before, trying several frequencies along a frequency range that includes the frequency of the trace. Therefore, one of these frequencies will correspond to the frequency of the trace and the phase angle calculated at this frequency will correspond to the phase of the trace. For this reason, we have to estimate the frequency of the trace to know which of the calculated phase angles correspond to the trace.

We use the real and imaginary parts of the Fourier transform (*X(k)* and *Y(k))* to calculate the magnitude of the correlation.

$$| Z(k) | = \sqrt{X(k)^2 + Y(k)^2} \tag{5.16}$$

The correlation magnitude will be maximum when the trace is correlated to a sine and cosine with the same frequency as a component in the trace. Therefore, determining the maximum values for the magnitude of the Fourier transform within the frequency range where we applied it, we can estimate the frequency components of the trace.

To have a better understanding of the process, Fig. 5.15 shows a graphical interpretation of the results obtained by the Fourier transform. In this figure we can see the two axis formed by the basis functions of the sine and the cosine, which represent the real and imaginary parts of the Fourier transform. The third axis, orthogonal to the first two, represents the frequency. The correlation process illustrated in Fig. 5.14 is repeated along this frequency axis during the Fourier transform process. Therefore, for each point along the frequency axis, the Fourier transform calculates the coordinates *X(k)* and *Y(k)* that correspond to the real and imaginary part of the Fourier transform. In this way, for each point of the frequency axis we can calculate a phase angle $\theta(k)$ and magnitude $|Z(k)|$, and the phase calculated at the frequency where the magnitude is maximum will correspond to the phase of the trace. Therefore, the phase angle is only indicated at the maximum point of $|Z(k)|$. This is illustrated in Fig. 5.16.

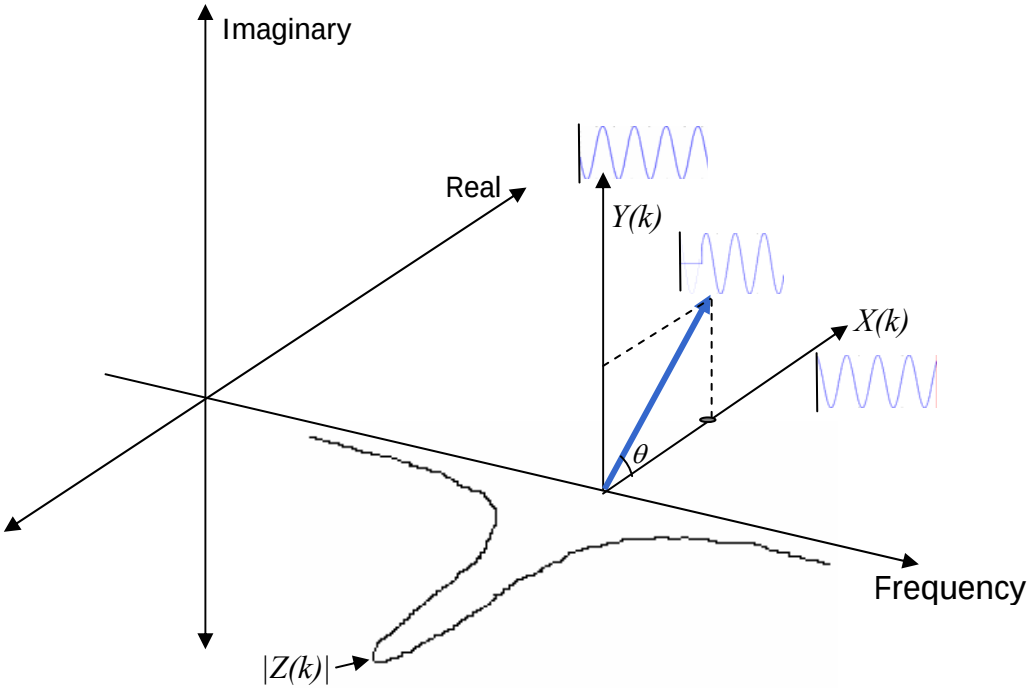

Fig. 5.15 Graphical representation of the Fourier transform

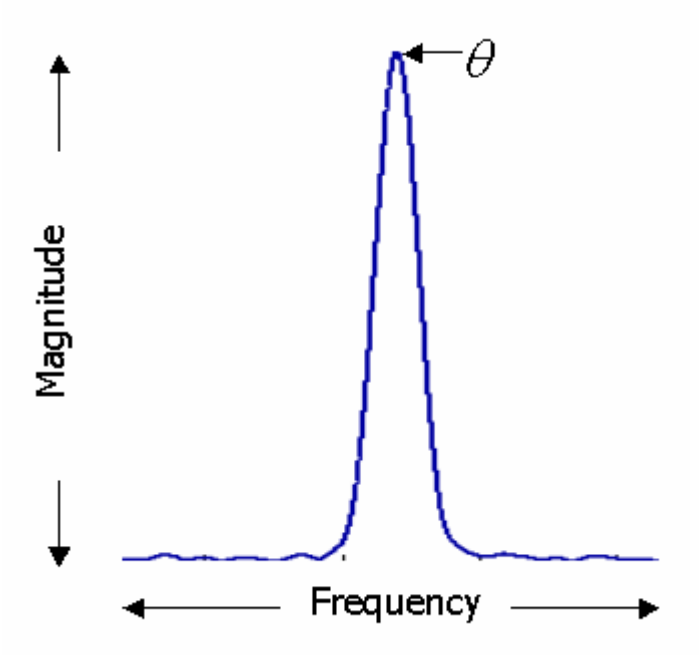

Fig. 5.16 Compact representation of the Fourier transform

5.6 Windowing of the Data

The sinusoidal trace is initially shaped by a decaying exponential due to the variable attenuation of the wire, and by a rectangular window, since the trace is limited to the frequency range from 50 kHz to 1.3 MHz. Fig. 4.16 shows an example of this sinusoidal trace that was obtained from a line with a single fault. This exponentially decaying shape of the trace and its limitation in length will cause spreading of the Fourier transform.

These problems cause loss of resolution in the measurements, and yields spurious reflection points. The problem can be improved by applying a weighted window to the trace. The effects of these windows are described next.

5.6.1 The windowing effect

Here we will explain the windowing effect to better understanding the effect caused by the windows that interact with the trace (rectangular window, exponential decaying window and weighted window)

Consider a discrete-time signal consisting of the sum of two sinusoidal components (that could be the case of a trace measured from a line with two faults); i.e.

$$x[n] = A_0 \cos(\omega_0 n + \theta_0) + A_1 \cos(\omega_1 n + \theta_1) \tag{5.17}$$

Multiplying *x[n]* by the window *w[n],* yields the windowed sequence *v[n]*.

$$v[n] = A_0 w[n] \cos(\omega_0 n + \theta_0) + A_1 w[n] \cos(\omega_1 n + \theta_1) \tag{5.18}$$

To obtain the discrete-time Fourier transform of *v[n]* we can expand equation 5.18 in terms of complex exponentials and it results:

$$v[n] = \frac{A_0}{2} w[n] e^{j\theta_0} e^{j\omega_0 n} + \frac{A_0}{2} w[n] e^{-j\theta_0} e^{-j\omega_0 n}$$
$$+ \frac{A_1}{2} w[n] e^{j\theta_1} e^{j\omega_1 n} + \frac{A_1}{2} w[n] e^{-j\theta_1} e^{-j\omega_1 n} \tag{5.19}$$

Utilizing the frequency-shifting property

$$e^{j\omega_0 n} w[n] \xleftrightarrow{F} W(e^{j(\omega-\omega_0)}) \tag{5.20}$$

the Fourier transform of the windowed sequence result:

$$V[e^{j\omega}] = \frac{A_0}{2} e^{j\theta_0} W[e^{j(\omega-\omega_0)}] + \frac{A_0}{2} e^{-j\theta_0} W[e^{j(\omega+\omega_0)}]$$
$$\frac{A_1}{2} e^{j\theta_1} W[e^{j(\omega-\omega_1)}] + \frac{A_1}{2} e^{-j\theta_1} W[e^{j(\omega+\omega_1)}] \tag{5.21}$$

According to this equation, the Fourier transform of the windowed signal consists of the Fourier transform of the window replicated at the frequencies $\pm\omega_0$ and $\pm\omega_1$. This result is also scaled by the complex amplitudes of the individual complex exponentials that make up the signal. This can be illustrated in the next figure. Fig. 5.17(a) shows the Fourier transform of a rectangular window function $|W(e^{j\omega})|$, described by equation 5.22, and Fig. 5.17(b) shows the Fourier transform of the windowed signal $|V(e^{j\omega})|$ ($x[n]w[n]$). In this example, the signal has two sinusoidal frequency components with frequencies $\frac{2\pi}{6}$ and $\frac{2\pi}{3}$.

$$w(\lambda) = A \cdot rec(\frac{\lambda}{\tau}) \xleftrightarrow{F} W(f) = \frac{A \cdot \sin(f\pi\tau)}{f\pi} \tag{5.22}$$

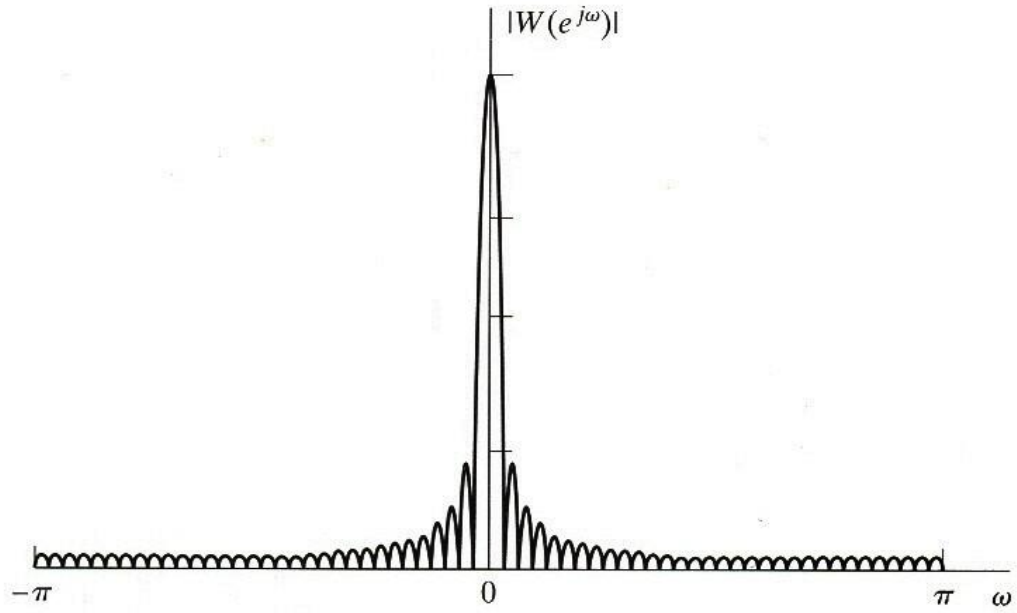

(a)

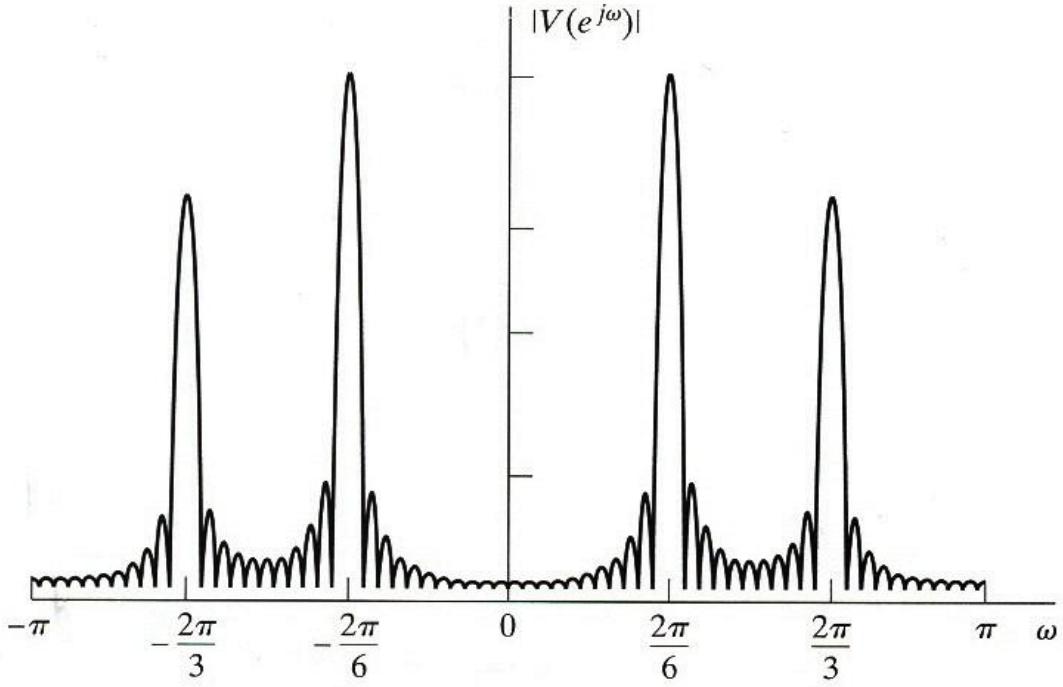

(b)

Fig. 5.17 (a) Fourier transform of window (b) Fourier transform of windowed signal having two frequency signals. (Figure taken from [12])

From this figure, we can see the effects of windowing a signal constituted by the sum of sinusoidals (which is the case of the traces that we obtain with the W-FDR system). This effect consists in the replication of the Fourier transform of the window (that reshapes the trace), at the frequencies of the sinusoidals that constitute the trace.

The effect of the exponential decaying window in a sinusoid trace, consists in the superposition of the Fourier transform of this window at the frequencies of the sinusoids that constitute the trace, as happens in the example of Fig. 5.17. Therefore, it spreads the lobes that correspond to the Fourier transform of the harmonics in the trace.

Since we are always affected by the effect of the rectangular window (because we can not have an infinite length sinusoid trace), the effect of the exponential decaying window just overlaps over the effect of the rectangular window, causing and extra spreading the final result. In our measurements this will result in the lost of resolution. The Fourier transform of the decaying exponential function is

$$w(\lambda) = e^{-\alpha \cdot \lambda} u(\lambda) \overset{F}{\longleftrightarrow} W(f) = \frac{1}{\alpha + j2\pi f} \tag{5.23}$$

where α is the decay rate.

To compensate for the spreading effect caused by the exponentially decaying window and the rectangular window, we multiply the trace by a weighted window. The primary effects of this window in the frequency domain are the reduction of spectral leakage (which is what we are looking for) and the reduction of resolution (which is not too significant). The reduction in resolution is influenced primarily by the width of the main lobe of $W(f)$ (Fourier transform of the window), while the degree of leakage depends on the relative amplitude of the main lobe and the side lobes of $W(f)$.

Table 5.1 shows a comparison of the commonly used windows (Hanning, Hamming, Blackman, Bartlett and Rectangular). In column one, we compare the peak side-lobe amplitude for the different windows. A larger magnitude yields to better reduction of spectral leakage. Column two compares the approximate width of the main lobe, which is related to the resolution of the window.

Type of window	**Peak side-lobe amplitude (dB)**	**Approximate width of main lobe**
Rectangular	-13	$4\pi/(N+1)$
Bartlett	-25	$8\pi/N$
Hanning	-31	$8\pi/N$
Hamming	-41	$8\pi/N$
Blackman	-57	$12\pi/N$

Table 5.1 Comparison of commonly used windows (data taken from [12])

For this project we used the Blackman window because it provides better reduction of spectral leakage than any of the other window, and the increased width of the main lobe is not significant when compared with the spreading due to the initial exponential window. Fig. 5.18, illustrates the resolution and spectral leakage of the Blackman window.

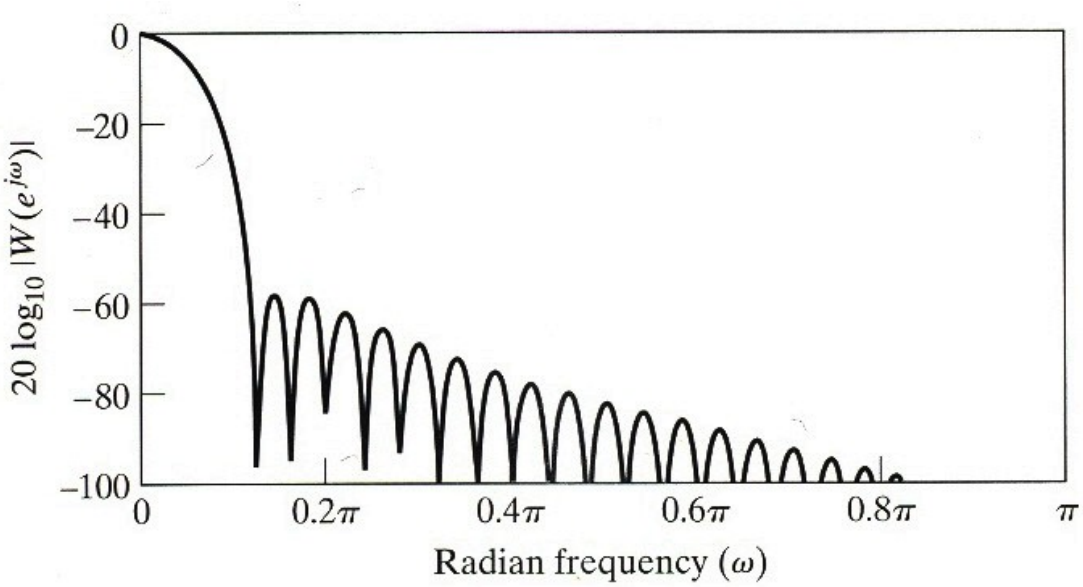

Fig. 5.18 Fourier transform of Blackman window (Figure taken from [12])

Fig. 5.19 shows the results obtained from the measurement of an open circuit at 1200 m after applying the Fourier transform without using the Blackman window to improve the results. Fig. 5.20 shows the same results after using the Blackman window. We can clearly see the improvement obtained after applying this window.

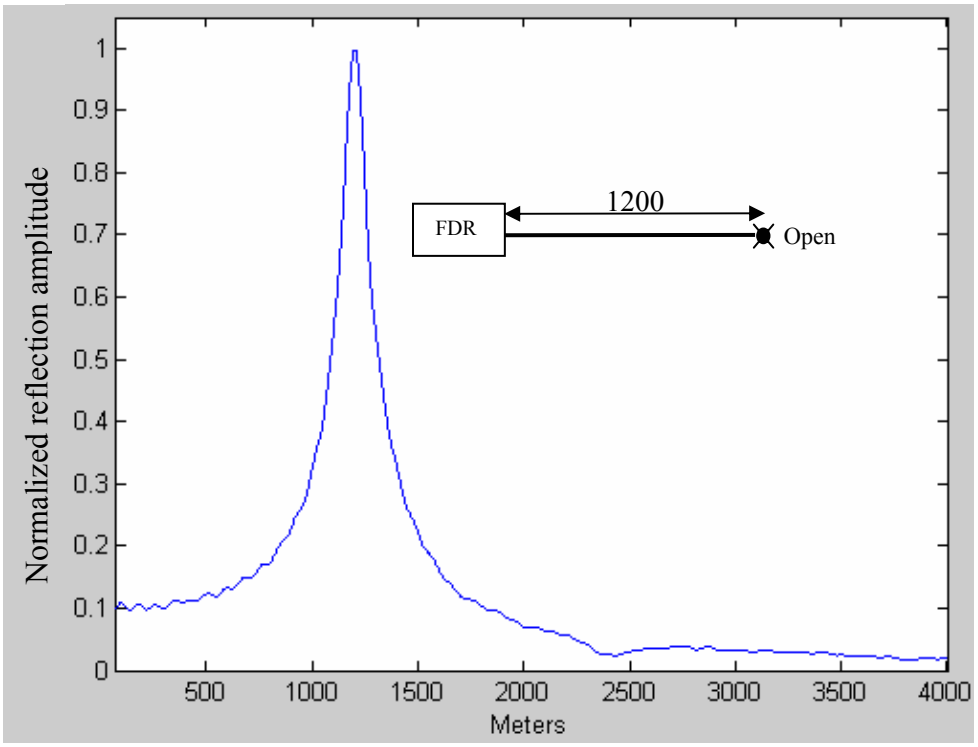

Fig. 5.19 Measurement of an O.C. at 1200 m without windowing

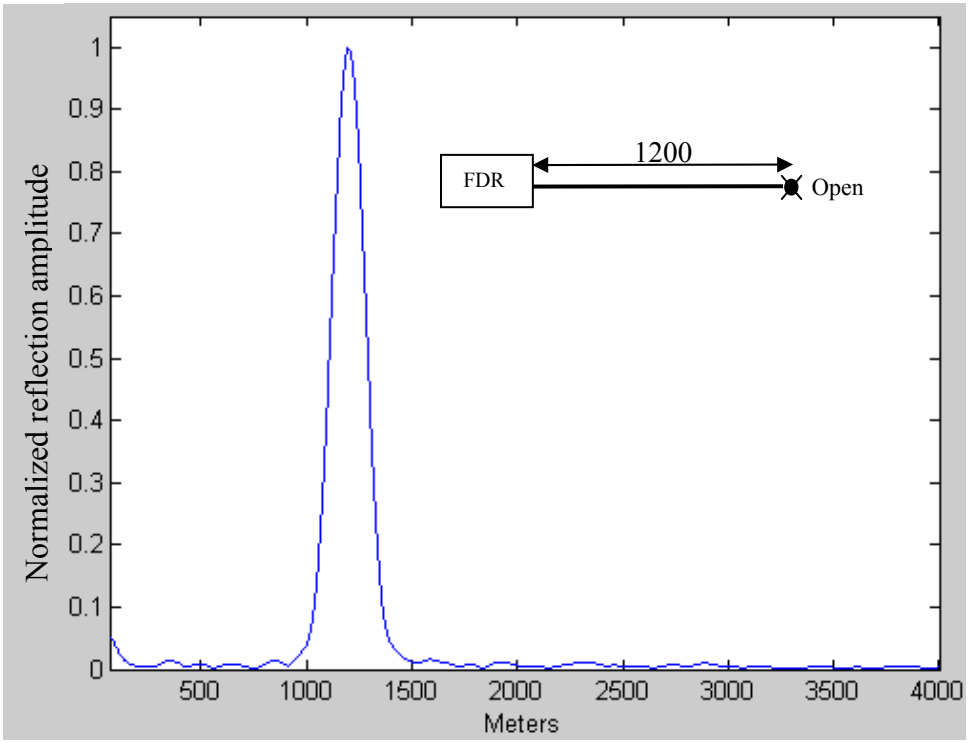

Fig. 5.20 Measurement of an O.C. at 1200 m using the Blackman window

5.7 Compensation for loss vs. distance to reflection

Due to the attenuation properties of the telephone wire, the reflected signal returning from a fault is more attenuated when the fault is more distant. For this reason, as we measure farther, the reflection magnitude that we obtain in the final result is more attenuated.

This can be illustrated in Fig. 5.21. This graph represents a measurement of a 200 m bridge tap at 800 m without using any distance loss compensation. In this graph we can see that the second reflection, which corresponds to the end of the bridge tap, is smaller than the first reflection that corresponds to the junction point. In reality the first reflection should have an amplitude 1/4 smaller than the amplitude of the second reflection. Nevertheless, the second reflection looks smaller due to attenuation, because it is 200 meters farther than the first one.

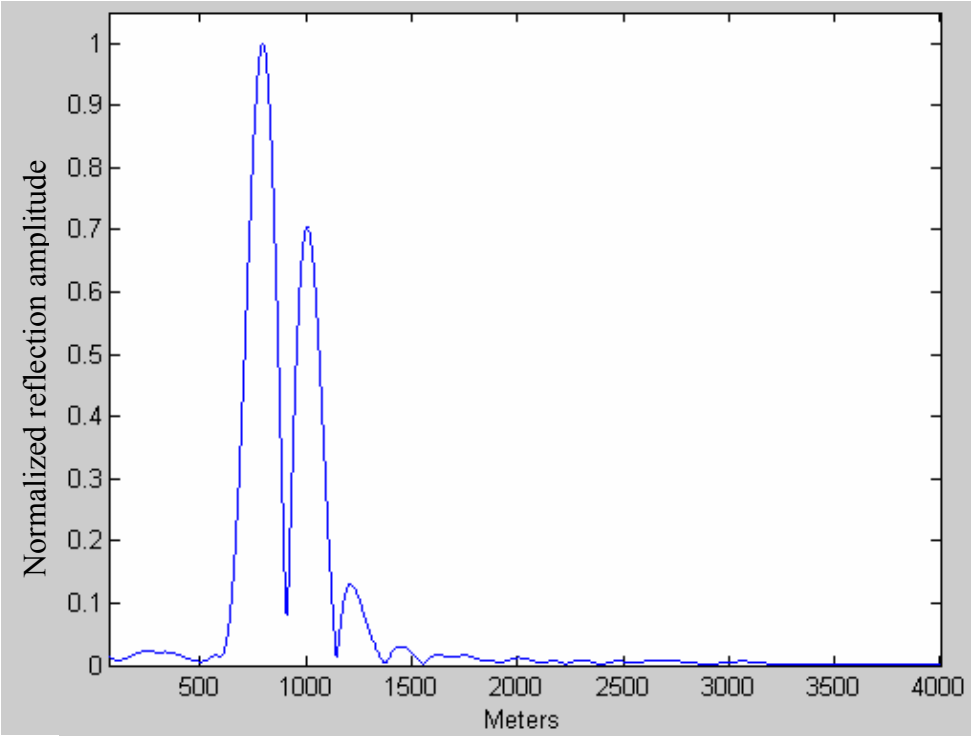

Fig. 5.21 Measurement of a 200 m bridge tap at 800 m, without using distance loss compensation

To compensate for this increasing attenuation with distance, we multiply the magnitude of the transform result, by a function that increases its magnitude with distance. This function was empirically determined and it is shown below.

$$\frac{1}{e^{-0.003 \cdot d} + 0.015 e^{-0.0015 \cdot d} + 0.01} \tag{5.24}$$

where d is distance in meters. The response of this function is shown in Fig. 5.22. As we can see in this figure, the gain rate decreases as farther is the distance. The reason for this is because as farther is the measurement, the noise level is higher and the gain rate has to decrease.

In Fig. 6.19 we can see the change after applying this function to the measurement shown in Fig. 5.21, which doesn't have a compensation for distance loss.

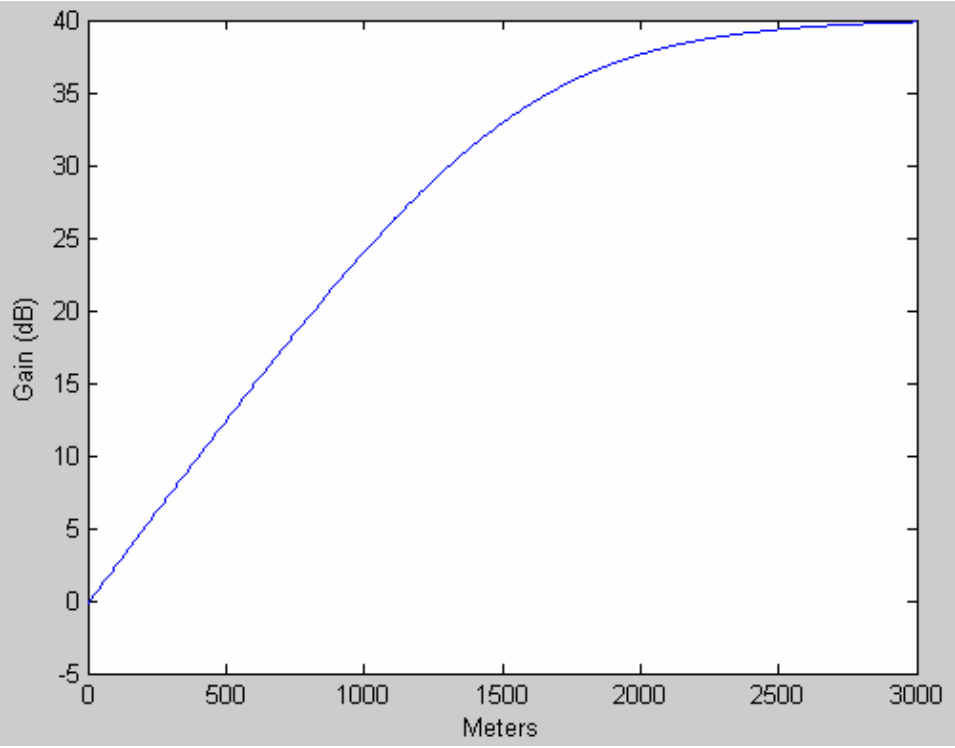

Fig. 5.22 Compensation for distance loss

5.8 Resolution

The distance resolution of the measurements can be determined calculating the time resolution, and then multiplying it by the propagation speed to convert it to distance. An estimate of the time resolution is given as $\frac{1}{\Delta f}$, where Δf is the useful frequency delta after applying the Blackman window, and the propagation velocity in the frequency range used is approximately 0.2 km/μs. In our measurements after applying the Blackman window, the useful frequency delta is approximately 500 kHz, which gives an estimate of 400 m.

5.8.1 Super-resolution

To make difficult measurements such as short bridge taps at long distances, we used a special algorithm "super-resolution" that improves, by several times, the resolution of the measurement. For example, with this algorithm we can estimate a 200 m bridge tap at 5 km, as is shown in Fig. 6.29.

To obtain the super resolution, the trace is zero padded down to 0 Hz and then, the algorithm flips the measured trace with respect to the *Y* axis. This duplicates the length of the trace and consequently, the number of cycles of the harmonics that form the trace. This increases the resolution of the measurement after applying the Fourier transform to the flipped trace. Fig. 5.23 shows a trace from an open circuit, which was flipped with respect the Y axis using this algorithm.

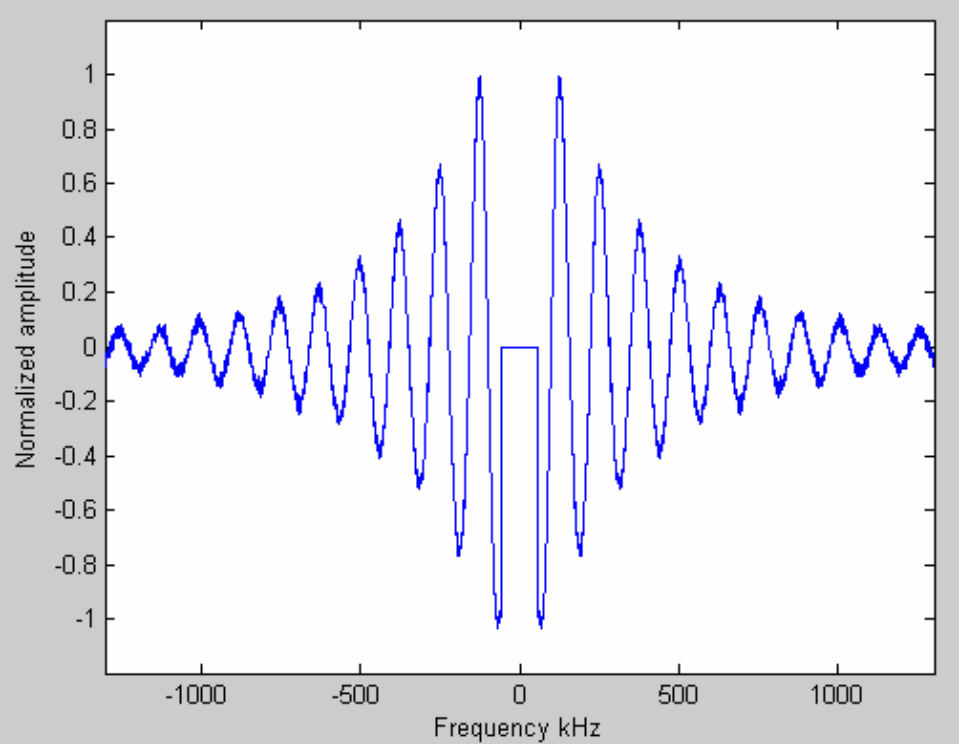

Fig. 5.23 Folded trace with respect to the Y axis

Once the trace has been duplicated by flipping it, then we window the full new trace. In this case, the low frequencies of the trace, which have the best amplitude, are not attenuated much by the window. This also helps in the improvement of the resolution. Recall that when we when we apply the window to a simple trace without flipping it, the lower frequencies are greatly attenuated.

After windowing the flipped trace, we increase the useful frequency delta (Δf) from 500 kHz (that we have in a simple trace) to approximately 1500 kHz. This gives an estimate distance resolution of 130 m.

It is important to highlight that this method can only be applied to measurements like open circuits, short circuits and bridge taps; where the reflection angle is ether 0° or 180° degrees. The reason is because these measurements have a trace with phase angle of 0° or 180° degrees, after being extrapolated down to 0 Hz.

Therefore, these traces are symmetric with respect to the *Y* axis, which makes possible to mirror the trace with respect to this axis.

Fig. 5.24 shows a measurement of an open circuit at 1200 m without using the super resolution, and Fig. 5.25 shows the same measurement, but this one processed using the super resolution. In these measurements, we can clearly see that the resolution improves significantly with the super resolution method.

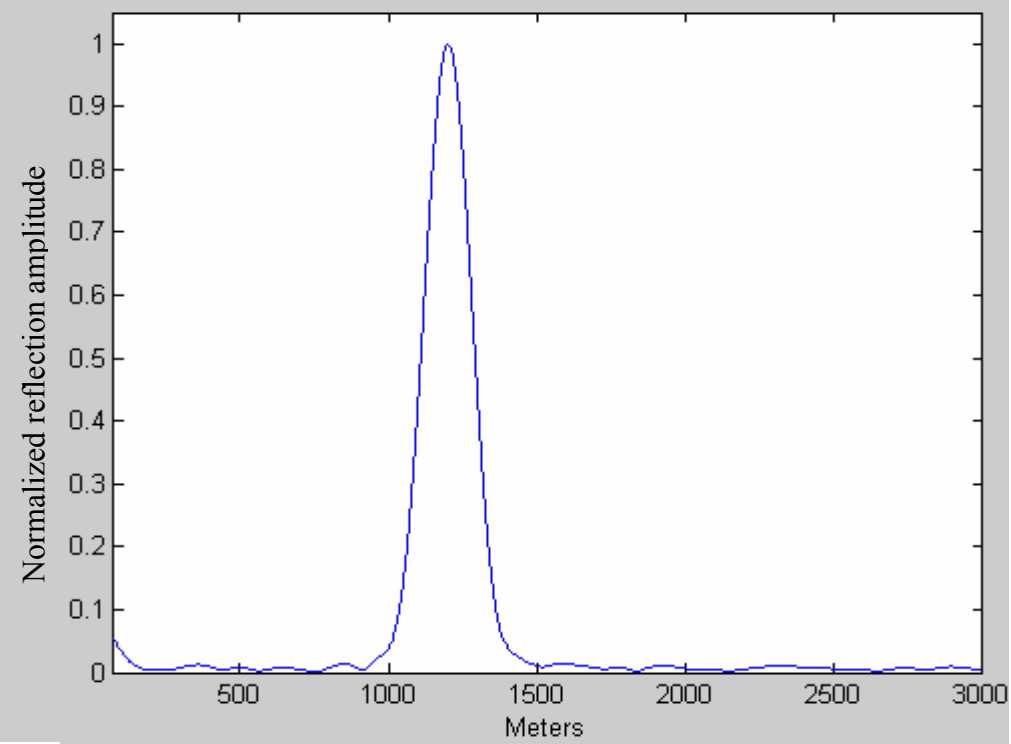

Fig. 5.24 Measurement processed without using super resolution

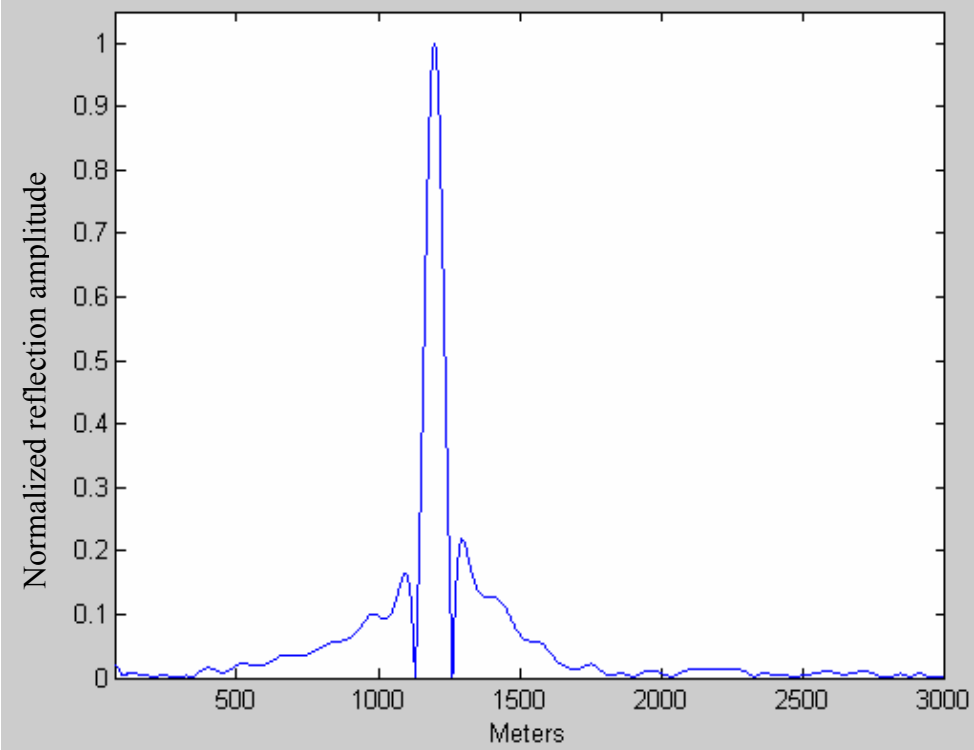

Fig. 5.25 Measurement processed using super resolution

6. System Results

This chapter describes the measurement system used to test lines using wideband frequency domain reflectometry (W-FDR). Measurement results are shown for a variety of faults in the telephone line.

6.1 Experimental setup

As we have explained, the W-FDR system performs a stepped frequency sweep to measure the line. For each frequency of the sweep the system measures the reflected signal and stores this value. The sequence of these values vs frequency forms a discrete trace. This system then saves the discrete trace into a file to be processed in MATLAB. Fig. 4.1 shows the block diagram of the W-FDR system used to perform the experiments.

To build this W-FDR system, we used a HP33120A waveform generator to produce the sinusoids at each frequency, and a TDS220 oscilloscope to digitize the reflected signal. This gave us the opportunity to obtain measurements of the trace with 2500 points of resolution. To control these two devices, we created a Labview program using the GPIB port to control the waveform generator and to receive data from the oscilloscope TDS220. This program sends a signal to the waveform generator to start producing the sinusoids of the stepped frequency sweep, and synchronizes the oscilloscope to capture a data point for each transmitted frequency. Once the sweep finishes, the oscilloscope, which is measuring the reflected signal from the fault, will have captured the entire trace. The time represented in the screen of the oscilloscope is exactly the same as the time that is taken for the sweep. After the oscilloscope has captured the trace, the labview program reads the trace from the oscilloscope through the GPIB port and stores the trace in a file to be processed in

MATLAB. Fig. 6.1 illustrates the connections of the hardware used for the experiments.

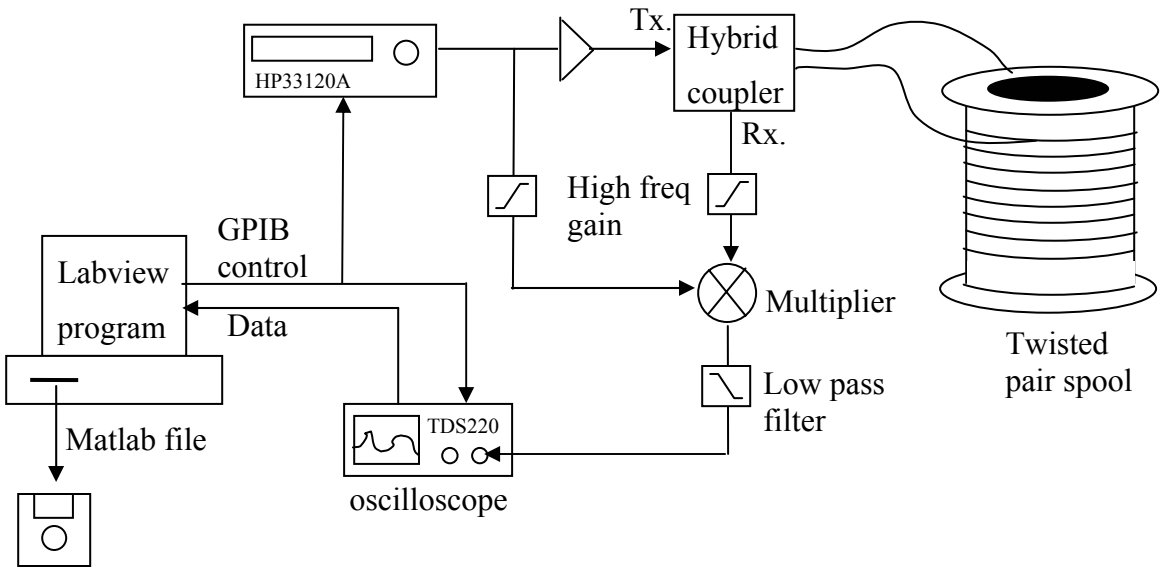

Fig. 6.1 W-FDR system connections

6.2 Open and short circuits

In this section are shown the results obtained after processing the measurement obtained with the W-FDR system (trace). These results were obtained measuring one single fault on the line. Next are shown several measurements from open and short circuits up to 5.2 km.

In the case of an open circuit, the reflection coefficient is $\rho = +1 = 1\angle 0^0$. Therefore, the reflection coefficient angle that we expect to obtain in these measurements is $\theta = 0^0$. For the case of the short circuit, the reflection coefficient is $\rho = -1 = 1\angle 180^0$, thus, the reflection coefficient angle that we expect to obtain in these measurements is $\theta = 180^0$.

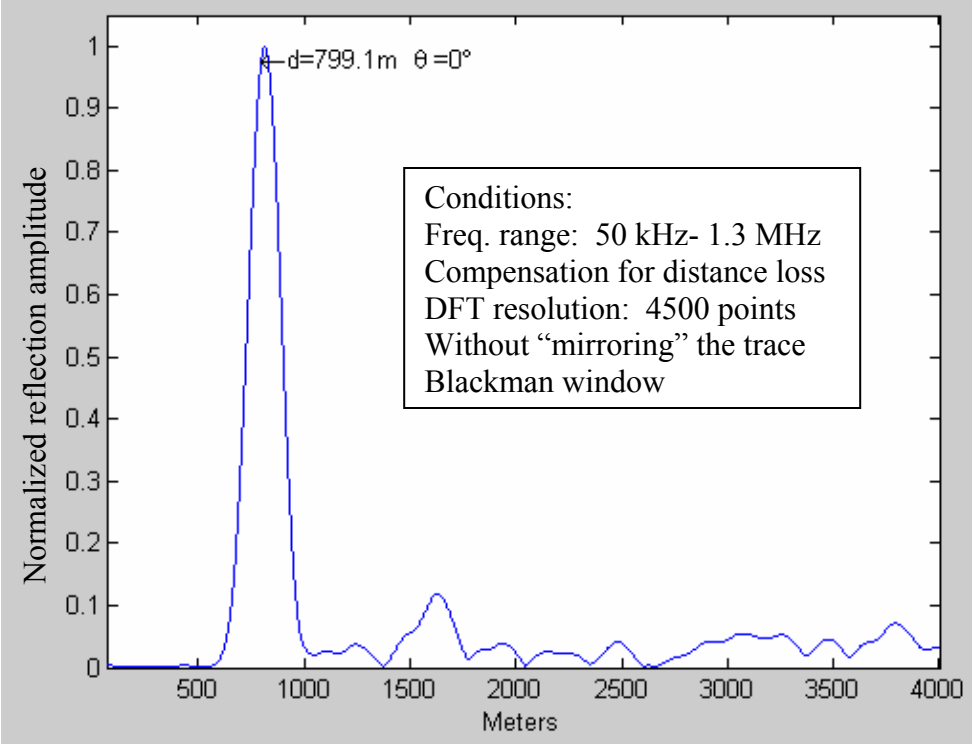

Fig. 6.2 Open circuit at 800 m

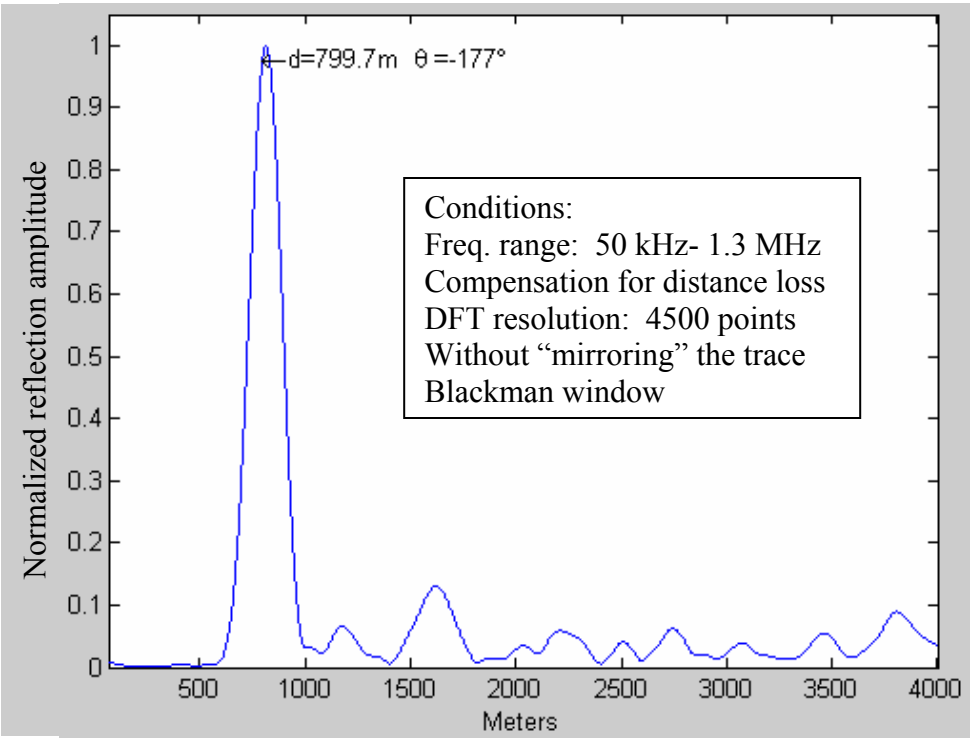

Fig. 6.3 Short circuit at 800 m

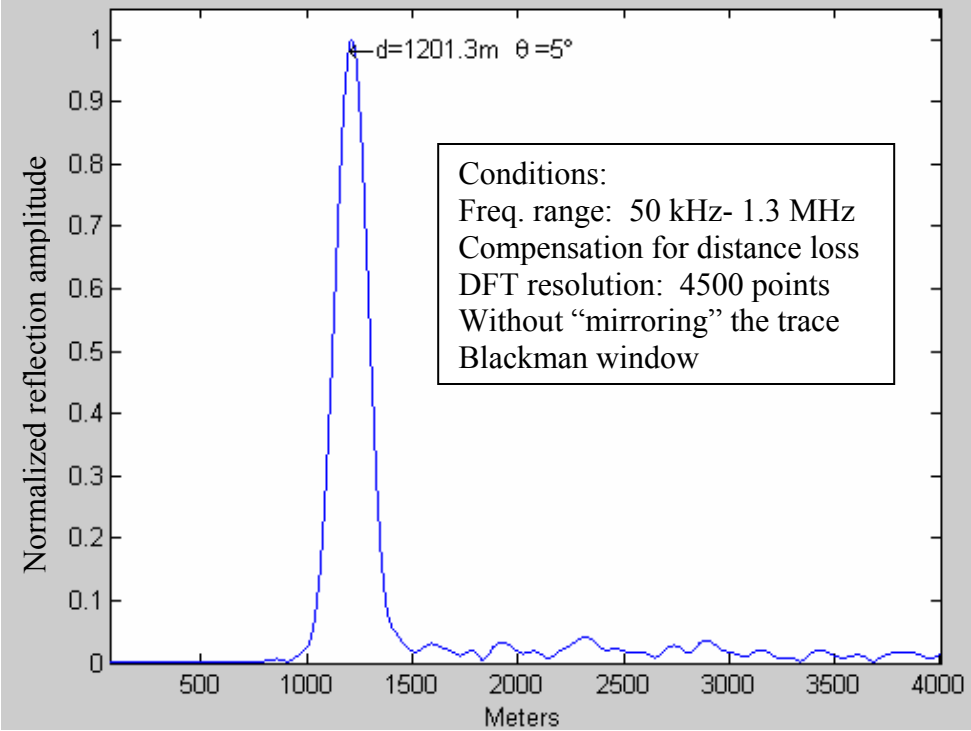

Fig. 6.4 Open circuit at 1200 m

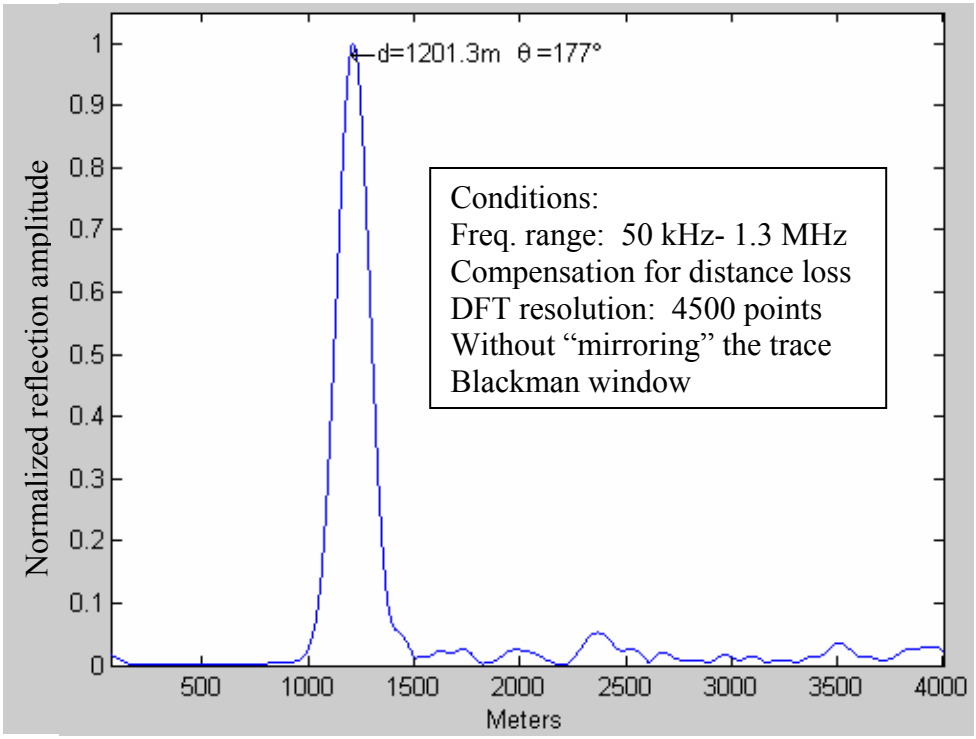

Fig. 6.5 Short circuit at 1200 m

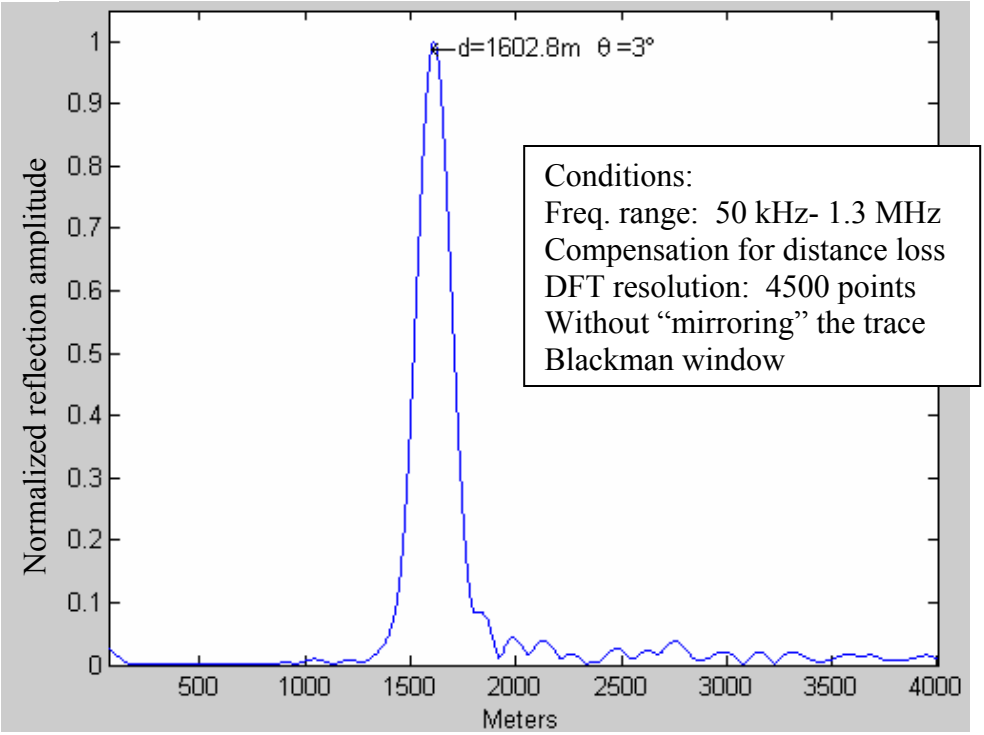

Fig. 6.6 Open circuit at 1600 m

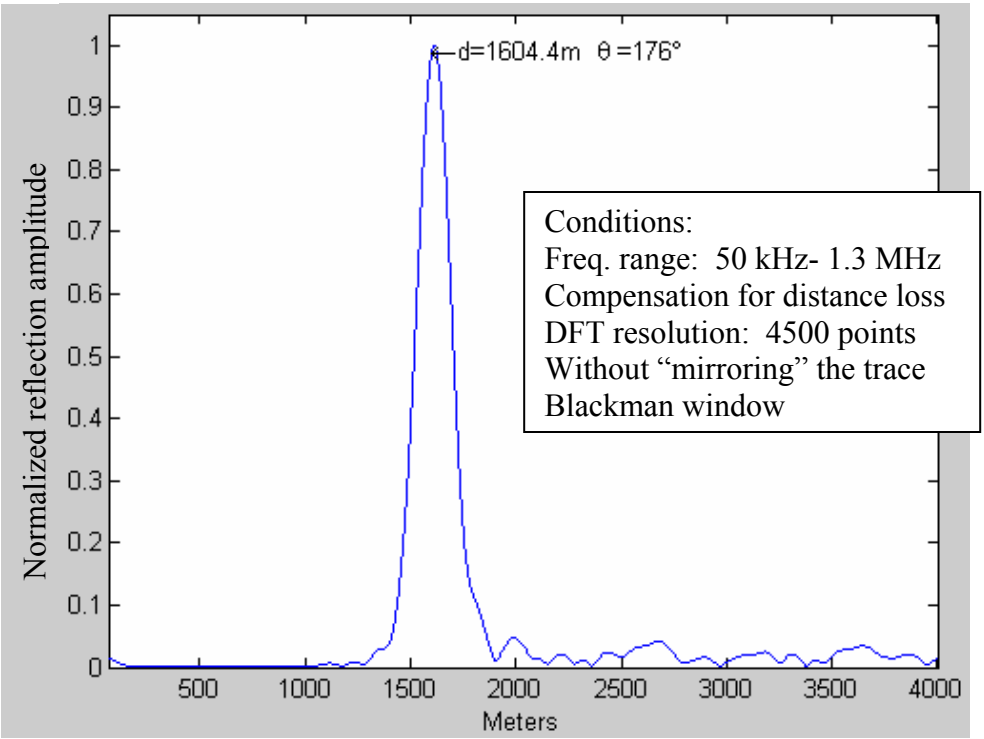

Fig. 6.7 Short circuit at 1600 m

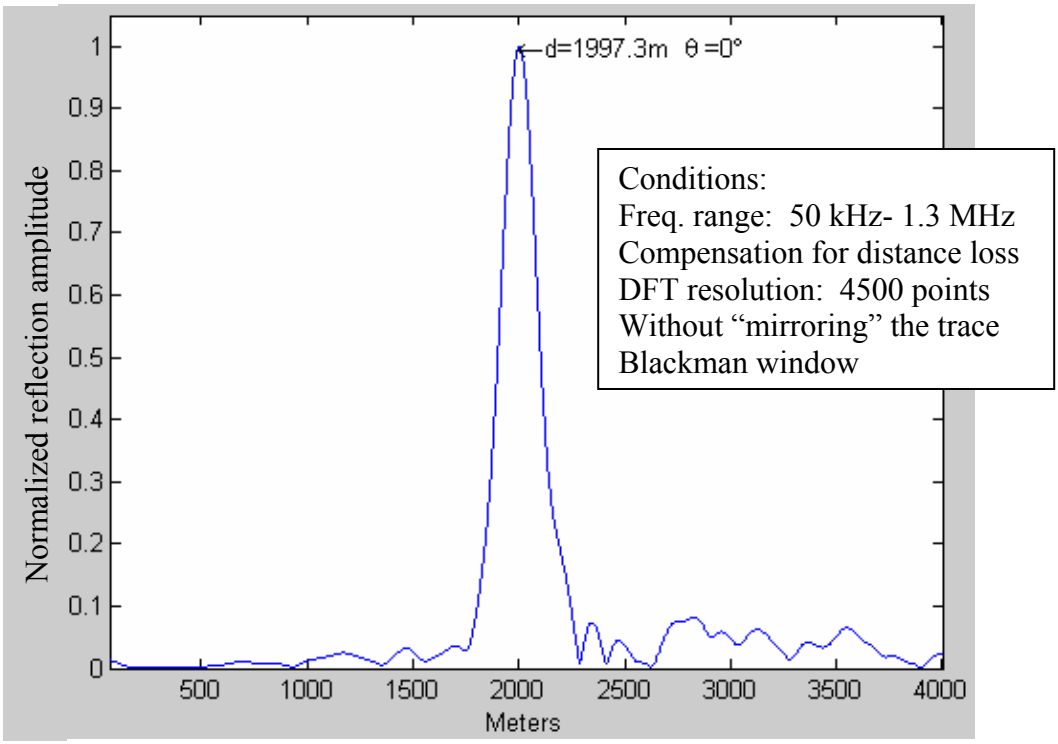

Fig. 6.8 Open circuit at 2000 m

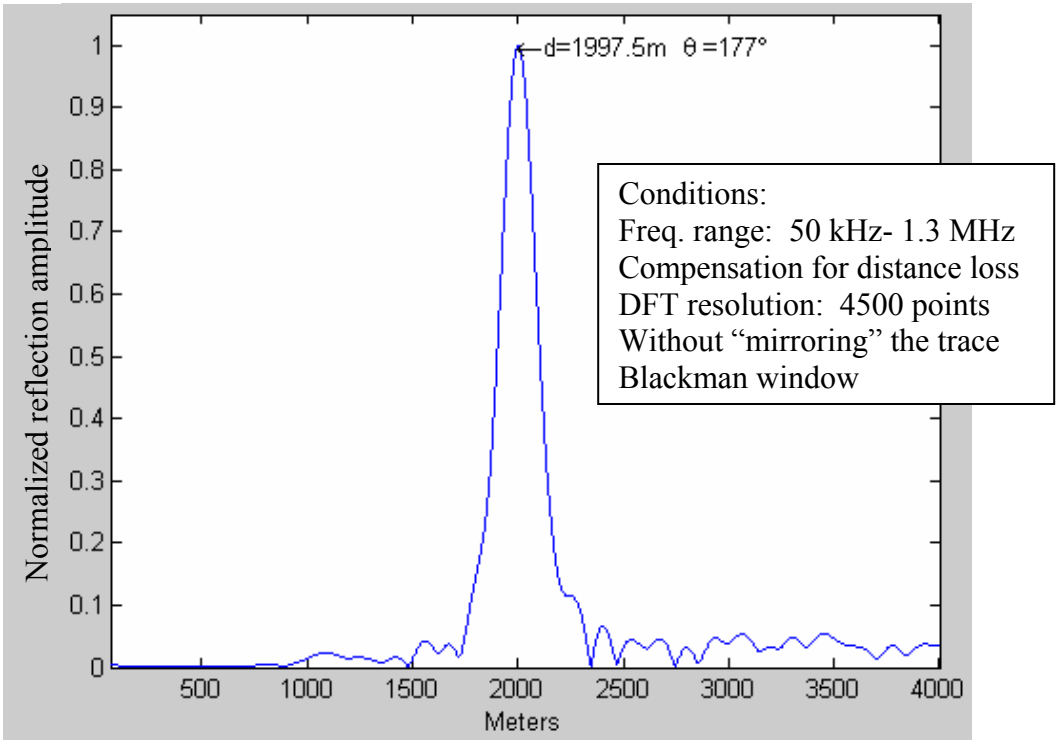

Fig. 6.9 Short circuit at 2000 m

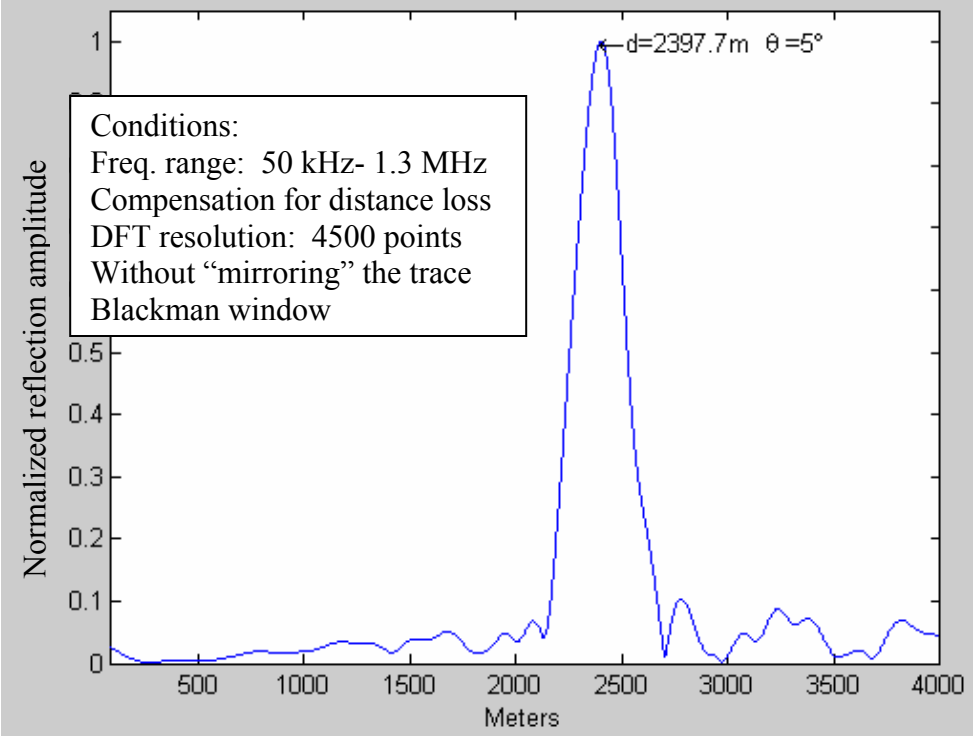

Fig. 6.10 Open circuit at 2400 m

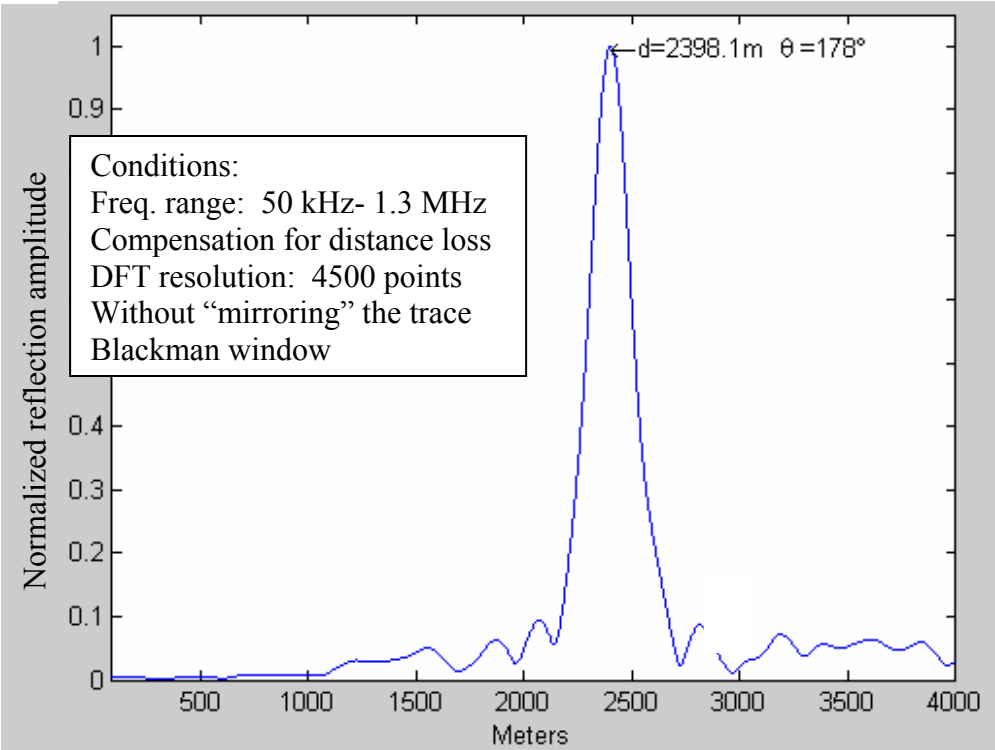

Fig. 6.11 Short circuit at 2400 m

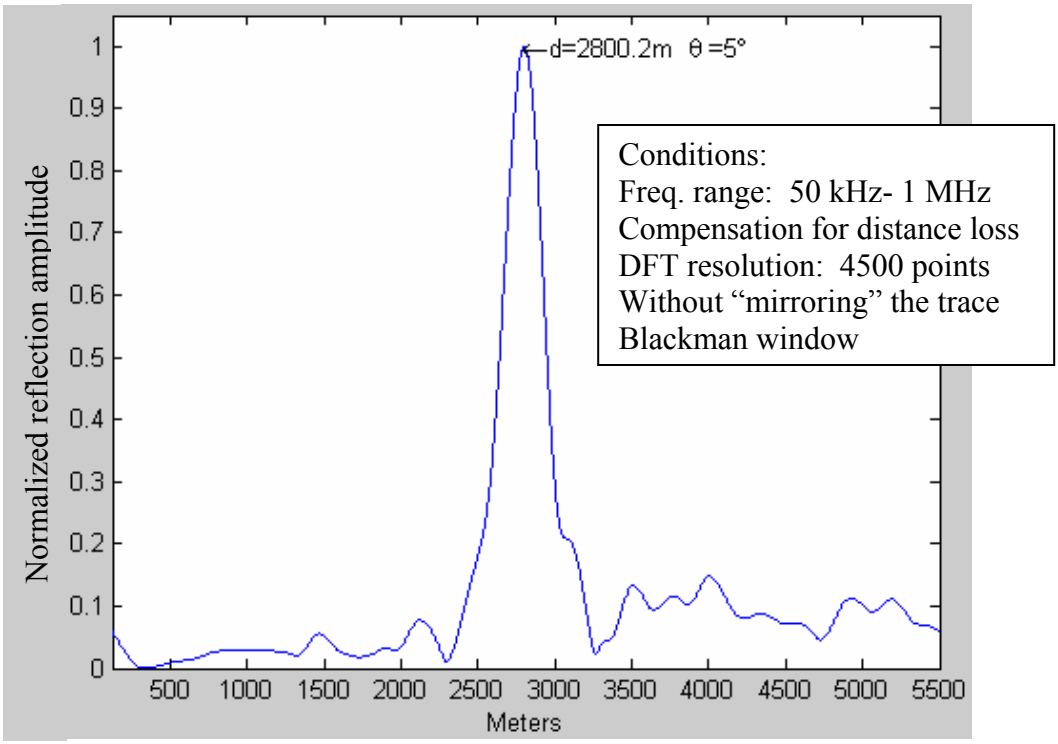

Fig. 6.12 Open circuit at 2800 m

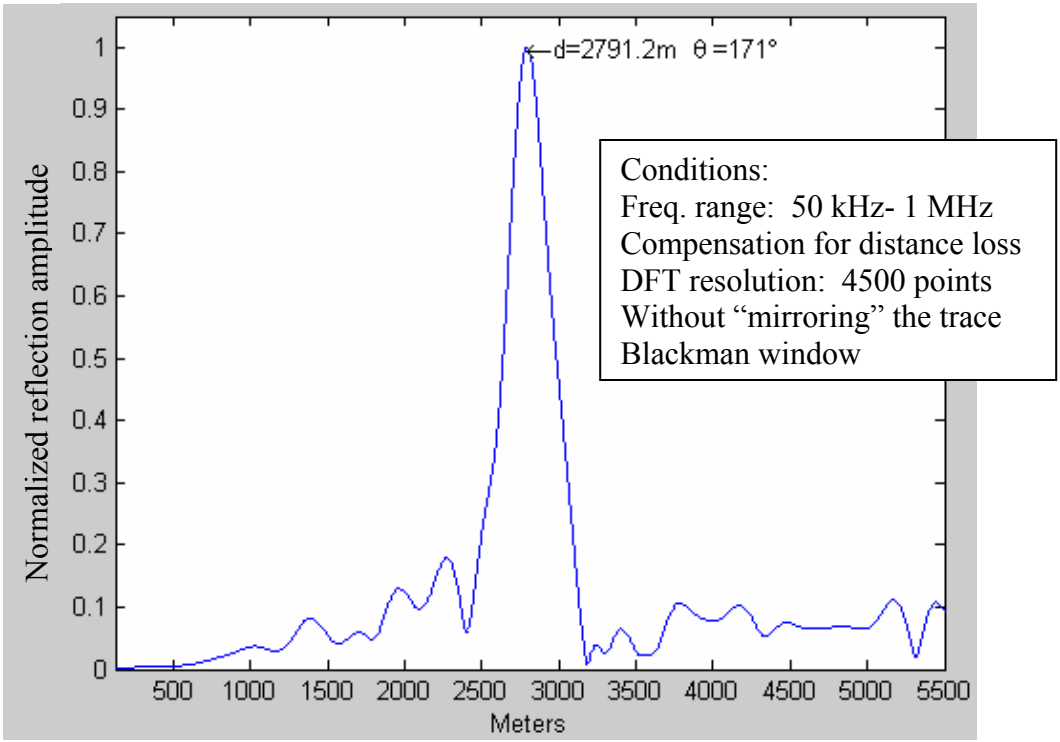

Fig. 6.13 Short circuit at 2800 m

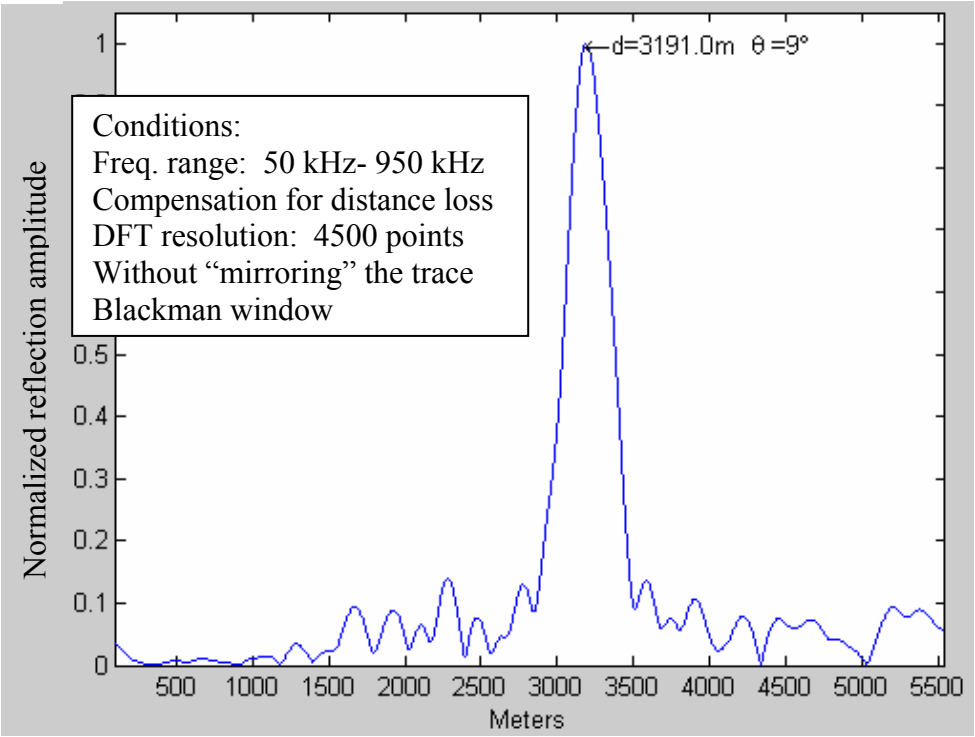

Fig. 6.14 Open circuit at 3200 m

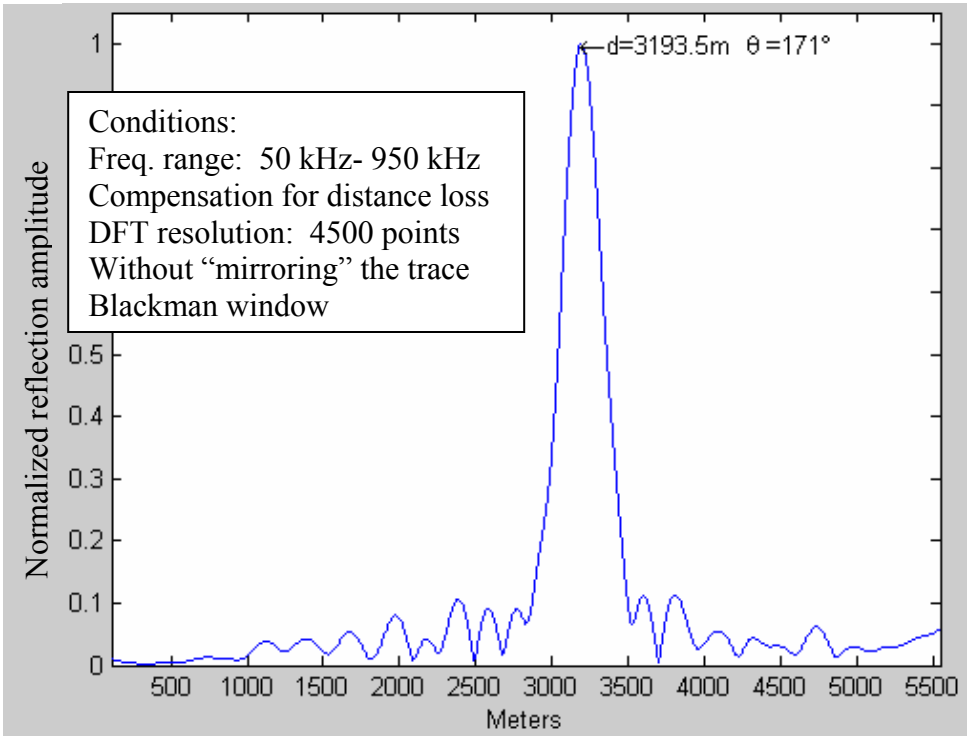

Fig. 6.15 Short circuit at 3200 m

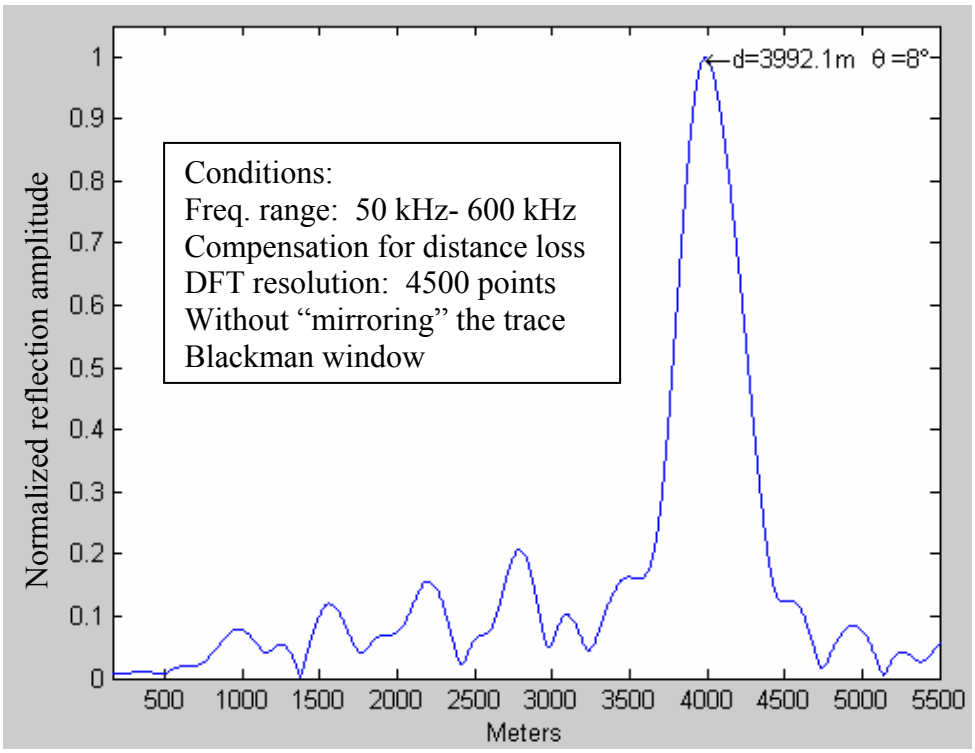

Fig. 6.16 Open circuit at 4 km

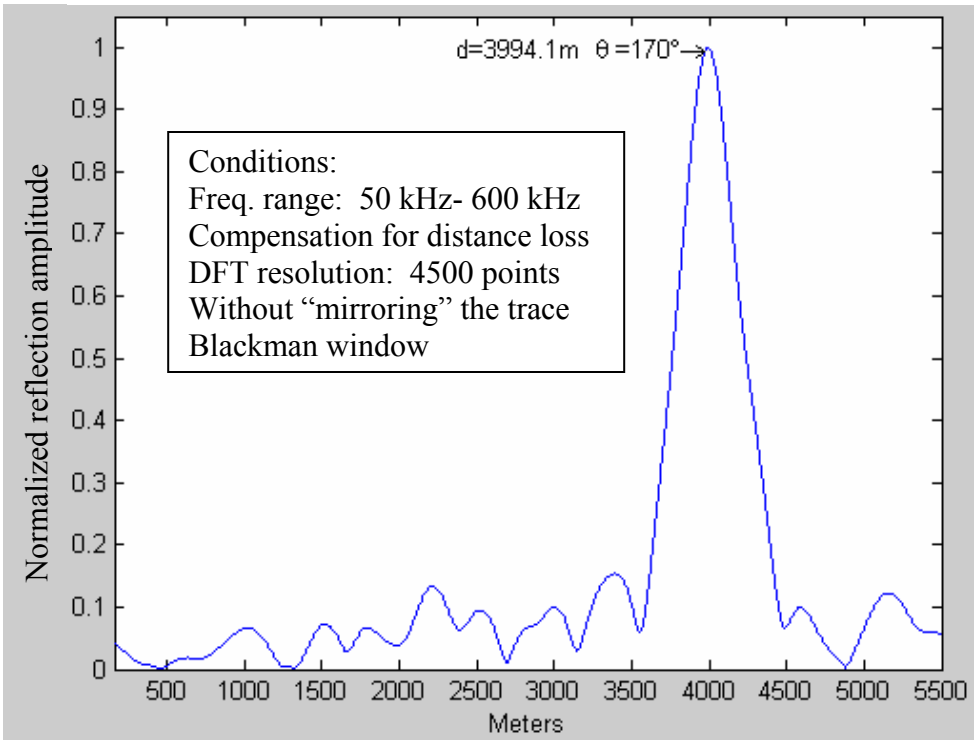

Fig. 6.17 Short circuit at 4 km

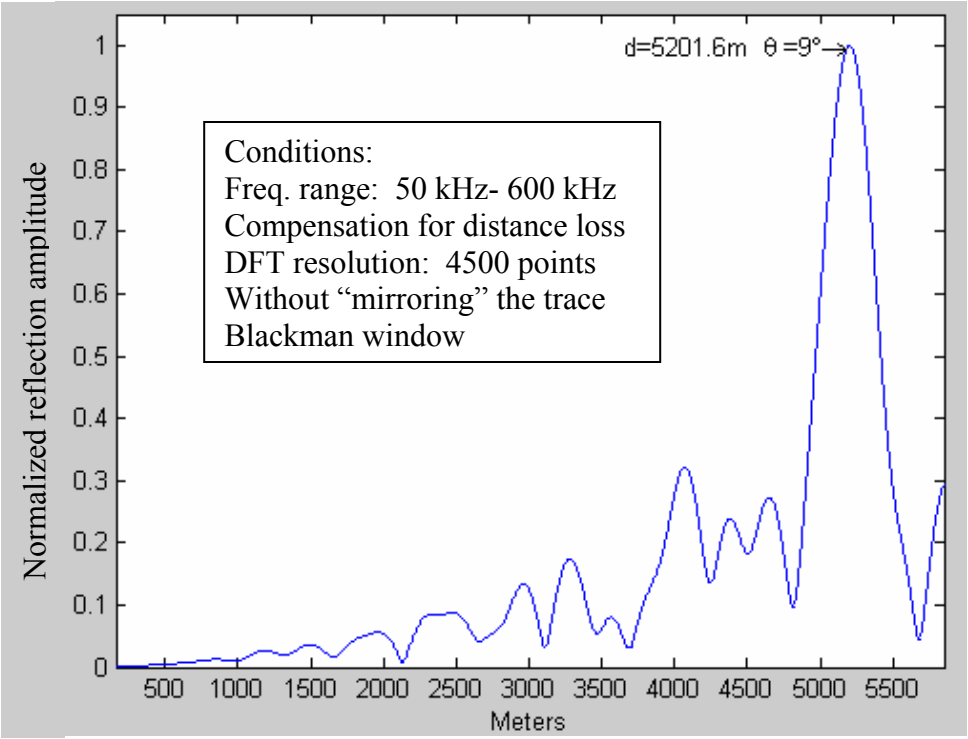

Fig. 6.18 Open circuit at 5.2 km

Figure above shows a measurement of an open circuit at 5.2 km. The width of the reflection peak in this measurement has increased, because the line attenuation limits the usable frequency range in the trace. For example, in this measurement the usable frequency range is from 50 kHz to 600 kHz, while in a measurement at 2.4 km, the usable frequency range is from 50 kHz to 1.3 MHz.

Spurious peaks in this measurement are assumed to be due to crosstalk in the 25 pair cable used for the measurement, because the cable is 400 meters long and the different pairs have been connected back and forth to give the required length of the line.

6.3 Complex loops

In this section we will show the results obtained from measuring complex loops with several faults. This includes measurements of one and two bridge taps terminated with an open or a short circuit.

Each figure shows a diagram of the line structure in test, with the distance of each section of the line. This includes the distance between the test instrument and the first bridge tap, the distance between bridge taps (in case of two bridge taps), and the length of the bridge taps. Also, shows how the bridge taps were terminated (in an open or a short circuit).

The following graphs show how W-FDR can accurately estimate the distance to each fault on the complex loop and the reflection angle of these faults. Using W-FDR, it is possible to estimate the structure of a complex loop.

Table 6.1 shows the reflection coefficient angle for the faults in the complex loops. In this way we can see the accuracy of the reflection angles estimated in the next measurements.

Fault	Angle
Bridge tap	180°
Open circuit	0°
Short Circuit	180°

Table 6.1 Reflection coefficient angles

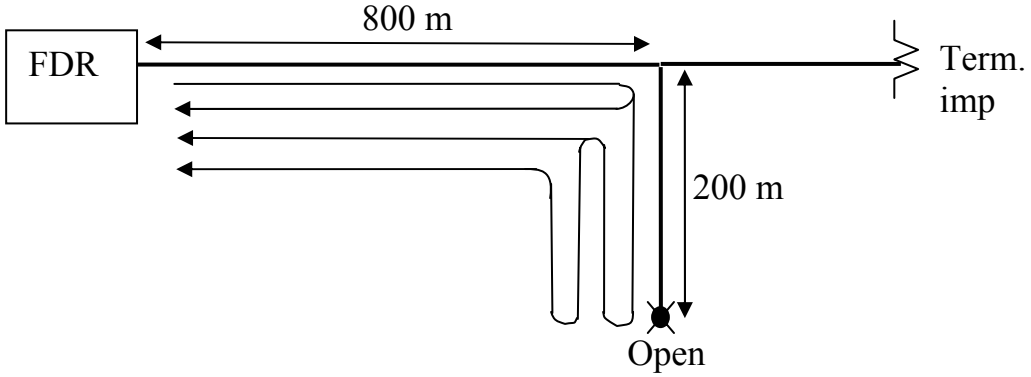

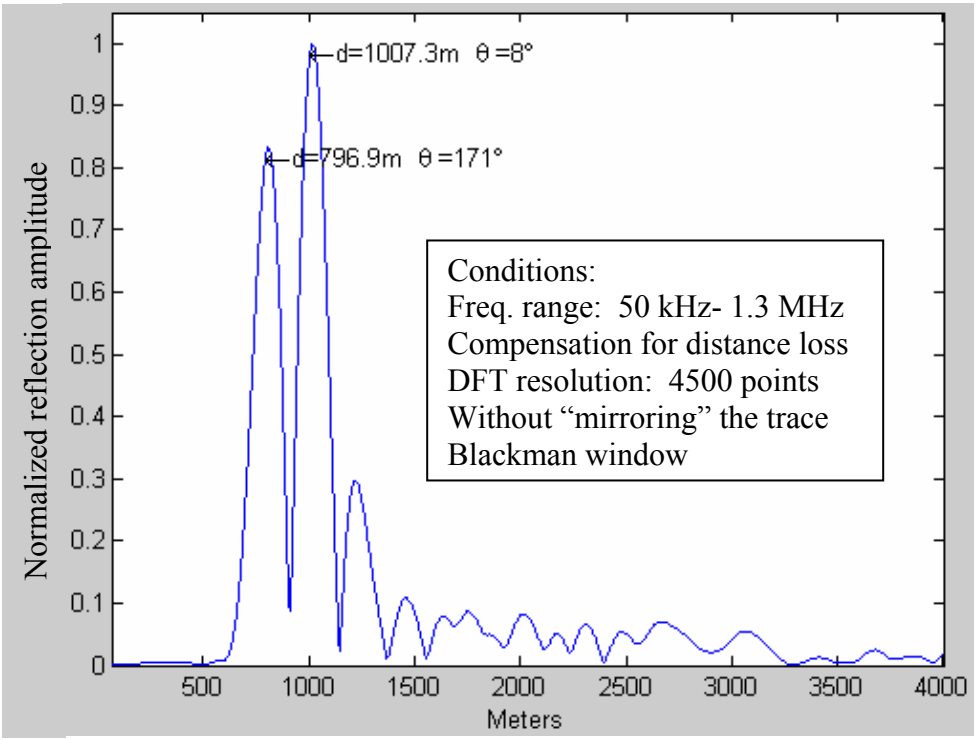

Fig. 6.19 200 m open circuit, bridge tap at 800 m

Next we show a measurement form a 400 m bridge tap. Fig. 6.20 shows the measured trace from this line using W-FDR. This trace is composed by two main frequencies that correspond to each reflection in the line. These are, from the junction of the bridge tap with the line, and from the end of the bridge tap. Fig. 6.21 shows the result after processing the trace. In this figure we can see that we can clearly estimate the location and length of the bridge tap after the processing of the trace, and even some secondary reflections caused by the bridge tap.

Figure below shows the structure of the line, where letter "A" represents the reflection from the junction, letter "B" represents the reflection from the open circuit at the end of the bridge tap, and "C" a secondary reflection from the bridge tap. These letters are also shown with their corresponding reflection peak in Fig. 6.21.

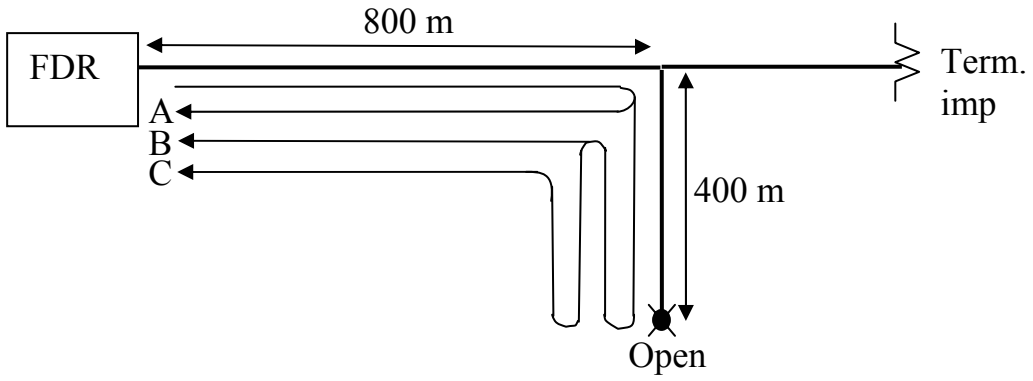

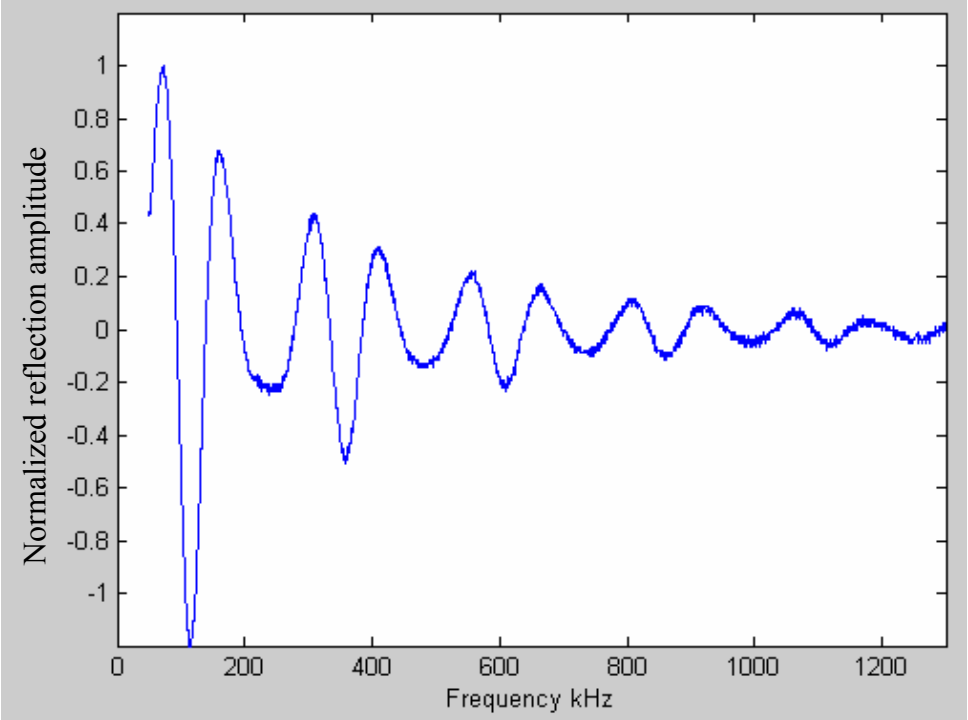

Fig. 6.20 Trace from a 400 m bridge tap at 800 m

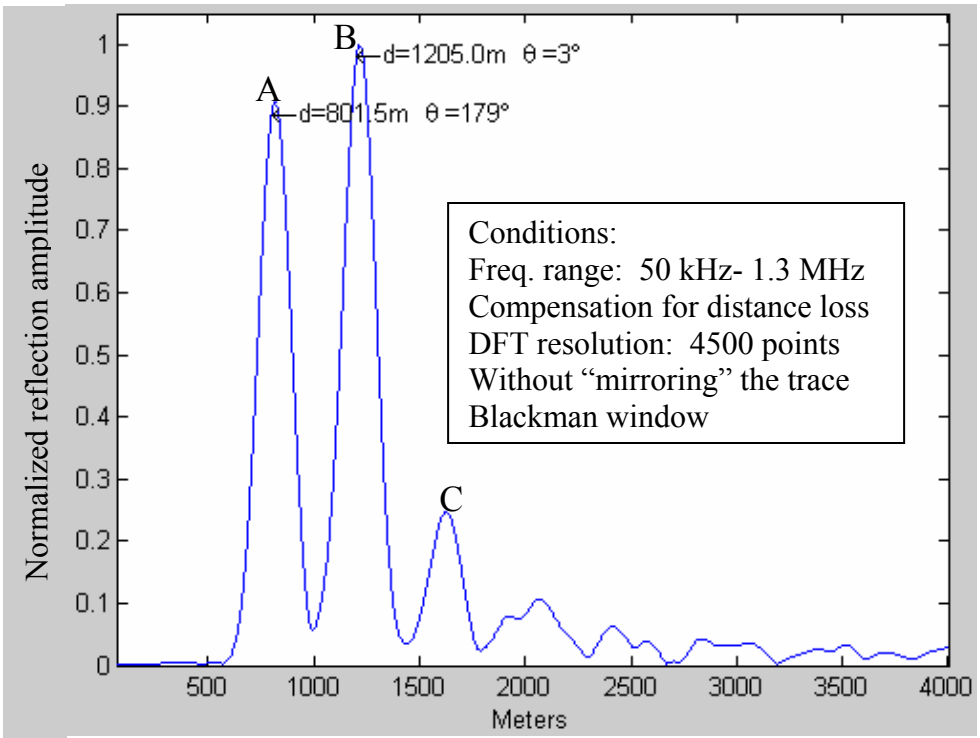

Fig. 6.21 400 m open circuit bridge tap at 800 m

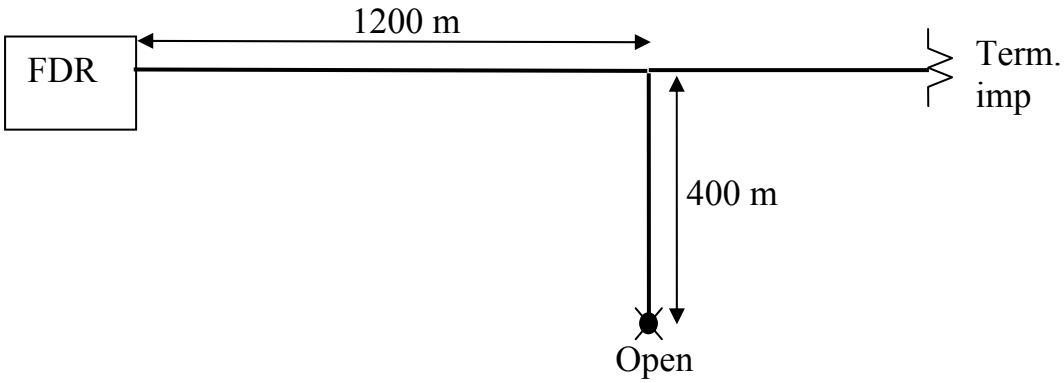

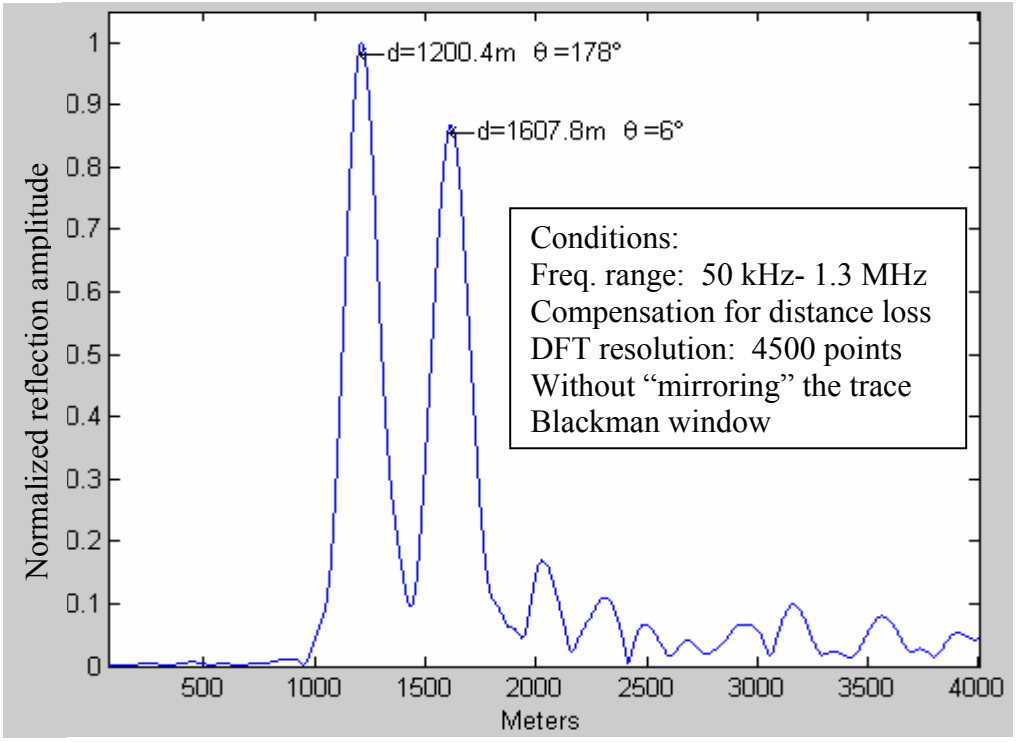

Fig. 6.22 400 m open circuit bridge tap at 1200 m

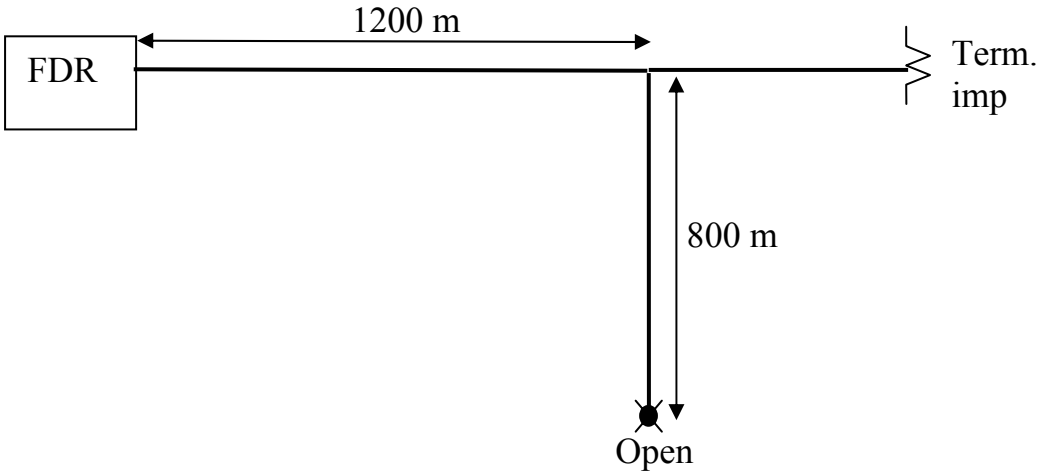

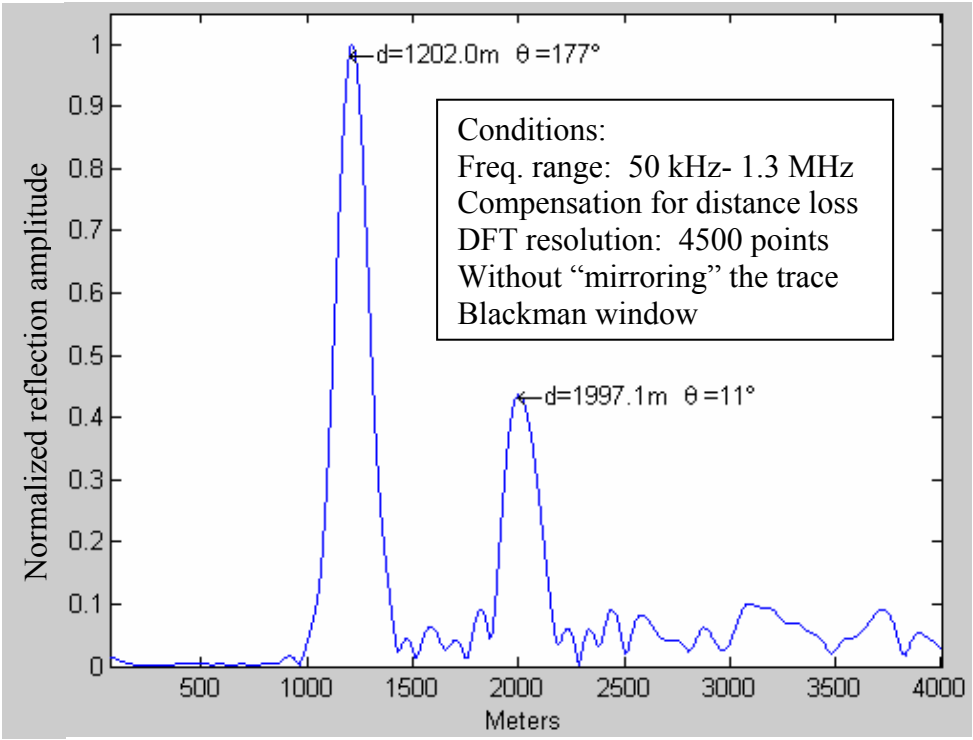

Fig. 6.23 800 m open circuit bridge tap at 1200 m

Next we show a measurement from a line that has 3 reflection points. This measurement presents an 800 m bridge tap that ends in a short circuit, and the line is terminated in an open circuit. This measurement shows that W-FDR can locate long bridge taps and estimate the reflection angle at the end of the bridge tap. In addition to the bridge tap, the measurement has one more reflection from the end of the line. This shows that this third reflection not only it does not affect the location of the long bridge tap, but also, this one is also clearly located and its reflection angle accurately estimated. Fig. 6.24 shows the trace of this measurement, which is constituted by 3 frequencies that correspond to the reflection points. Fig. 6.25 shows the result after processing the trace, where we can see how the 3 reflections were located, and the reflection angle of each one were also estimated.

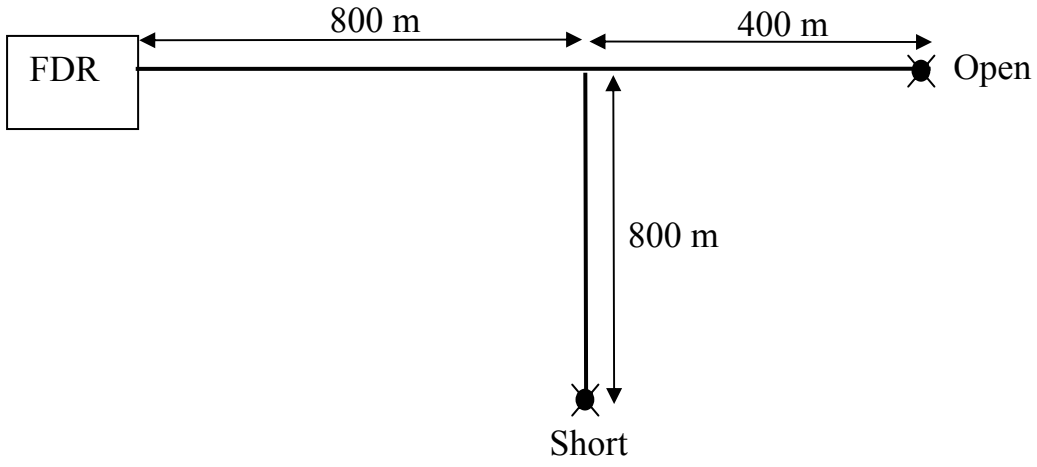

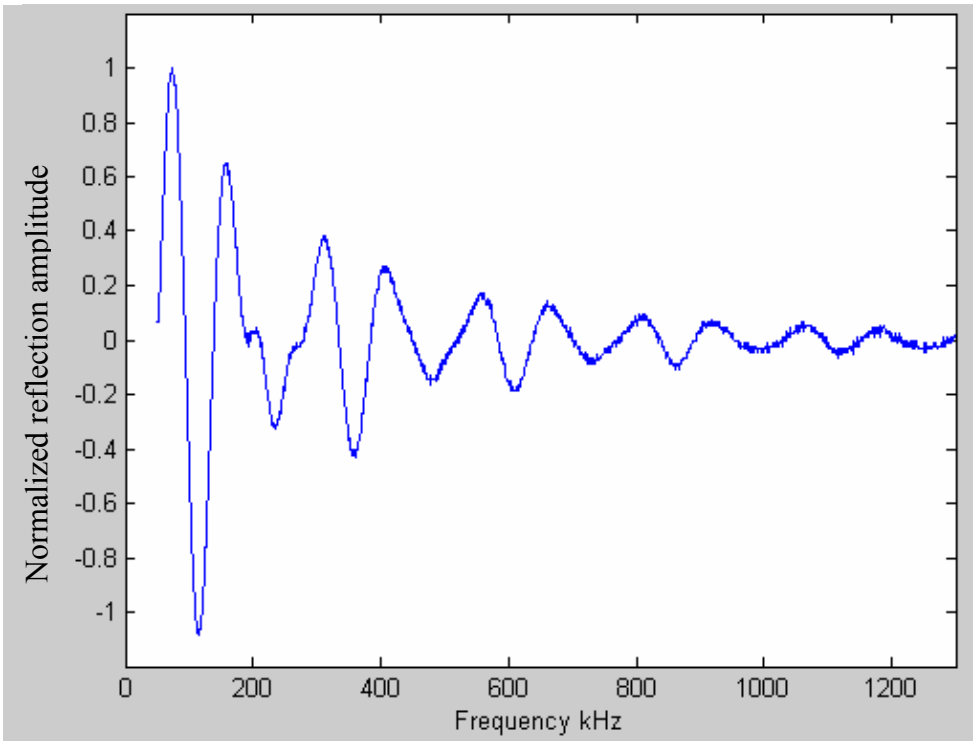

Fig. 6.24 Trace from an 800 m S.C. bridge tap with O.C. at end of line

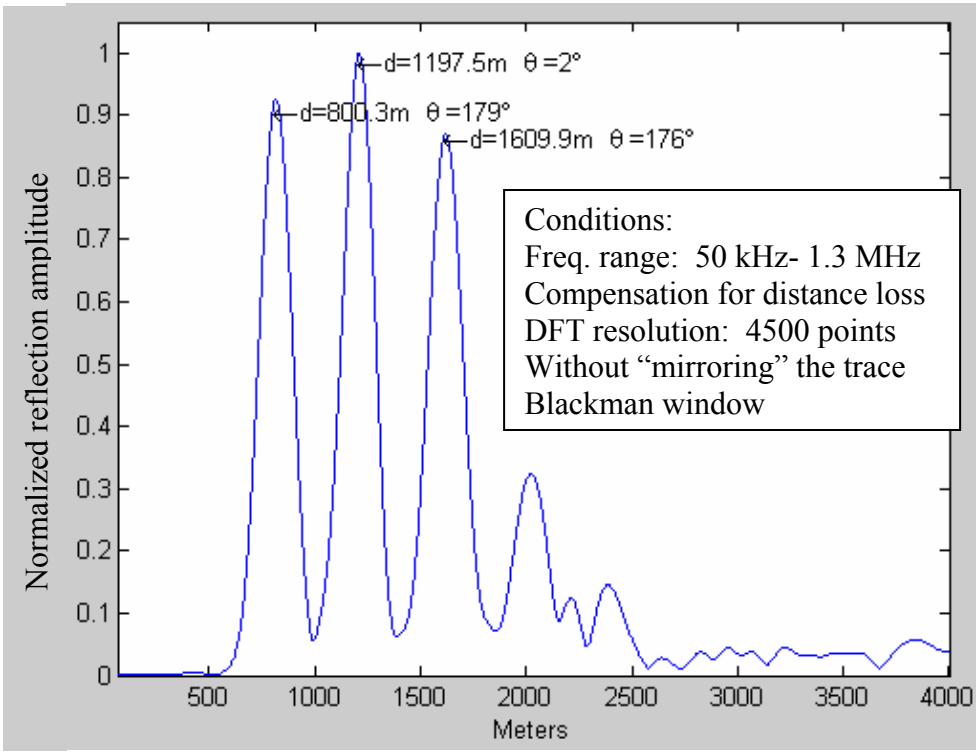

Fig. 6.25 800 m short circuit bridge tap with O.C. at end of line

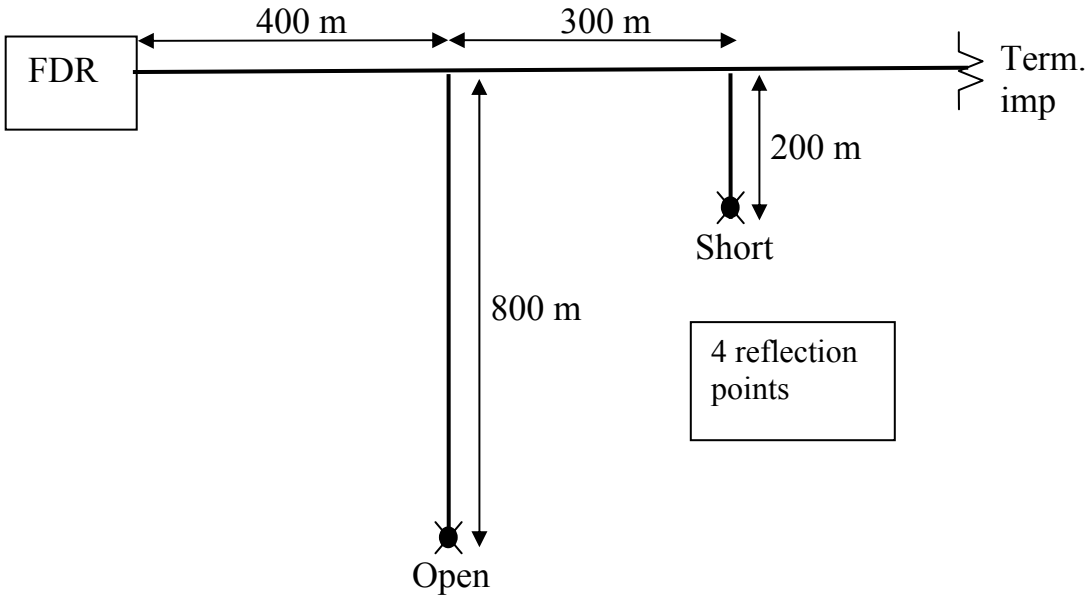

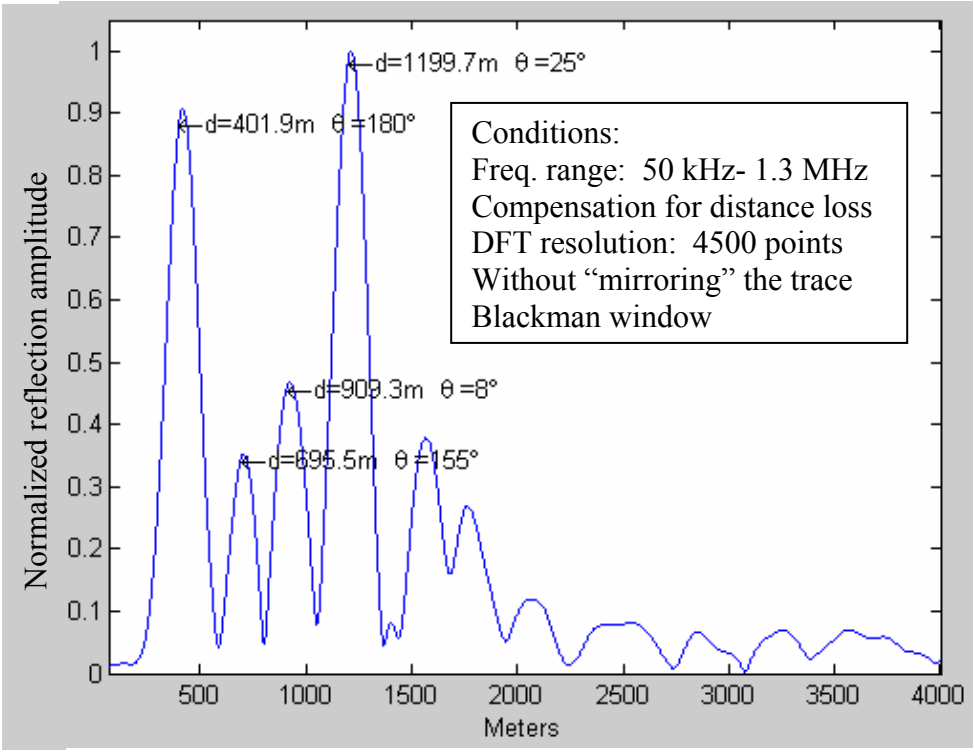

Fig. 6.26 Double open and short circuit bridge taps

Next we show a measurement of a complex loop that has 4 reflection points. The line has two bridge taps, the first one is 800 m long and terminated in a short circuit, and the second one is a short bridge tap (200 m) terminated in an open circuit. This measurement is interesting for several reasons. First, it shows that W-FDR can clearly locate two bridge taps with good resolution. Second, it shows that despite the number of reflections, it can accurately estimate the reflection angle for each fault, which tells the type of fault that is locating and helps to determine the structure of the line. Finally, the measurement also shows that W-FDR can locate in the same line from short to long bridge taps and estimate the length of these ones. Fig. 6.27 shows the trace of this measurement that is constituted by 4 frequencies that correspond to the reflection points of the line. Fig. 6.28 shows the result after processing the trace. In this figure we can clearly see the location of the 4 reflections, and the reflection angle of each, despite of the complexity of the line.

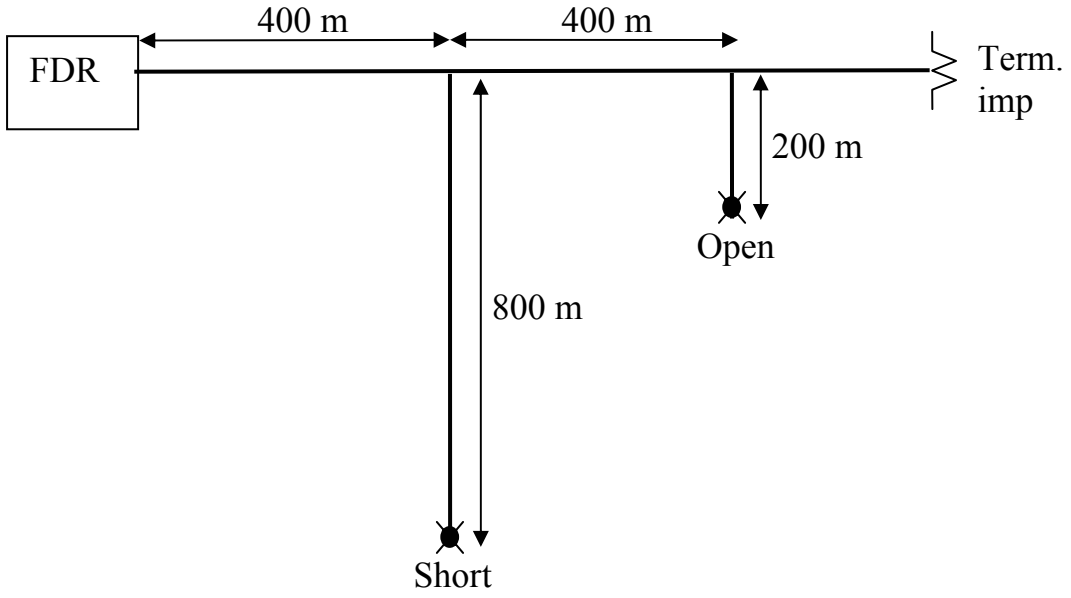

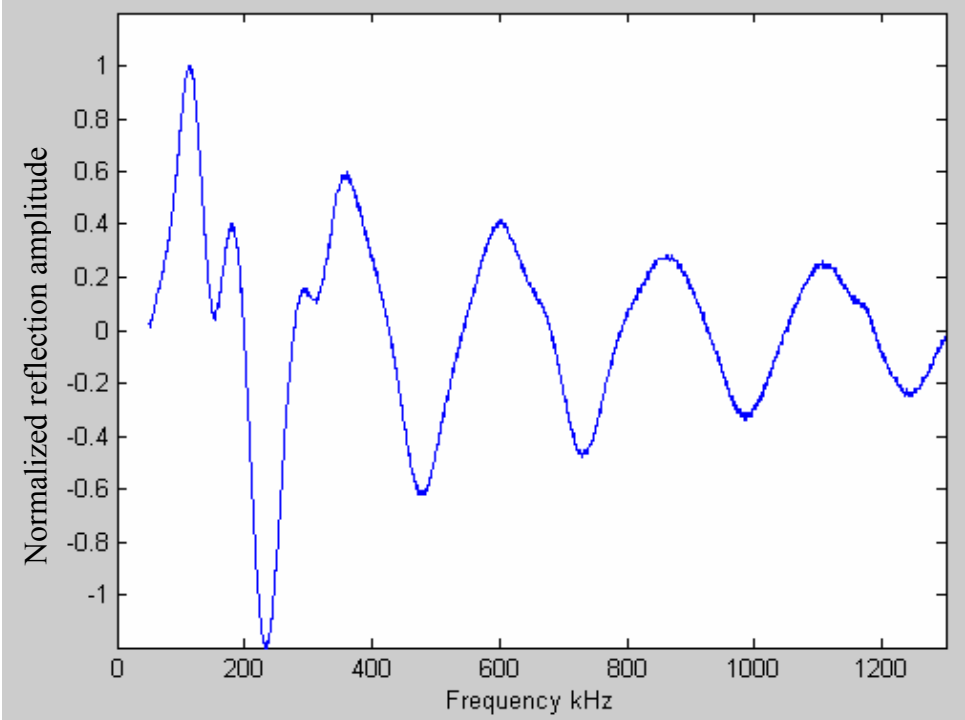

Fig. 6.27 Trace from a two bridge taps terminated in open and short circuit

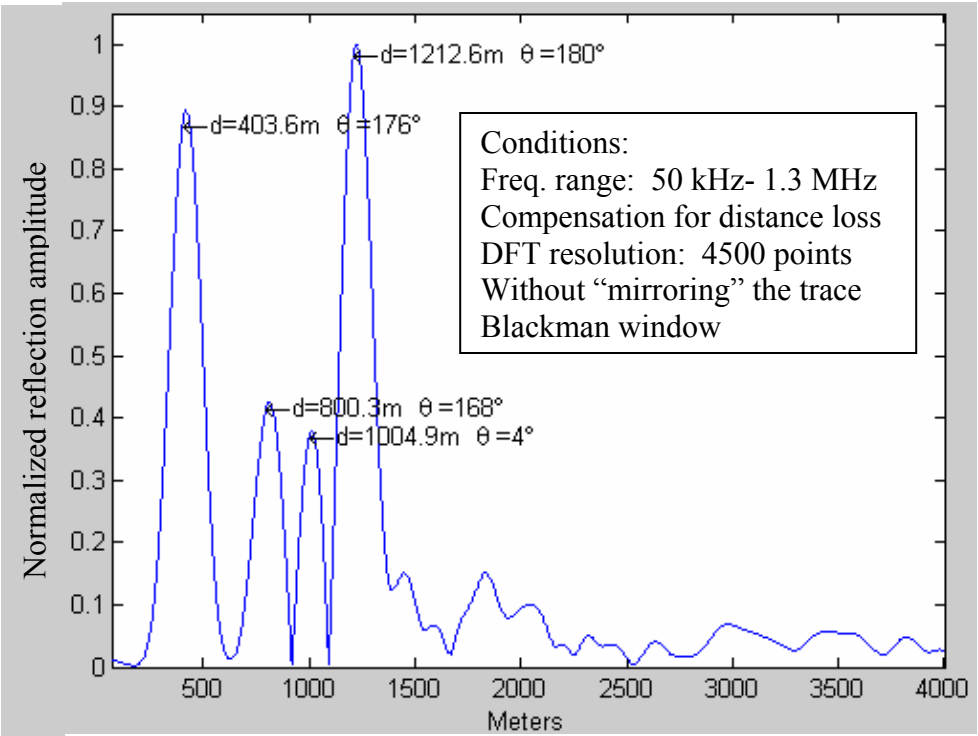

Fig. 6.28 Two bridge taps terminated in open circuit and short circuit

Fig. 6.29 shows an important measurement that demonstrates that with this technology is possible to estimate a 200 m bridge tap at 5 km. This is an important achievement, because normally measurements at far distances have a poor resolution. The spread of the reflection normally makes impossible to see the second reflection from the end of the bridge tap when the two reflections are close. For this reason, a measurement like this one demands a very high resolution. In order to solve this measurement, we used the "super resolution" method explained in Chapter 5. We can see that this method is useful to solve complex measurements that demand very high resolution.

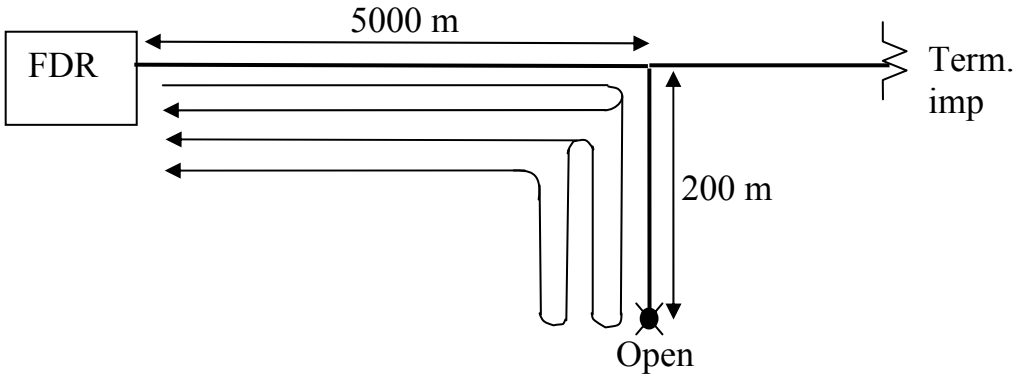

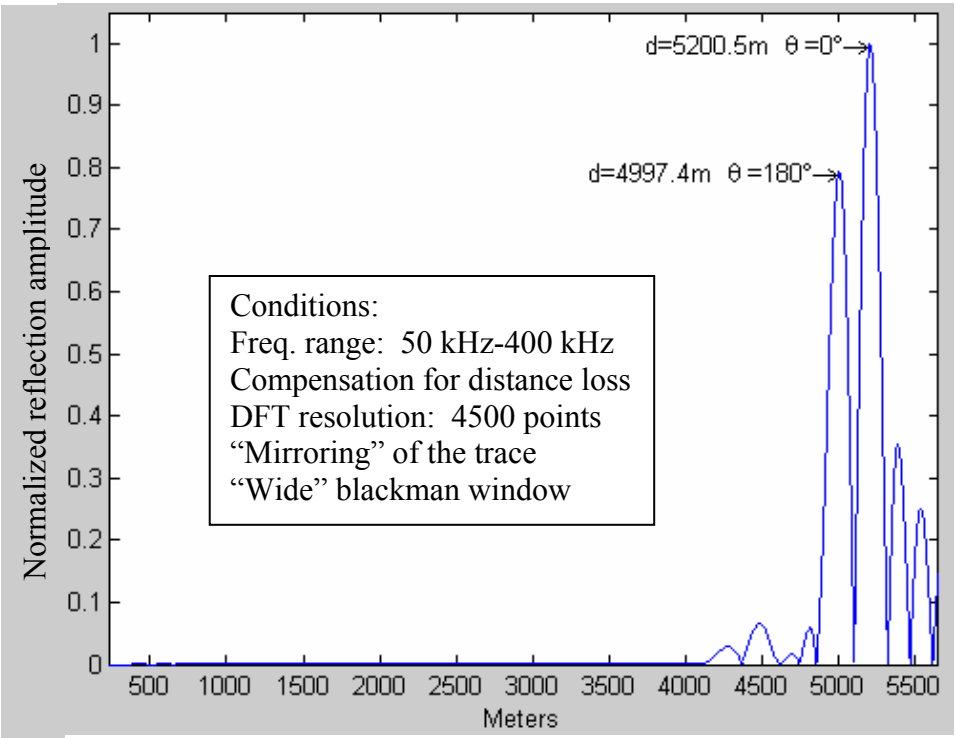

Fig. 6.29 200 m open circuit bridge tap at 5200 m

6.4 Inductance and capacitance faults

In this section we first show how W-FDR can locate inductance faults in the telephone lines. Inductance faults are caused by coils on the line, for example loading coils, which were added to telephone lines in the past to improve the quality of the voice, but now they have to be located and removed to prepare the line for high speed data transmission.

The reflection angle caused by a coil will depend on the inductance. Recall from Chapter 3, the reflection coefficient is

$$\rho = \frac{Z_r - Z_0}{Z_r + Z_0} \tag{6.1}$$

where Z_0 is the impedance of the line, that is approximately $100\Omega \angle 15°$ in the range of frequencies from 50 kHz to 1.3 MHz, and Z_r represents the impedance of the coil, which is $\omega L \angle 90°$. Therefore, substituting these values of impedance in equation 6.1, the reflection coefficient will depend of L, the inductance of the coil. For illustration purposes, in the next measurements we used 15 uH coils that gives a reflection angle close to -90°.

Since the impedance of the coil also depends on the frequency ω, the reflection coefficient of the coil will also change with frequency. The frequencies that form the trace, will not have an entirely constant rate of variation along the frequency axis. For this reason, the coil locations are estimated farther than its actual location. Nevertheless, this difference is almost insignificant.

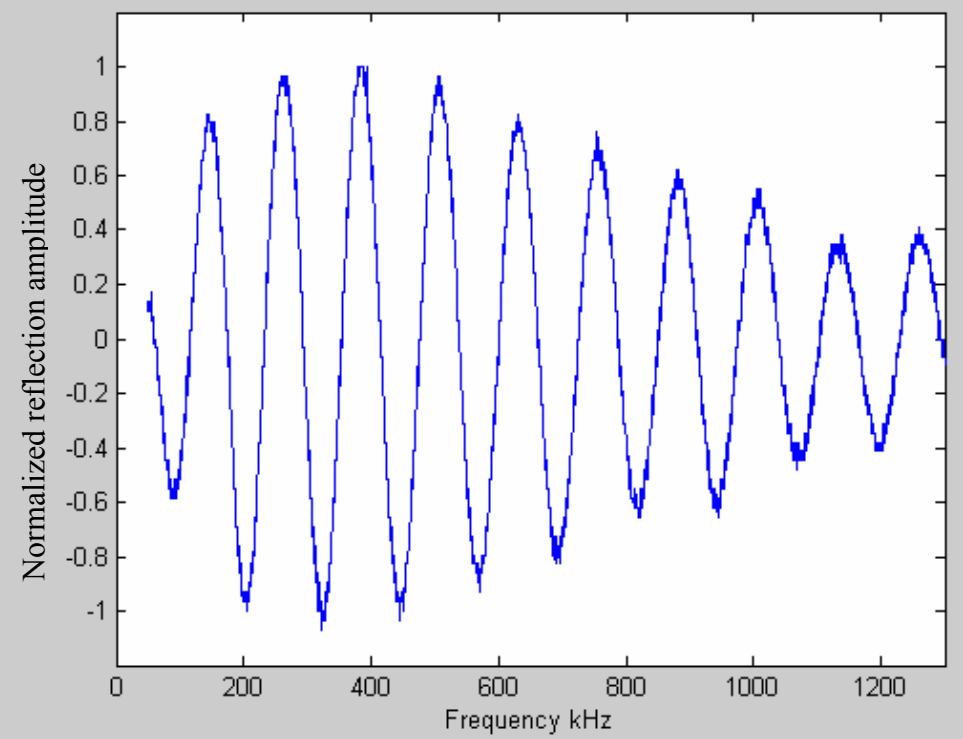

Fig. 6.30 Trace from a coil at 800 m

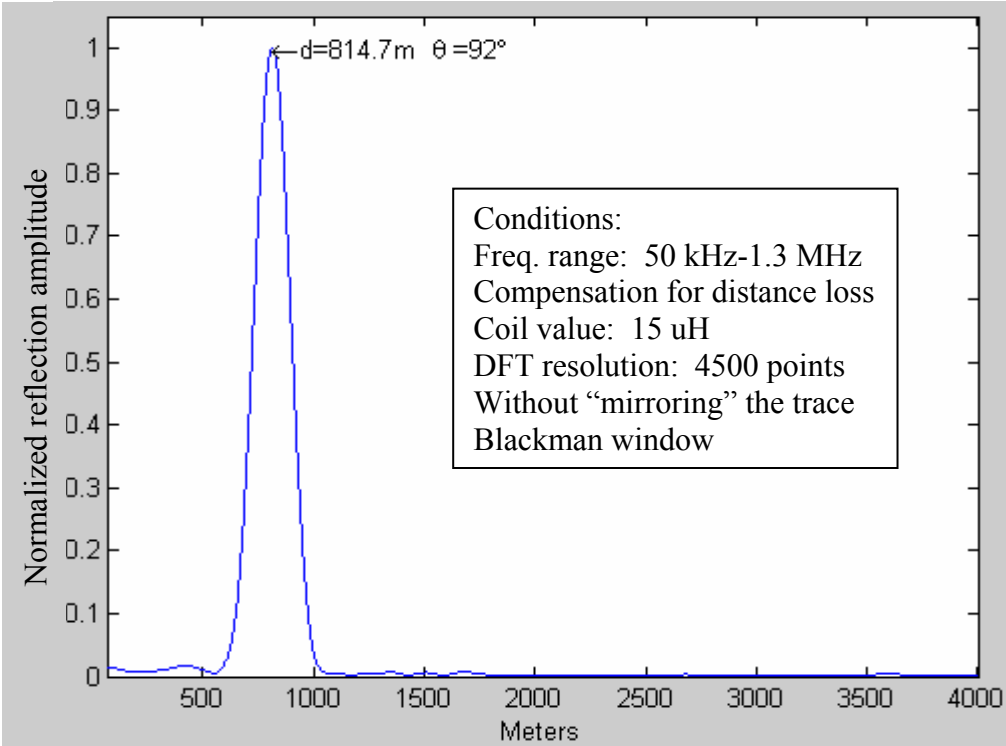

Fig. 6.31 Coil at 800 m

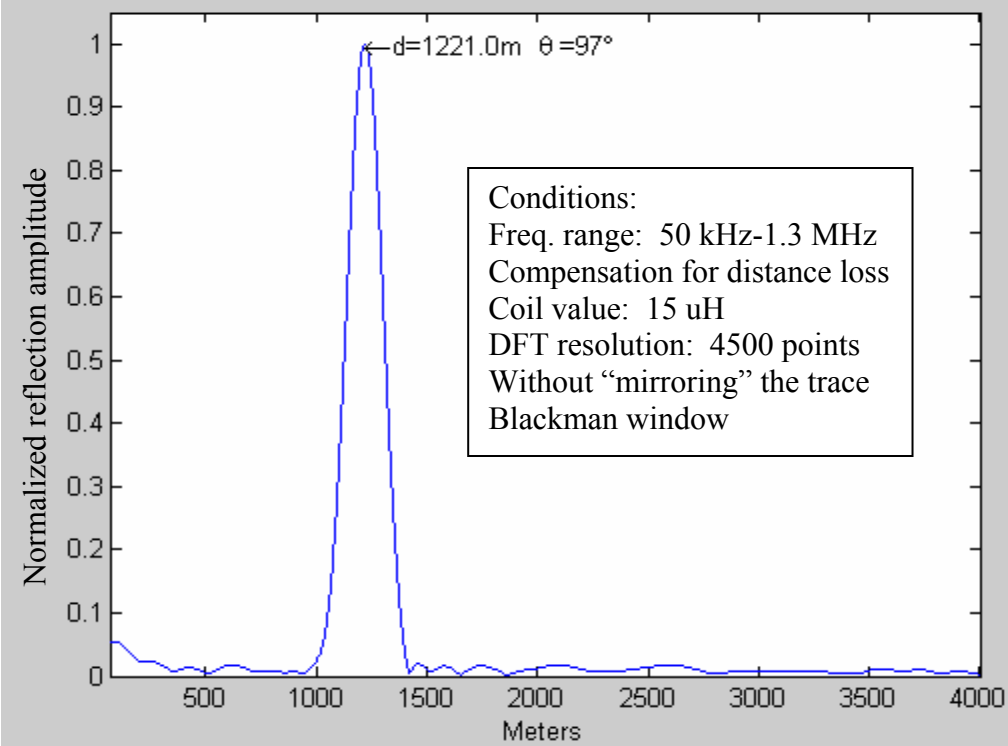

Fig. 6.32 Coil at 1200 m

Next we show some measurements that show that W-FDR can locate multiple coils in the line. Fig. 6.33 shows how the coils were connected to the twisted pair line during the experiments, which is the same way as the loading coils are connected in the telephone lines.

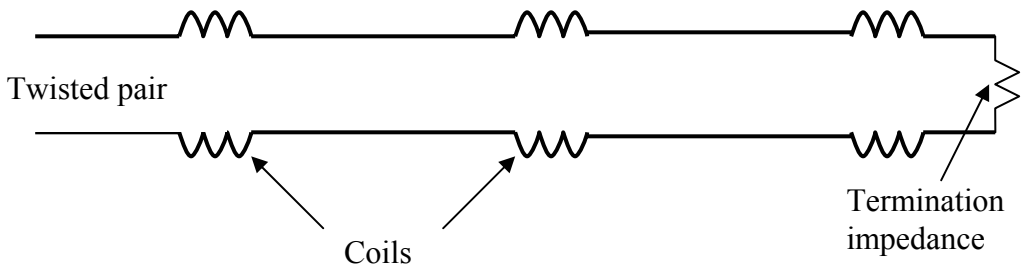

Fig. 6.33 Coils in the twisted pair line

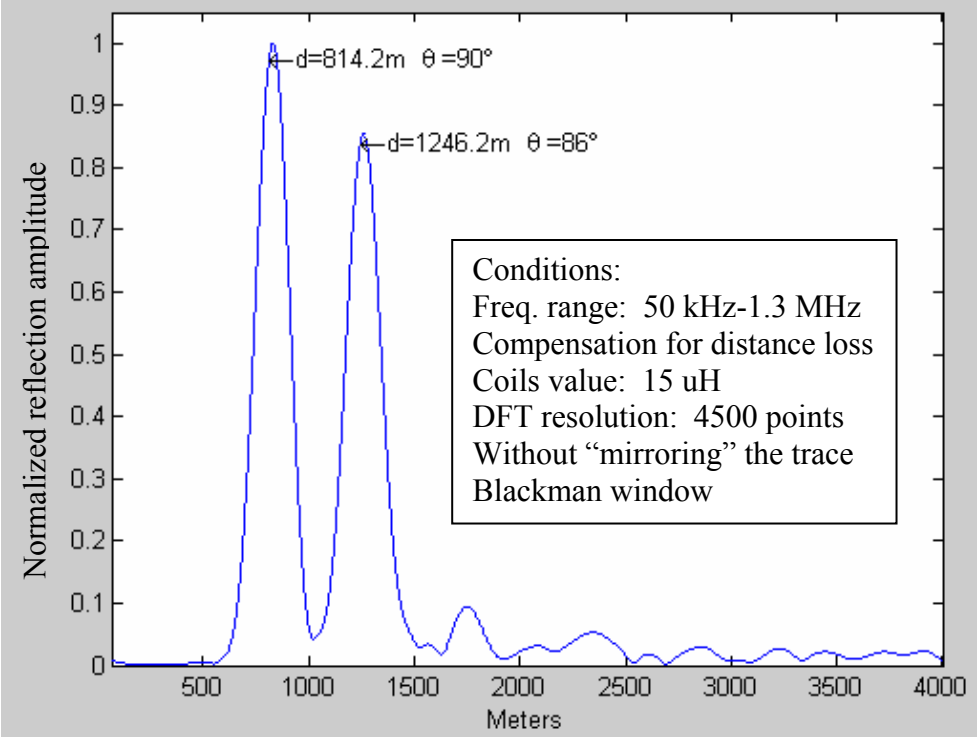

Fig. 6.34 Double coil (800 m, 1200 m)

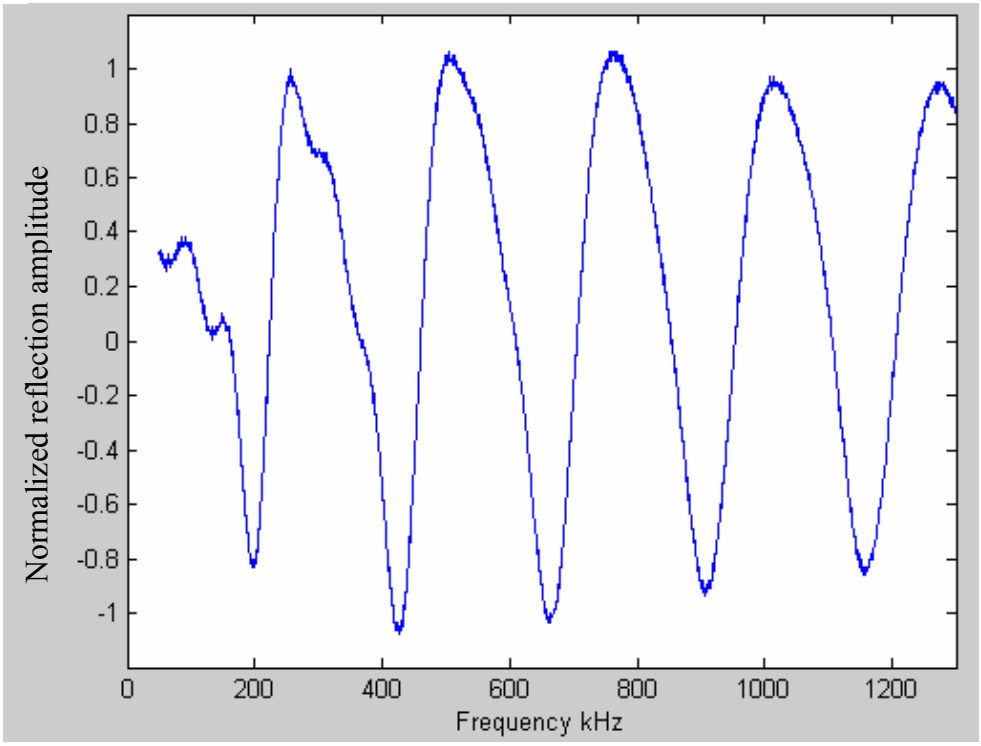

Fig. 6.35 Trace from a line with 3 coils (800 m, 1200 m, 1600 m)

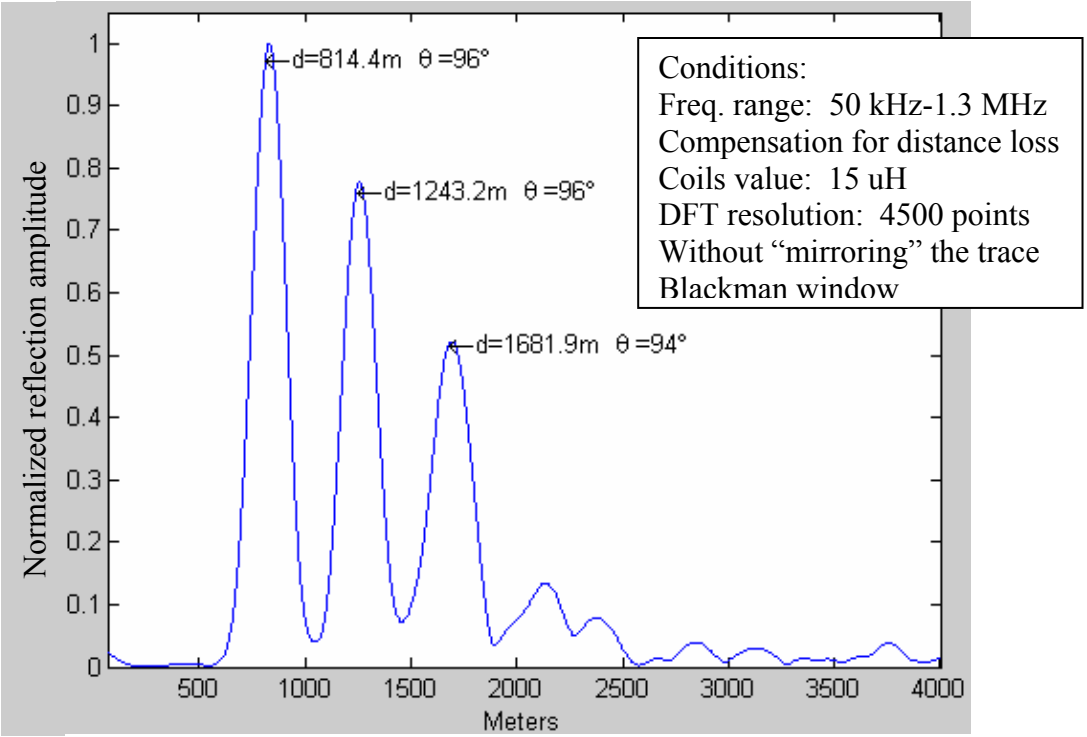

Fig. 6.36 Triple coil (800 m, 1200 m, 1600 m)

Next we show some measurements of a line terminated in a capacitor. The impedance of a capacitor is $\frac{1}{\omega C}\angle -90°$. Therefore, similar to the case of the coils, the reflection coefficient from a capacitor will depend of the capacitance *C*. For illustration purposes, in these measurements we used 8 nF capacitors, to obtain a reflection angle close to +90°. The location of the capacitors also appears to be slightly farther than its actual location. This is caused for the same reason that was explained for the case of the coils. Fig. 6.37 shows how the capacitor was connected to the twisted pair line in the measurements.

Fig. 6.37 Coils in the twisted pair line

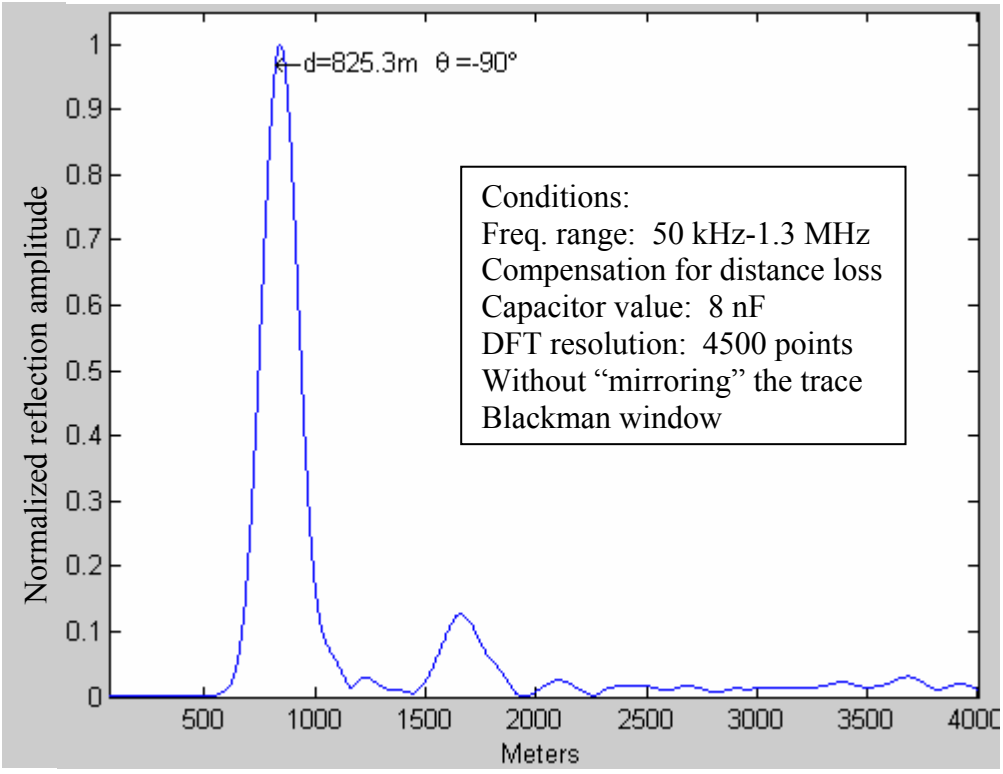

Fig. 6.38 Capacitor at 800 m

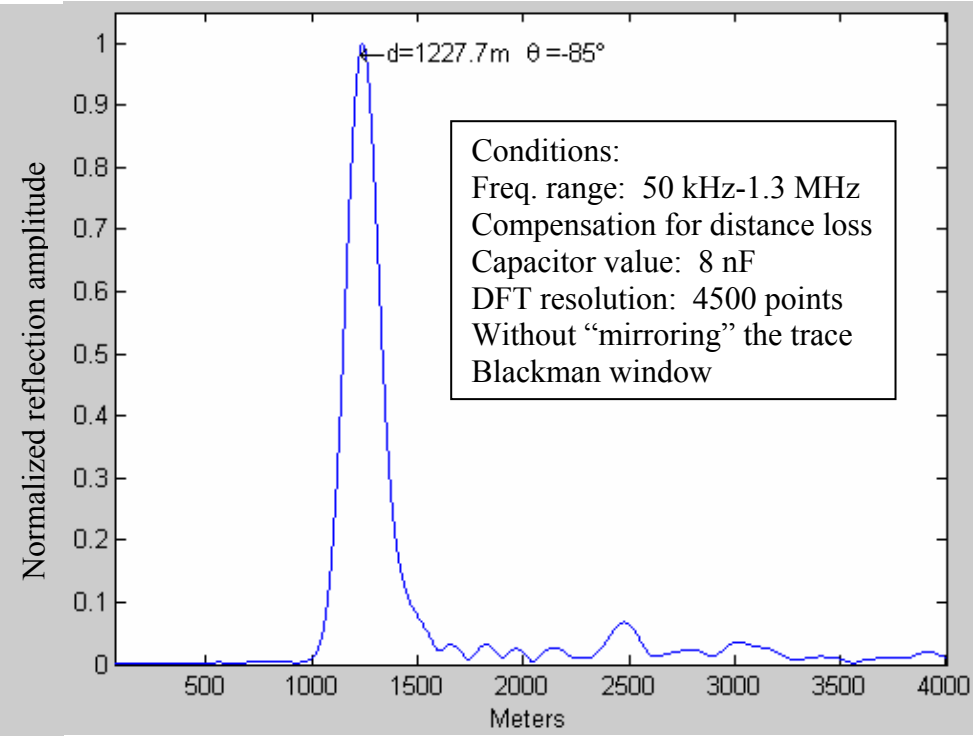

Fig. 6.39 Capacitor at 1200 m

6.5 The effect of water

Water is a common problem in telephone lines that technicians have to locate in order to fix the line. When a twisted pair line gets into water, this changes the capacitance and the characteristic impedance of the part of the line that has water. This change in characteristic impedance of the line at the points where the water starts and ends, causes a portion of the signal traveling on the line to be reflected back at these points.

Next we show a measurement of a properly terminated line that has 300 m of the line under water, starting at 1200 m. In this measurement we can see the first reflection at 1203 m, which corresponds to the point where the water starts. The second reflection, which corresponds to the end of the water, appears to be at 1724

m instead 1500 m that is the actual location. The reason why this reflection is 224 m farther than its real location, is because when the signal passes through the 300 m of line under water, the signal travels slower. This gives the appearance that the section under water is longer than what it really is. For this reason the second reflection appears at 1724 m.

We can also see in this measurement that the reflection angle where the water starts is 162° and 25° where the water ends. These reflection angles help to recognize and differentiate a reflection caused by water on the line, from reflections like bridge taps, open circuits or short circuits, where the reflection angle is ether 180° or 0°.

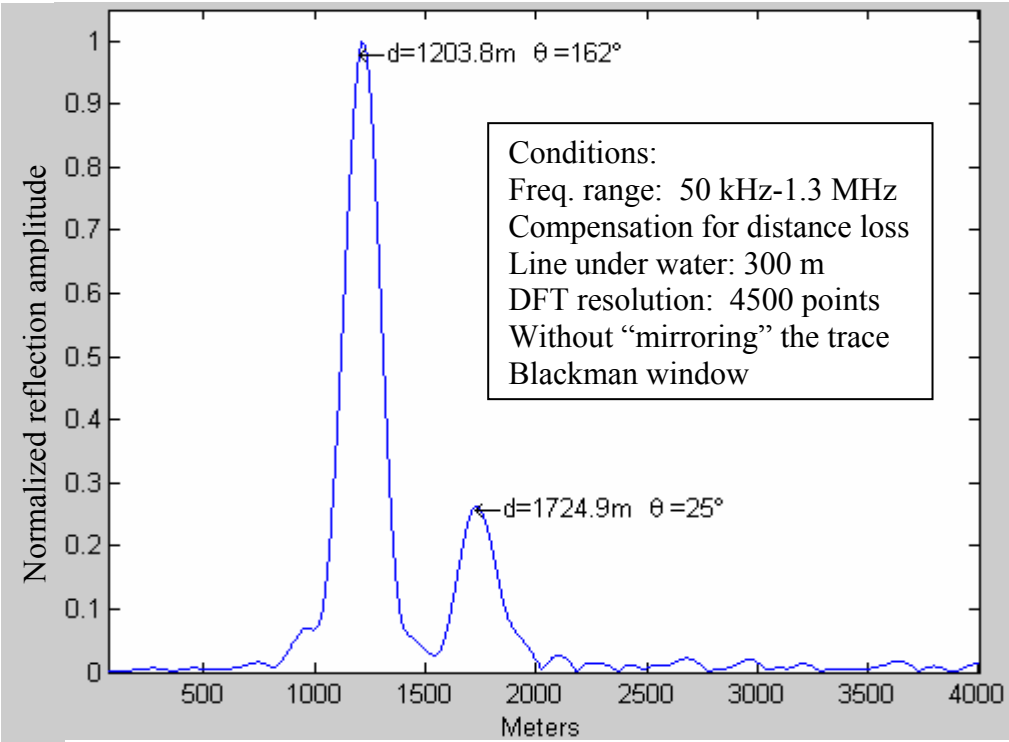

Fig. 6.40 300 m line under water (starting at 1200 m)

7. Conclusions

Wideband frequency domain reflectometry (W-FDR) is a new technique to locate faults in telephone lines. This measurement technique was investigated as an alternative to the well known technique called time domain reflectometry (TDR). This new technique performs a stepped frequency sweep on the line, instead of sending a pulse (like TDR). The reflected waveform is passed through a coherent detector and captured to be processed and estimate the location of the fault.

This new measurement technique presents the novel advantage; as well as determining the location of the fault, it can also estimate the reflection coefficient angle of the fault. This angle is used to estimate the type of the fault. In this way, it is possible to distinguish a reflection from an open circuit, loading coil, bridge tap, water, etc.

The W-FDR system that was built in the lab to test this new technique has a range that exceeds 5 km. This allows telephone lines to be measured from a central location such as a central office or a field cross-connect. This facilitates low-cost deployment of DSL, since measurements do not involve human intervention at the customer location.

W-FDR can accurately locate different kinds of faults on the telephone line. In this thesis, we presented measurements from different kinds of faults at distances up to 5 km. The results of these measurements show a good accuracy in the location of the faults and the measurement of the reflection coefficient angle.

With W-FDR, it is possible to locate multiple faults on the same line and estimate the reflection angle of each fault. In this thesis we present measurements of complex loops that present up to 4 impairments in the same line. These results show that W-FDR can locate each fault and estimate each reflection coefficient angle, and even show secondary reflections from the bridge taps.

In addition, with W-FDR is possible to locate multiple coils on the telephone line. These coils have been used by telephone companies in the past to improve the quality of voice. Nevertheless, these coils prevent high speed data transmission and must be removed in order to provide high speed data services like ADSL. In this thesis, we present measurements of 15 uH coils on the line, which were clearly located with W-FDR.

Based on the results obtained with W-FDR, which are shown in Chapter 6, we conclude that with this measurement technique, is possible to achieve better resolution, measure longer distances and more clearly estimate multiple faults in the same line when compared with the instruments currently on the market. Besides this, W-FDR presents the advantage that it can estimate the reflection coefficient angle, allowing us to obtain information about the nature of the fault. Therefore, this technique can be a better option than the traditional TDR.

7.1 Future work

A prototype of a W-FDR system was built in this thesis, to test in a real telephone line. This prototype system is not a marketable product. To test the telephone lines, it uses a waveform generator, an oscilloscope to digitize the reflected signal, and a computer to control these instruments and process the measurements. Therefore, this is an expensive system and is not practical to be used in the field. For this reason, a portable instrument to test telephone lines using W-FDR needs to be designed.

Also, future work could improve the hardware of the W-FDR system. The prototype system used an 8 bit oscilloscope as a digitizer. To improve the measurements obtained with W-FDR, a digitizer with better resolution (for example 12 bits) should be implemented in a future portable instrument. Also, a better pre-amplifier can be designed to improve the measurement range of the device, and a better hybrid coupler to reduce or even eliminate the baseline.

The results obtained with the W-FDR system show the location of the fault. However, these measurements do not indicate whether or not the line impairments will affect the quality of internet service. Future work in this area should include the development of a database to cross reference results to quality service. These results could be gathered from existing service records along with field analysis of the given lines.

W-FDR applications can be also extended to other areas different than qualifying twisted pair lines. Future applications of W-FDR could include ultrasound which presently uses variations of TDR.

References

[1] Terence William Monteith, "Locating telephony loop impairments with Frequency Domain Reflectometry", Thesis, University of Saskatchewan, 2002.

[2] "DSL Forum", Statistics on DSL growth for Canada and United States. URL: http://www.dslforum.org , March 2, 2004

[3] "Internet Software Consortium", Internet domain survey

URL: http://www.isc.org/index.pl?/ops/ds/ , January 2004

[4] Walter Goralski, "xDSL Loop Qualification and Testing", IEEE Communications Magazine, vol. 37, no. 5, May 1999, pp. 79-83.

[5] Consultronics, Information about the cable shark plus (DSL cable qualifier)

URL: http://www.consultronics.com/cshark.htm, April 2004

[6] Fluke Networks, Fault location using 990DSL Coper-pro URL: http://portweb.flukenetworks.com/storage/efulfillment/2105869_6517_ENG_A_EFUL_1501.pdf

[7] 'Power Divider for FMCW Radar', White paper on FMCW Power Dividers, URL: http://www.ee.duke.edu/gsm/projects/fmcw-pd/fmcw.html, March 12, 2001.

[8] David. E. Dodds, EE816 Telephony Notes, University of Saskatchewan, Saskatoon, Saskatchewan, 1996

[9] Whitham D. Reeve, *Subscriber Loop Signaling and Transmission* Handbook. Digital. New York, NY: IEEE Press, 1995

[10] Hugh Hildreth Skilling, *Electric transmission lines*. New York, NY: McGraw-Hill Book Company, 1951

[11] Leon W. Couch II, *Digital and Analog Communication Systems*. New York, NY: MacMillan Publishing Company, 1990.

[12] Alan V. Oppenheim, *Discrete-time signal processing- 2nd ed.,* New Jersey, Prentice-Hall, 1999

[13] John G. Proakis, Dimitris G. Manolakis, *Digital Signal Processing,* Second edition, New York, NY: Macmillan, 1992

[14] "The DSL Sourcebook", Paradyne white paper on DSL Technology, URL: http://www.paradyne.com/cgi-bin/universal.perl , April 19, 2004

[15] TRlabs presentation, "DSL line tester", Edmonton, presenter-Terence Monteith, May 3, 2000.

[16] Greg J. Erker, David E. Dodds W. A. Krzymien, "Digital line extension using MID span amplification", paper, TRlabs, Edmonton, Alberta

[17] Merrill I. Skolnik, *Introduction to radar systems- 2nd ed*, New York, NY, McGraw-Hill, 1980

[18] Stefano Galli and David L. Waring, "*Loop Makeup Identification Via Single-Ended Testing: Beyond Mere Loop Qualification*," IEEE JSAC, Vol.20, No.5, June 2000.

[19] Bell telephone laboratories, Charles W. Kaiser, "*Loop fault locator*", US patent No. 3751606, Aug 1973.

[20] Bell telephone laboratories, John T. Peoples, "*Loop fault locater*", US patent No. 3904839, Sep 1975.

[21] John T. Peoples, "*Determining the composition of subscriber loops from frequency domain measurements*", US patent No. 0146095 A1, Oct 2002.

[22] Sunrise telecom, Raymond L. Chong, "*Detection of bridge tap using frequency domain analysis*", US patent No. 6417672 B1, Jul 2002.

A. Primary constant curve fitted equations

In order to calculate the warping function, it is necessary to estimate the phase delay β in the range of frequency used during the sweep. For this reason, it is necessary to have the values of the primary constants along this frequency range. Therefore, to have enough values of these primary constants in the frequency range needed, the tabulated values of the primary constants were curve fitted to obtain equations that describe these primary constants. The tabulated values of the primary constants at several frequencies can be seen in table A.1 and A.2.

The obtained equations that describe these primary constants, for 24 and 26 AWG telephone wire were developed by Monteith [1] and are shown below. The per unit capacitance was not curve fitted because it is almost constant over the frequency range used.

24 AWG:

Resistance:

$$r = 51.4 - 7.4x10^{-4} f + 7.7x10^{-5} f \cdot \ln(f) - 2.7x10^{-7} f^{1.5} + 4.2x10^{-11} f^{2}$$

Inductance:

$$l = 0.13 + \frac{3.1x10^{-3}}{1 + (3.1x10^{-3})(4.2x10^{-2})f} + \frac{4.5x10^{-2}}{1 + (4.5x10^{-2})(4.1x10^{-5})f}$$

Conductance:

$$g = 5.7x10^{-2} + 4.0x10^{-5} f - 9.8x10^{-20} f^{3} - 6.4x10^{-3} \cdot \ln(f) - \frac{1.7x10^{-2}}{f}$$

26 AWG:

Resistance:

$$r = 82.4 + 2.0x10^{-4} f - 4.6x10^{-12} f^2 \cdot \ln(f) + 2.2x10^{-14} f^{2.5} - 4.2x10^{-3} f^{0.5} \cdot \ln(f)$$

Inductance:

$$l = 0.14 + \frac{4.8x10^{-3}}{1 + (4.8x10^{-3})(2.5x10^{-2}) f} + \frac{4.3x10^{-2}}{1 + (4.3x10^{-2})(2.4x10^{-5}) f}$$

Conductance:

$$g = 5.7x10^{-2} + 4.0x10^{-5} f - 9.8x10^{-20} f^3 - 6.4x10^{-3} \cdot \ln(f) - \frac{1.7x10^{-2}}{f}$$

Table A.1 26 AWG PIC 70, taken from [4]

FREQ. (kHz)	***r*** **(Ohm/km)**	***l*** **(mH/km)**	***g*** **(uS/km)**	***c*** **(nF/km)**
10	274.29	0.6106	0.532	51.58
15	274.59	0.6093	0.755	51.58
20	274.95	0.6083	0.968	51.58
30	275.83	0.6060	1.378	51.58
50	278.26	0.6004	2.149	51.58
70	281.54	0.5932	2.881	51.58
100	287.94	0.5860	3.927	51.58
150	301.88	0.5784	5.588	51.58
200	318.81	0.5725	7.179	51.58
300	357.40	0.5630	10.214	51.58
500	434.73	0.5479	15.929	51.58
700	505.18	0.5351	21.346	51.58
1000	594.45	0.5207	29.112	51.58
1500	717.33	0.5063	41.426	51.58

Table A.2 24 AWG PIC 70, taken from [4]

FREQ. (kHz)	***r*** **(Ohm/km)**	***l*** **(mH/km)**	***g*** **(uS/km)**	***c*** **(nF/km)**
10	172.71	0.6099	0.532	51.58
15	173.11	0.6086	0.755	51.58
20	173.60	0.6070	0.968	51.58
30	174.81	0.6040	1.378	51.58
50	178.22	0.5952	2.149	51.58
70	182.88	0.5880	2.881	51.58
100	191.64	0.5807	3.927	51.58
150	209.56	0.5719	5.588	51.58
200	229.31	0.5647	7.179	51.58
300	268.16	0.5522	10.214	51.58
500	336.60	0.5325	15.929	51.58
700	392.77	0.5187	21.346	51.58
1000	463.61	0.5063	29.112	51.58
1500	561.02	0.4938	41.426	51.58

B. TDR test equipments

The CableShark instrument, manufactured by Consultronics Ltd of Toronto, appears to be the best equipment available on the market to locate faults on telephone lines using TDR. This equipment has a better resolution than other equipment on the market. Fig. B.1 shows a picture of the CableShark equipment [5].

Fig. B.1 CableShark DSL test equipment (picture taken from [5])

Fig. B.2 and Fig. B.3[5] show the measurements of a short circuit and a bridge tap respectively obtained with the CableShark instrument.

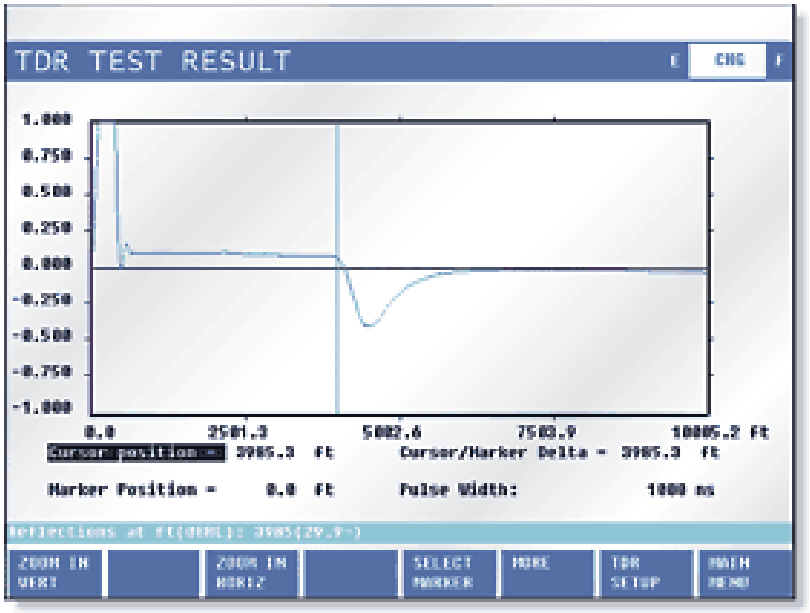

Fig. B.2 Measurement of a short circuit at 1220 m (3995 ft) (picture taken from[5])

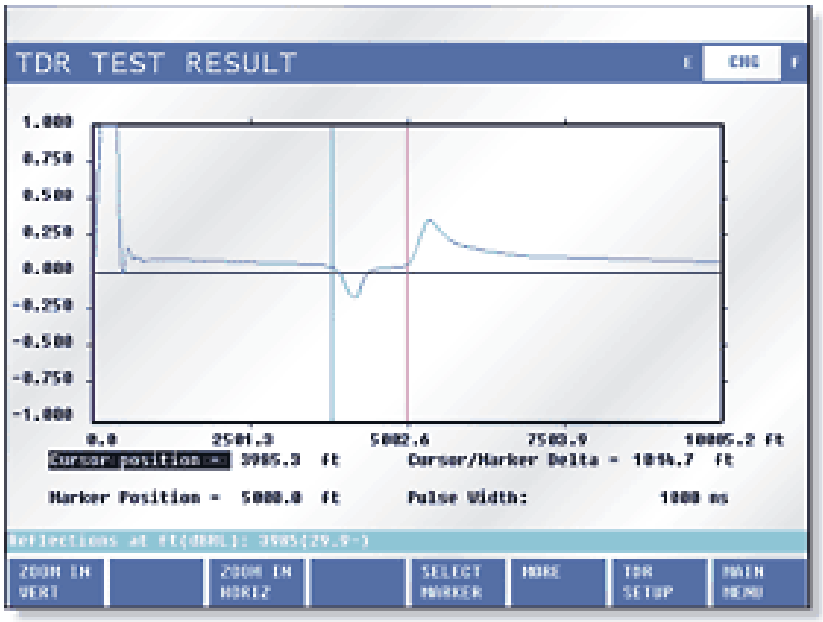

Fig. B.3 Measurement of 305 m (1000 ft) bridge tap at 1220 m (picture taken from [5])

The 990DSL Copperpro manufactured by Fluke Inc. of USA, is another DSL test equipment to locates faults in telephone lines. This device doesn't have resolution as good as CableShark, but still is an excellent DSL test equipment. Fig. B.4 shows a picture of the 990DSL Copperpro equipment.

Fig. B.4 990DSL Copperpro DSL test equipment (picture taken from [6])

Figures below taken from [6] shows the measurements of a short circuit and a bridge tap obtained with 990DSL Copper-pro.

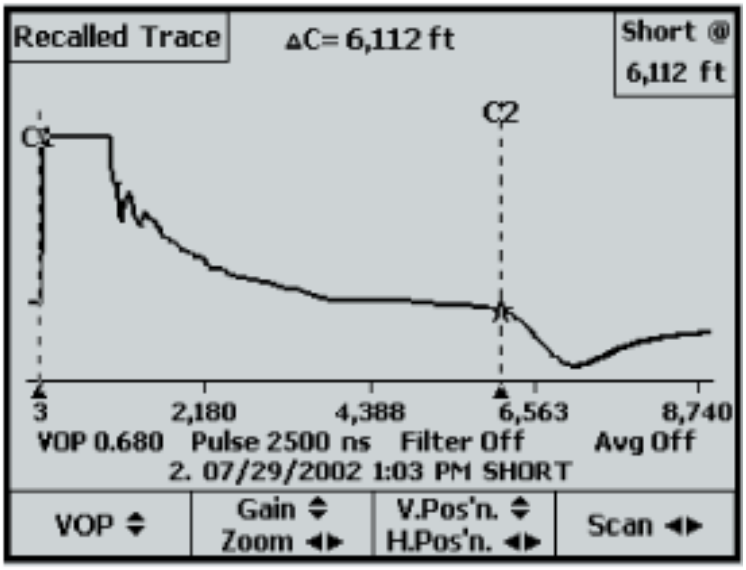

Fig. B.5 Copperpro measurement of a short circuit at 1866 m (6112 ft) (picture taken from [6])

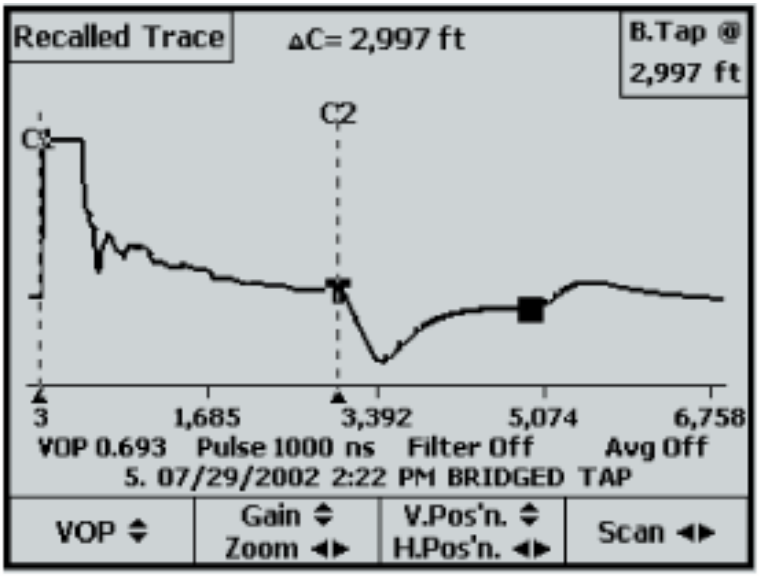

Fig. B.6 Copperpro measurement of a bridge tap located at 1090 m (2997 ft) (picture taken from [6])

C. MATLAB code

Main code:

```
clear mag
y=ope12;      %Name of the vector that has the measurement after subtracting the
              %baseline
y=y(1:2500);  % 2500 represents 1.3 MHz. The data can be limited to fewer samples
scale=4000;   % Maximum distance to plot (it can reach up to 6000 m)
shift=0;      % Shift the compensation for distance loss in case of long distance
              % measurements (shift=meters)
start_sweep=50e3;  %Start frequency of the sweep(50 kHz)
y=y/max(y);   % Normalizes the trace

% Calculation of the last frequency of the sweep when the data is limited to less
% than 2500 samples
sweep_end=((1.3e6-start_sweep)/(2500-1))*length(y)+start_sweep-((1.3e6-
start_sweep)/(2500-1));

% Calculation of the number of 0's to pad the trace down to 0 Hz
ph=round(start_sweep/((sweep_end-start_sweep)/length(y)));
y=[zeros(1,ph),y];  %Zero padding the trace
x=linspace(0.001,sweep_end,length(y)); % Creates the frequency axis to be warped
x=warp(x,24);  %warping of the frequency axis
[x,y]=resam(x,y);  %resample function

%y=mirror(y);  % Used only when super resolution is desired

y=y.*blackman(length(y))';  %Blackman window


N=length(y);
[mag,distance]= ft(y, x(end),1/x(end),scale*2, 4500);  %Fourier transform
distance=(distance/2);  % Divide distance by 2, to don't consider the distance of the
                        % entire round trip
mag=mag/max(mag(200:end));  %Normalizes measurement and avoids normalized
                            % to spurious reflections at close distances

peaks=peak(mag);      % Determine location of the fault, to make zoom in each one
                      % and obtain a high precision resul.
```

```
% Compensation for distance loss
mag=mag.*(1./(exp(-.003*(distance-shift))+.015*exp(-.0015*(distance-
shift))+.010));

%Normalizes measurement after the compensation
mag=mag/max(mag(200:end));
plot(distance,mag)  %Plots result
axis([distance(1),distance(end),0,1.05])  %Adjust scale
xlabel('Meters');
ylabel('Normalized reflection amplitude');


% This cycle makes a Fourier transform in the frequency range where is each
% reflection, to obtain the exact location and angle of each fault (makes zoom).
for i=1:length(peaks),
   n=peaks(i);
   [zoom_mag,zoom_freq,ang,spec]=ft(y(1:end-0),x(end),freq(n-1),freq(n+1),2500);
   [n_zoom,n_zoom]=max(zoom_mag);
   phase(i)=(ang(n_zoom)+0);
   dist(i)=zoom_freq(n_zoom)/2-0;
   text(distance(n),mag(n),['\leftarrowd=',num2str(dist(i),'%4.1f'),'m','  \theta
=',num2str(phase(i),'%3.0f'),'\circ'])  %displays result
end
```

Fourier transform function:

```
% This function calculates the DFT of the trace, estimates the reflection angle and
% obtains the distance axis of the measurement

function [mag,freq,ang,spec]= ft(y,x,startF,endF,points);
%y=trace, x=last value of the warped frequency axis, startF and endF define
%the range of frequency for the DFT, points=number of points in the DFT

clear spec;

x=linspace(0,x,length(y));  % Creates the x axis for the trace. In case of using super
% resolution, this line should be replaced by x=linspace(-x,x,length(y)); because
% then, the trace has double length
f=linspace(startF,endF,points); % vector of the frequencies for the DFT

for n=1:points,
spec(n)=sum( y.*(cos(2*pi*f(n)*x)-i*sin(2*pi*f(n)*x)));  %Correlates the trace
% with a sine and a cosine, which is the DFT
freq(n)=f(n); % The DFT converts the inverse wave length from cycles/meter to
```

```
                % meters. Therefore, the frequency is in reality the distance
mag(n)=abs(spec(n));
ang(n)=angle(spec(n))*180/pi; %Saves the angle in degrees
end
```

Warping function:

```
% This function converts the frequency axis to inverse wave length, based
% in the proprieties of the wire (24 or 26 AWG)

function x_axis = warp( frequency , gauge ) ; %frequency= Hz,
                                               %gauge= 24 or 26 AWG

if ( gauge == 26)

% unit resistence ( ohms/ kft )
r = 82.490828-0.00083896972.*frequency + 7.7360828e-5.*frequency.*log(
frequency )-7.2662322e-10.*( frequency.^2) + 4.3271278e-11.*(
frequency.^2).*log( frequency );

% unit inductance (H/ kft )
l = 1e-3*(0.13560646 + 0.0045586458./(1 +
0.0045586458.*0.029993745.*frequency )+ 0.042974221./(1 +
0.042974221.*2.4978083e-5.*frequency ) ) ;

% unit conductance ( S/ kft )
g = 1e-6*(0.056975378 + 3.9604488e-5.*frequency -9.7592923e-20.*(
frequency.^3 ) -0.0064187937.*log ( frequency )-0.017247963./frequency );


elseif ( gauge == 24)

% unit resistence ( ohms/ kft )
r = 51.454871 - 0.00081480804.*frequency + 8.4036765e-5.*frequency.*log(
frequency ) -2.9944726e-7.*( frequency.^1.5) + 4.7368441e-11.*( frequency.^2) ;

% unit inductance (H/ kft )
l = 1e-3*(0.13270211 +
0.0034384324./(1+0.0034384324.*0.033834621.*frequency )+
0.044967001./(1+0.044967001.*3.9171495e-5.*frequency ) ) ;

% unit conductance ( S/ kft )
g = 1e-6*(0.056975378 + 3.9604488e-5.*frequency - 9.7592923e-20.*(
frequency.^3 ) -0.0064187937.*log ( frequency ) - 0.017247963./ frequency ) ;
```

```
else

dispstring = [ 'Inavalid gauge type. Use 24 or 26.'] ;
disp ( dispstring );
end

w = 2*pi*frequency ; %converts frequency to rad/sec

% Calculation of the warping factor
term1 = r.^2 + (w.^2 ).*( l.^2 ) ;
term2 = g.^2 + (w.^2 ).*( ( 15.7e-9).^2);
term3 = sqrt ( term1.*term2 ) ;

beta = sqrt (0.5*( term3 - r.*g + (w.^2).*l.*15.7e-9));
beta = beta /304.8;    % Convert to 1/m.   304.8 m in 1 kft

warpfactor = beta ./w;  % Warping factor

x_axis = frequency.*warpfactor ;  %Return warped data
```

Resampling function:

```
%This function resample the warped frequency axis that has an irregular
%space between samples, to make uniform the space between its samples

function [ x_new , y_new ] = resam(x,y) ; %x=warped frequency axis
                                          %y=trace


N = length ( x ) ; % Number of points in vector
samplesize = x( length(x))-x(length(x)-1); % resample step size
points = floor ((max(x)-min(x))/ samplesize ) ; % number of points in new vector
overlap = 0; % Initialize overlap counter

y_axis (1) = y (1) ; % Initialize with first sample
x_axis (1) = x (1) ; % Initialize with first sample

%Loop to determine new X and Y axis
for i = 2: points
 x_axis ( i ) = x_axis(1) + samplesize*( i-1); %Calculate new X axis points
```

```
 if ( x_axis ( i ) < x( i-1-overlap )) %Determine if overlap occurred
 overlap = overlap +1; % overlap occurred , increment counter
 end

 % Use linear interpolation to find new Y axis points
 y_axis ( i ) = (( y( i-overlap )-y( i-1-overlap ))*( x_axis ( i )-x( i-1-overlap ))/( x( i-
overlap )-x( i-1-overlap )))+ y( i-1-overlap );
end

x_new = x_axis ; %Return new x axis
y_new = y_axis ; %Return new y axis
```

Fault location function (peak location):

```
%This function is used to locate the peaks in the graph of normalized
% reflection magnitude, to make zoom in each reflection

mag=mag/max(mag(100:end)); %Normalizes measurement and avoids normalized
                                % to spurious reflections at close distances

peaks=1;
[n,n]=max(mag(100:end));  %Determine the location of all peaks on the plot
n=n+99; % Compensate for the 100 points that we skip in previous function.
count=0;
flag=0;
factor=round((length(mag)/2500)*60);

for i=n-10:length(mag)-61,  % Cycle to check every peak on the plot and
%  determine which ones are real and which ones are just noise.
   if( mag(i)>mag(i-1) && mag(i)>=mag(i+1) )  %Checks if it is a peak
      if(mag(i)>0.140)  % Checks if the peak level is above 0.14, to make sure that it
                        %  is not noise from the line.

%Checks the slope level before and after the peak, to make sure that the peak quite
large and it is not a peak from noise
if((mag(i)-mag(i-factor))>0.045 && (mag(i)-mag(i+factor))>0.045)

 for k=i:i+round(factor*2/3), if((mag(k+1)-mag(k))>12e-4) flag=1; end; end
%Makes one last check to make sure the peak is not just noise
            if(flag==0)
               count=count+1;
               peaks(count)=i; %Stores the position of the reflection (peaks)
            else flag=0;
            end
         end
```

```
      end
   end
end
```

Super resolution function (mirror):

```
%This function is used to mirror the trace respect to the Y axis, to obtain
%super resolution

function y2=mirror(y); %y= trace

N=length(y);
for i=0:N-1, y2(i+1)=y(N-i); end  % Mirror the trace in a new vector y2

y2=[y2,y]; %Put the two vectors together (Trace and mirror trace)
```

D. Schematic diagrams

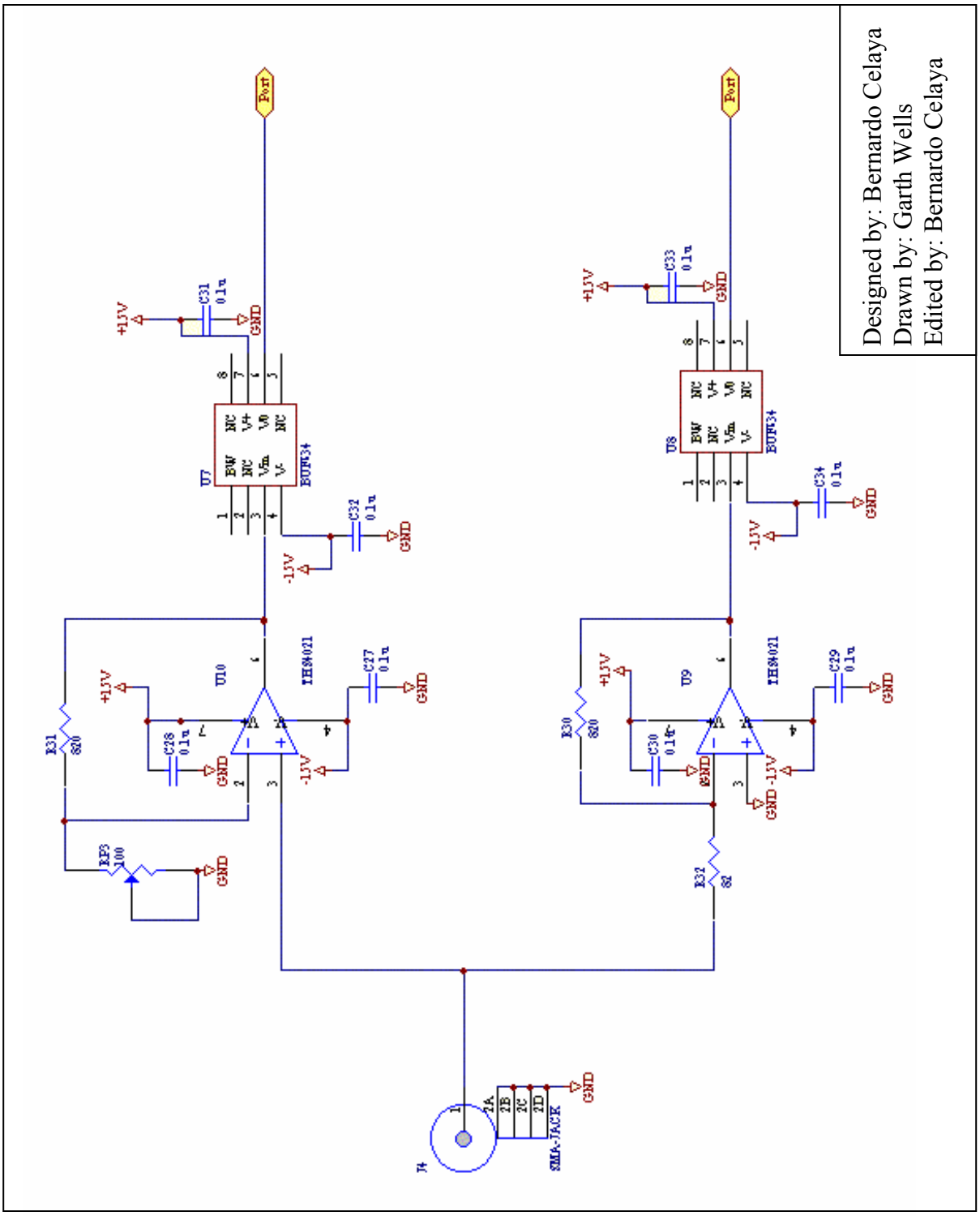

Fig. D.1 Differential amplifier

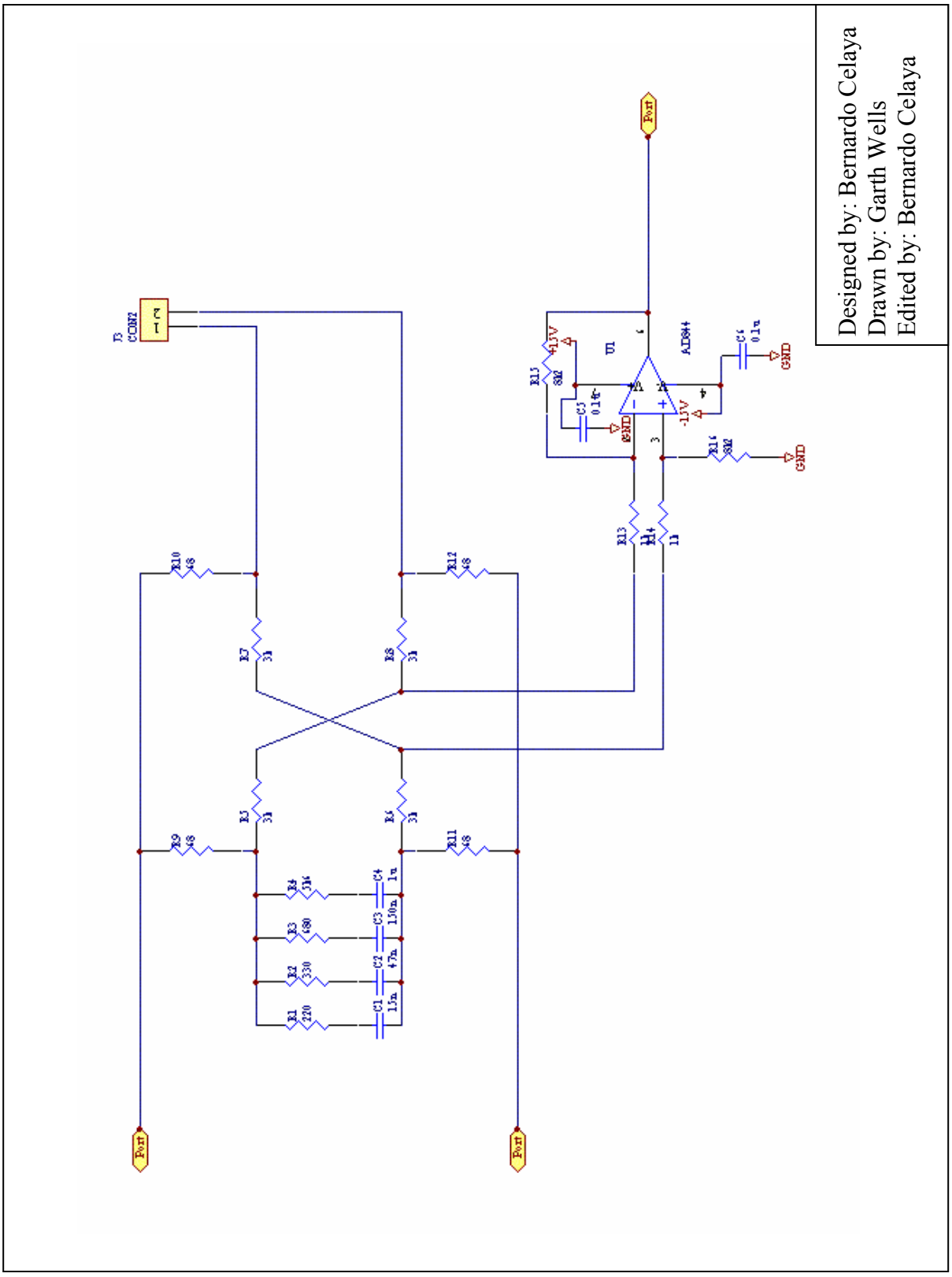

Fig. D.2 Hybrid coupler with differentiator

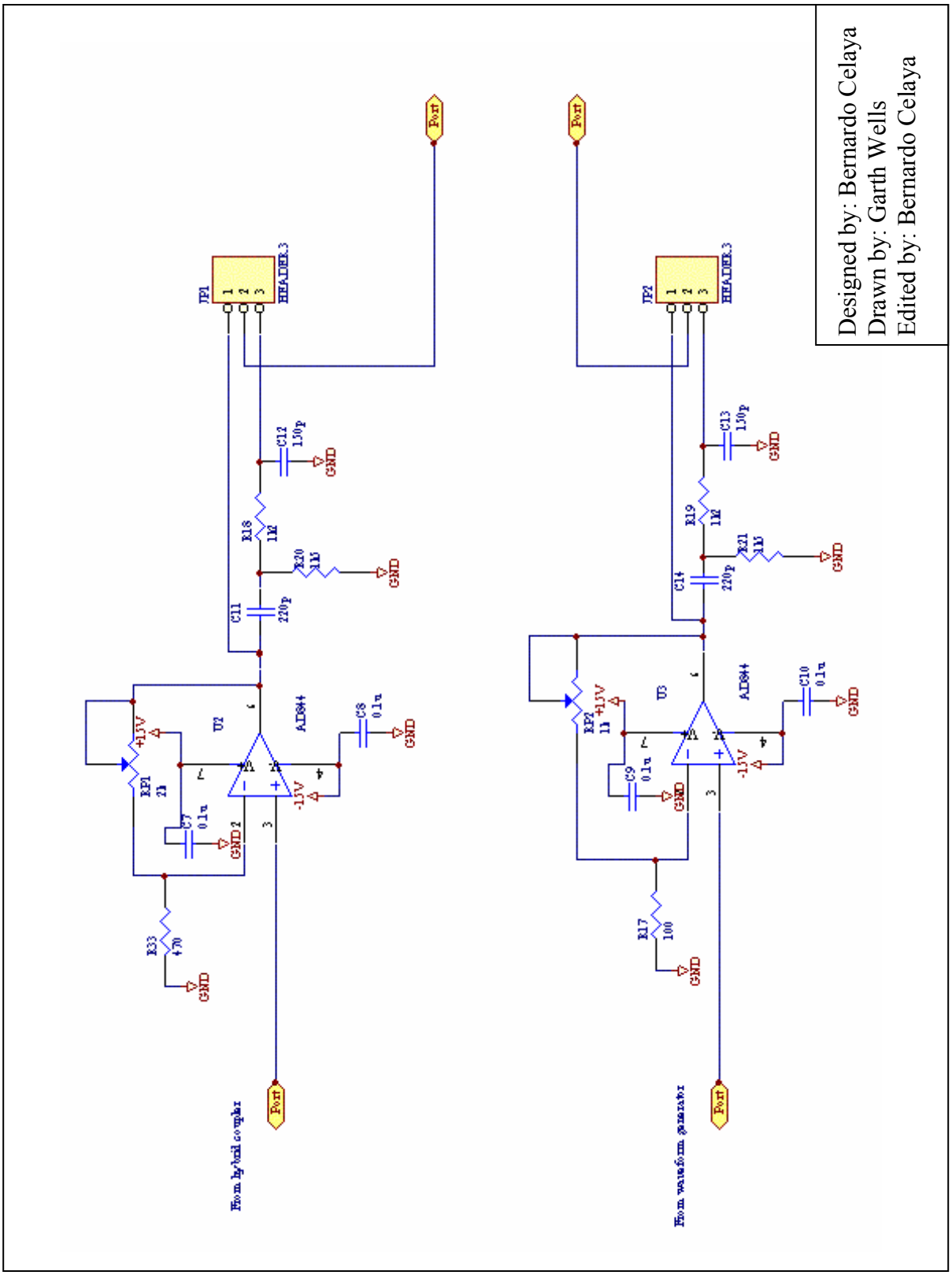

Fig. D.3 Circuit for high frequency compensation

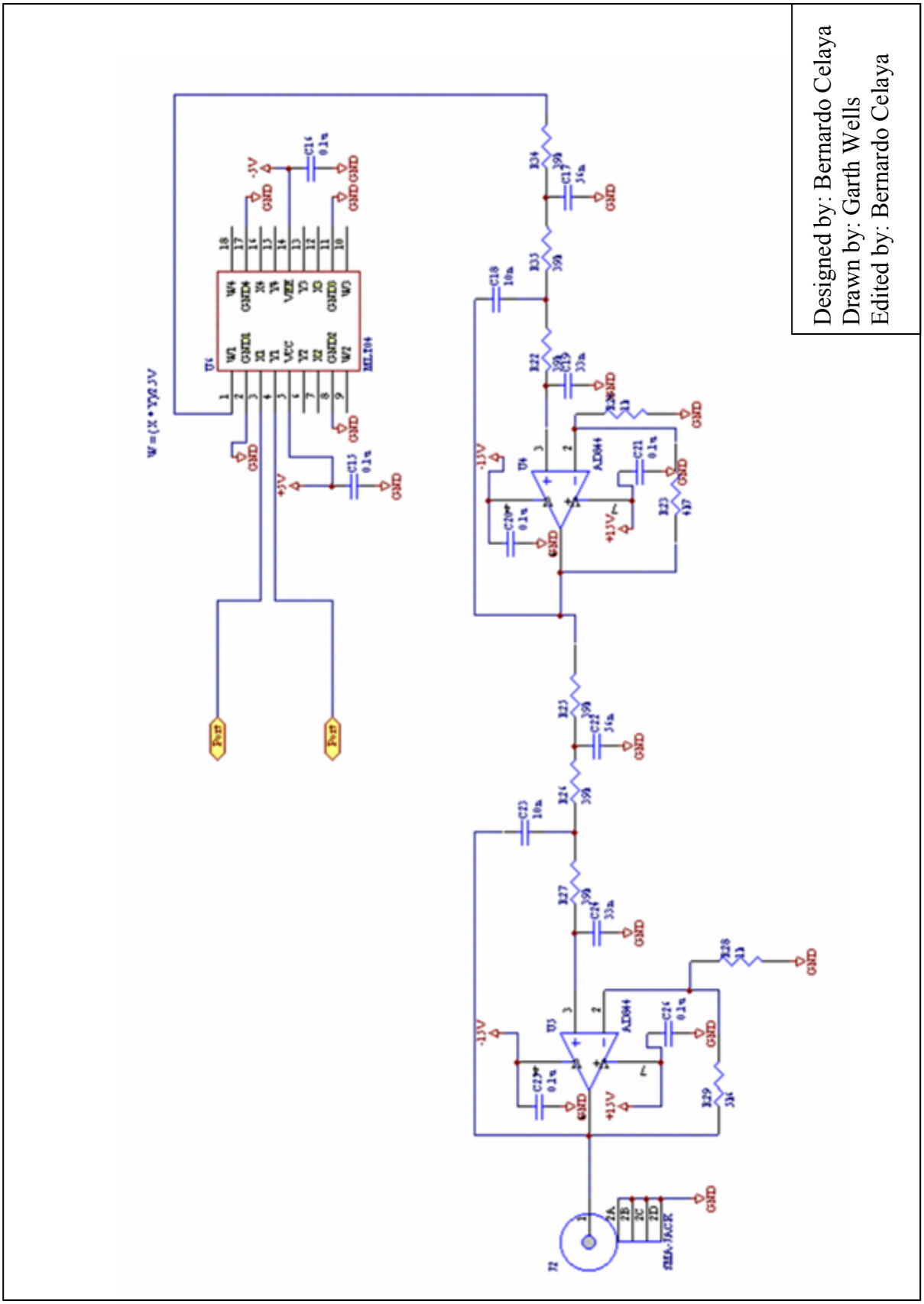

Fig. D.4 Coherent detector (multiplier and low pass filter)

E. Experiment pictures

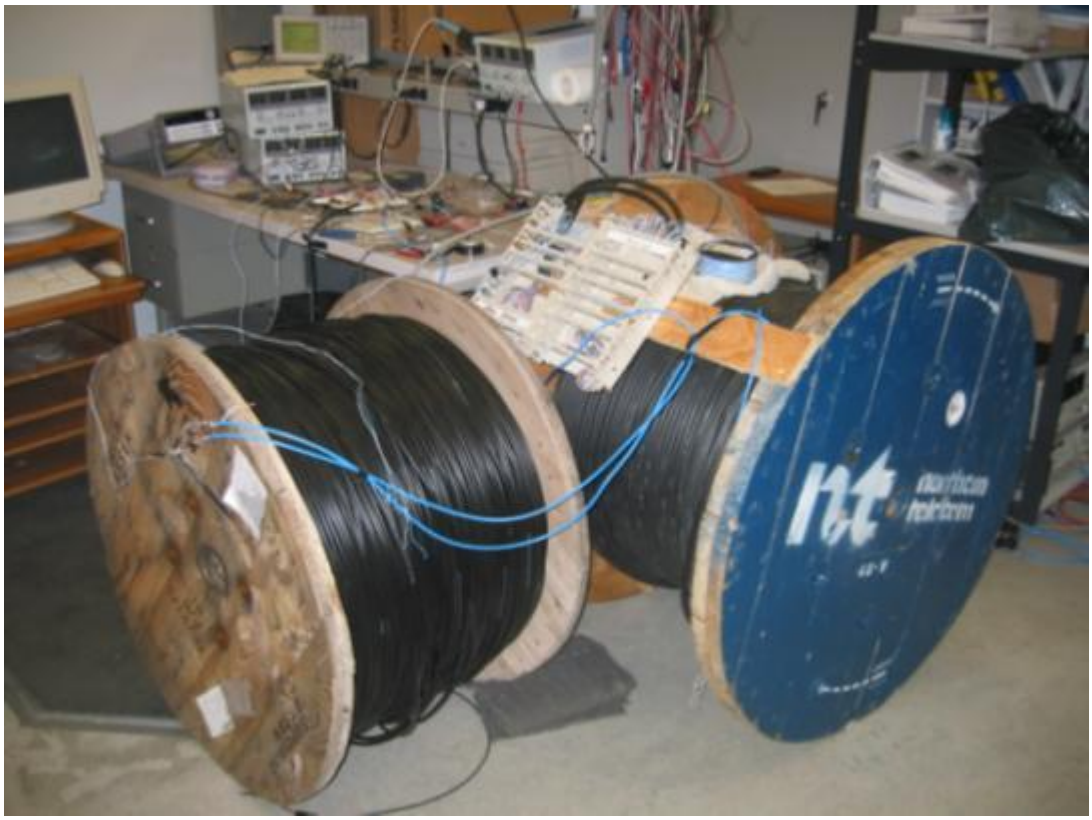

Fig. E.1 Spool cables used for the experiments

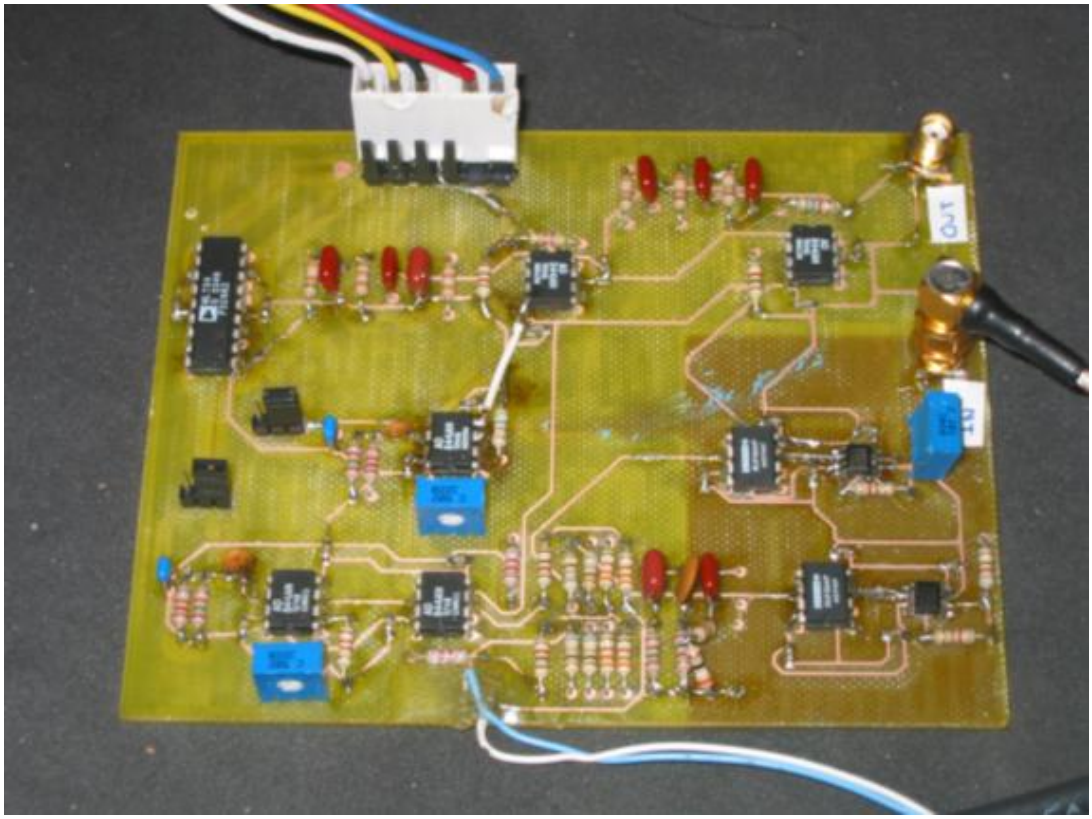

Fig. E.2 W-FDR system circuit board